JYVÄSKYLÄ STUDIES IN BIOLOGICAL AND ENVIRONMENTAL SCIENCE
292

Moona Huttunen

Enterovirus-Induced Non-Acidic Entry Pathway and its Relation to the Epidermal Growth Factor Receptor Pathway

JYVÄSKYLÄN YLIOPISTO

JYVÄSKYLÄ STUDIES IN BIOLOGICAL AND ENVIRONMENTAL SCIENCE 292

Moona Huttunen

Enterovirus-Induced Non-Acidic Entry Pathway and its Relation to the Epidermal Growth Factor Receptor Pathway

Esitetään Jyväskylän yliopiston matemaattis-luonnontieteellisen tiedekunnan suostumuksella
julkisesti tarkastettavaksi yliopiston Ambiotica-rakennuksen salissa YAA303,
lokakuun 31. päivänä 2014 kello 12.

Academic dissertation to be publicly discussed, by permission of
the Faculty of Mathematics and Science of the University of Jyväskylä,
in building Ambiotica, hall YAA303 on October 31, 2014 at 12 o'clock noon.

UNIVERSITY OF JYVÄSKYLÄ

JYVÄSKYLÄ 2014

Enterovirus-Induced Non-Acidic Entry Pathway and its Relation to the Epidermal Growth Factor Receptor Pathway

JYVÄSKYLÄ STUDIES IN BIOLOGICAL AND ENVIRONMENTAL SCIENCE 292

Moona Huttunen

Enterovirus-Induced Non-Acidic Entry Pathway and its Relation to the Epidermal Growth Factor Receptor Pathway

UNIVERSITY OF JYVÄSKYLÄ

JYVÄSKYLÄ 2014

Editors
Varpu Marjomäki
Department of Biological and Environmental Science, University of Jyväskylä
Pekka Olsbo, Ville Korkiakangas
Publishing Unit, University Library of Jyväskylä

Jyväskylä Studies in Biological and Environmental Science
Editorial Board

Jari Haimi, Anssi Lensu, Timo Marjomäki, Varpu Marjomäki
Department of Biological and Environmental Science, University of Jyväskylä

URN:ISBN:978-951-39-5859-6
ISBN 978-951-39-5859-6 (PDF)

ISBN 978-951-39-5858-9 (nid.)
ISSN 1456-9701

Copyright © 2014, by University of Jyväskylä

Jyväskylä University Printing House, Jyväskylä 2014

“Where should I go?” -Alice.
“That depends on where you want to end up.” -The Cheshire Cat.

— Lewis Carroll,
Alice's Adventures in Wonderland & Through the Looking-Glass

ABSTRACT

Huttunen, Moona
Enterovirus-induced non-acidic entry pathway and its relation to the epidermal growth factor receptor pathway
Jyväskylä: University of Jyväskylä, 2014, 52 p.
(Jyväskylä Studies in Biological and Environmental Science
ISSN 1456-9701; 292)
ISBN 978-951-39-5858-9 (nid.)
ISBN 978-951-39-5859-6 (PDF)
Yhteenveto: Enterovirusten indusoima neutraali sisäänmenoreitti ja sen vuorovaikutukset epidermaalisen kasvutekijäreseptorireitin kanssa
Diss.

Echovirus 1 (EV1) and coxsackievirus A9 (CVA9) are members of the human *Enterovirus B* species in the family *Picornaviridae*. Both of these viruses bind to integrins on the plasma membrane (PM) before entering the cells via endocytosis. On the PM, EV1 clusters its receptor, α2β1 integrin, subsequently entering into tubulovesicular structures that gradually form intraluminal vesicles (ILVs), giving rise to multivesicular bodies (MVBs). The entry of EV1 is dependent on macropinocytosis regulators. However, the structures related to CVA9 internalization and uncoating are as yet unidentified. The aims of this thesis were to study the nature and importance of MVBs along the EV1 infection pathway and to study the infectious entry pathway and endocytic structures of CVA9. Moreover, we were interested in the effect of EV1 entry on epidermal growth factor receptor (EGFR) sorting and downregulation. We were able to show that the clustering of α2β1 integrin induces the formation of neutral MVBs, separate from EGFR-positive MVBs. Remarkably, CVA9 was also sorted into neutral MVBs after internalization. Endosomal sorting complexes required for transportation (ESCRTs) were necessary for both viral infections. As the ESCRT machinery is mainly responsible for ILV formation, we concluded that multivesicularity was needed for both infections. A set of endocytosis regulators almost identical to that of EV1 was needed for CVA9 infection. In addition, both viruses avoided the canonical endocytic structures, and acidification was not needed for successful infection. Despite the separate entry pathways, EV1 caused an accumulation of EGFR at the PM and in cytoplasmic endosomes and concomitantly caused enhanced EGFR signaling and reduced downregulation. This is probably due to higher protein kinase C α (PKCα) activation, which has been shown to direct EGFR sorting to recycling instead of degradation.

Keywords: Coxsackievirus A9; echovirus 1; endocytosis; epidermal growth factor receptor; multivesicular body.

Moona Huttunen, University of Jyväskylä, Department of Biological and Environmental Science, P.O. Box 35, FI-40014 University of Jyväskylä, Finland

Author's address Moona Huttunen
Department of Biological and Environmental Science
P.O. Box 35
FI-40014 University of Jyväskylä
Finland
moona.huttunen@jyu.fi

Supervisors Docent Varpu Marjomäki, Ph.D.
Department of Biological and Environmental Science
P.O. Box 35
FI-40014 University of Jyväskylä
Finland

Professor Timo Hyypiä
Department of Virology
Haartman Institute
P.O. Box 21
00014 University of Helsinki

Reviewers Docent Tero Ahola, Ph.D.
Department of Food and Environmental Sciences
Division of Microbiology and Biotechnology
P.O. Box 56
00014 University of Helsinki

Docent Vesa Olkkonen, Ph.D.
Minerva Institute for Medical Research
Biomedicum Helsinki U2
Tukholmankatu 8
00290 Helsinki

Opponent Professor Renate Fuchs
Department of Pathophysiology and Allergy Research
Medical University of Vienna
Waehringer Guertel 18-20
A-1090 Vienna, Austria

CONTENTS

LIST OF ORIGINAL PUBLICATIONS

ABBREVIATIONS

1 INTRODUCTION 9

2 REVIEW OF THE LITERATURE 10
2.1 Enteroviruses 10
2.1.1 Echovirus 1 and coxsackievirus A9 and cell membrane receptors 11
2.2 Endocytosis 12
2.2.1 Early and recycling endosomes 14
2.2.2 Endosomal carrier vesicles and multivesicular bodies 15
2.2.3 Late endosomes and lysosomes 17
2.2.4 Endosome acidification 17
2.2.5 Endosome motility 18
2.2.6 EV1 and CVA9 endocytosis, uncoating, and replication 18
2.3 Epidermal growth factor receptor 25
2.3.1 EGFR endocytosis 26
2.3.2 Ligand-mediated EGFR activation and receptor signaling 28

3 AIMS OF THE PRESENT STUDY 29

4 OVERVIEW OF THE METHODS 30

5 RESULTS AND DISCUSSION 31
5.1 CVA9 endocytosis and uncoating 31
5.2 CVA9 and EV1 do not enter the canonical endocytosis pathway, and the infections are independent of acidification 33
5.3 EV1 and CVA9 accumulate in MVBs, and ESCRT machinery is needed in the infections 34
5.4 EGFR and EV1 are closely associated during virus infection 36
5.5 EV1 infection slows down the degradation of EGFR 37
5.6 Changes in EGFR sorting and signaling during EV1 infection 38

6 CONCLUDING REMARKS 40

Acknowledgements 42

YHTEENVETO (RÉSUMÉ IN FINNISH) 43

REFERENCES 45

LIST OF ORIGINAL PUBLICATIONS

The thesis is based on the following original papers, which will be referred to in the text by Roman numerals I–III.

My responsibilities and the contributions of the other authors in each of the articles are described in the table at the bottom of the page.

I Karjalainen M., Rintanen N., Lehkonen M., Kallio K., Mäki A., Hellström K., Siljamäki V., Upla P., Marjomäki V. 2011. Echovirus 1 infection depends on biogenesis of novel multivesicular bodies. *Cellular Microbiology* 13(12): 1975–1995.

II Huttunen M., Waris M., Kajander R., Hyypiä T., Marjomäki V. 2014. Coxsackievirus A9 infects cells via nonacidic multivesicular bodies. *Journal of Virology* 88(9): 5138–5151.

III Huttunen M., Turkki P., Mäki A., Paavolainen L., Ruusuvuori P., Marjomäki V. 2014. Echovirus 1 Internalization Negatively Regulates EGFR Downregulation. Manuscript.

Author contributions. Initials stand for the following authors: **MH**, Moona Huttunen; MK, Mikko Karjalainen; NR, Nina Rintanen; KK, Katri Kallio; AM, Anita Mäki; KH, Kirsi Hellström; VS, Valtteri Siljamäki; PU, Paula Upla; MW, Matti Waris; RK, Ritva Kajander; PT, Paula Turkki; LP, Lassi Paavolainen; PR, Pekka Ruusuvuori; TH, Timo Hyypiä; VM, Varpu Marjomäki

	I	II	III
Original idea and planning	MK, VM	TH, VM, **MH**	VM, **MH**
Transfections	MK, NR, VS	**MH**	-
siRNA experiments	MK, NR	-	-
Quantitative real-time PCR	KH	**MH,** MW	-
Viral (EV1 or CVA9) infections	MK, NR, **MH,** VS	**MH,** RK	**MH,** PT
Integrin clustering experiments	MK, NR, AM	**-**	AM
Endosomal pH measurement	MK, KK, NR	**MH**	-
Immunofluorescence and confocal microscopy	MK, NR, **MH,** AM, VS	**MH**	**MH,** PT
Computational methods	MK	**MH**	**MH**, LP, PR
Electron microscopy	MK, NR	**MH**	-
Statistical testing	MK, NR	**MH**	**MH**
Live cell microscopy	MK	**MH**	AM
SDS-PAGE and immunoblotting	-	-	**MH**
Writing	MK, VM	**MH,** VM, TH	**MH**, VM, PT

ABBREVIATIONS

β2M	β2-microglobulin
Arf6	ADP-ribosylation factor 6
BMD/LBPA	bis(monoacylglycero)phosphate/lysobisphoshatidic acid
CI-MPR	cation-independent mannose 6-phosphate receptor
CME	clathrin mediated endocytosis
CtBP1/BARS	C-terminal binding protein1/brefeldin A–ADP-ribosylated substrate
CVA9	coxsackievirus A9
DN	dominant negative
ECM	extracellular matrix
ECV	endocytic carrier vesicle
EE	early endosome
EEA1	early endosome antigen 1
EGF	epidermal growth factor
EGFR	epidermal growth factor receptor
EIPA	ethylisopropylamiloride
ESCRT	endosomal sorting complexes required for transport
EV1	echovirus 1
HEV	human enterovirus
Hrs	hepatocyte growth factor receptor substrate
ILV	intraluminal vesicle
Lamp	lysosomal-associated membrane protein
LDL	low-density lipoprotein
LE	late endosome
MAPK	mitogen-activated protein kinase
MVB	multivesicular body
NR	neutral red
Pak	p21-activated kinase
PI	phosphatidylinositol
PI3K	phosphoinositide-3-kinase
PI3P	phosphatidylinositol-3-phosphate
PIP_2	phosphatidylinositol 4,5-bisphosphate
(p)PKC	(phosphorylated) protein kinase C
PLC	phospholipase C
PMA	phorbol myristate acetate
RGD	Arg-Gly-Asp
PM	plasma membrane
RE	recycling endosome
Tf	transferrin
TGN	trans-Golgi-network
V-ATPase	vacuolar ATPase
WT	wild type

1 INTRODUCTION

Our understanding of cell biology, and especially of endocytosis, has evolved substantially in recent decades. Curiosity regarding the mechanisms and roles of endocytosis increased rapidly in the late 1970s, and in the early 1980s, the transitional, acidic structures between the primary endocytic vesicles and the degradative lysosomes were named "endosomes." Clathrin-mediated endocytosis (CME) was long thought to be the only endocytosis route, and other pathways only became widely appreciated as late as the 1990s. Although physiological ligands (e.g., epidermal growth factor [EGF]) and their receptors have a central role in the research of endocytosis, viruses have also been widely used to study this phenomenon. As a result, researchers gather knowledge concurrently from basic cell biology and from virology. Endocytosis is more than just a simple process of transporting molecules across the plasma membrane. Generally speaking, it is indistinguishably linked with almost all aspects of cellular signaling. Nowadays, it is increasingly evident that in addition to signaling from cargo molecules, endosomes and their maturation processes also play a crucial role in regulating cellular signaling events. Understanding the endocytic pathways of viruses and cellular receptors is important, for instance, in the development of new antiviral treatments and vaccines.

The aim of this thesis was to increase the knowledge of two enteroviruses, echovirus 1 (EV1) and coxsackievirus A9 (CVA9), and more specifically, of their infectious entry pathways and the structures involved. We found remarkable similarities between these two enteroviruses. Based on the findings of this thesis, it seems likely that the enterovirus internalization pathway could be similar among numerous human enterovirus group B viruses. This finding implies that future antiviral drugs could be effective against several enteroviruses. The results of this thesis also showed that EV1 has specific effects on epidermal growth factor receptor (EGFR) trafficking and downregulation, causing increased growth factor signaling, which may have beneficiary effects on EV1 infection.

2 REVIEW OF THE LITERATURE

2.1 Enteroviruses

The Enterovirus genus belongs to the *Picornaviridae* family. There are 12 species of viruses in the Enterovirus genus: nine human enterovirus species (HEVs) (including polioviruses, coxsackieviruses, echoviruses, and other enteroviruses) and three human rhinovirus species. All HEVs have a positive-polarity, single-stranded RNA genome approximately 7.5-kb long. The genome is enclosed in a non-enveloped, icosahedral protein capsid (30 nm in diameter) consisting of 60 copies of each of the four different structural proteins (VP1–4). Ubiquitous HEVs are important human pathogens that cause illnesses ranging from the common cold to paralysis and other infections of the central nervous system, carditis, and severe disease syndromes in newborns. In addition, EV1, CVA9, and enteroviruses in general have been associated with type 1 diabetes (Hyöty *et al.* 1995, Roivainen *et al.* 1998, Graig *et al*. 2013). Transmission of HEVs occurs via direct contact with the virus, shed from the gastrointestinal or upper respiratory tract. HEVs are acid-stable; this feature distinguishes them from other picornaviruses, which are unstable in acidic conditions.

In a simplified model (Fig. 1), HEV infection begins when a virus attaches to its receptor at the cell surface. After endocytosis, the HEV uncoats and releases its genome into the cytoplasm, where it is translated by the host cell translation machinery. The resulting polyprotein is cleaved by virus-encoded proteases. The genome is replicated on cytoplasmic membranes by RNA-dependent RNA polymerase, creating a negative strand template that is then used for positive strand replication. The positive RNA genome is packaged into the newly formed capsids and released upon maturation, usually by cell lysis.

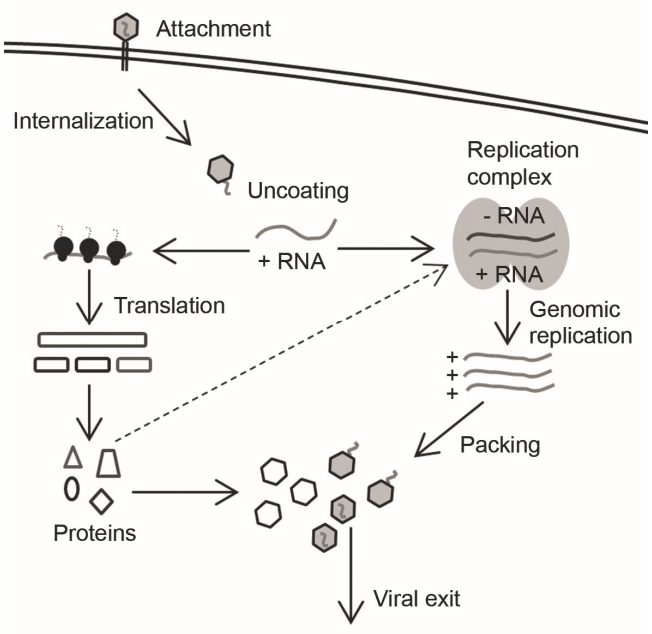

FIGURE 1 Human enterovirus (HEV) replication cycle in cell. HEVs bind to a cellular receptor, and after virus internalization, the genome is released into the cytoplasm, where viral replication takes place. First, the genomic RNA is translated to produce the viral polyprotein, which is processed to produce various proteins needed for virus replication. The RNA synthesis occurs in the replication complex. Replicated RNA is packed into newly synthesized viral particles that are later released from the cell.

2.1.1 Echovirus 1 and coxsackievirus A9 and cell membrane receptors

Both EV1 and CVA9 belong to the *Enterovirus B* species (Hyypiä *et al.* 1997) and use integrins as their receptors or co-receptors for cell entry (Bergelson *et al.* 1992, Roivainen *et al.* 1994, Williams *et al.* 2004, Heikkilä *et al.* 2009). Integrins are transmembrane receptors on the plasma membrane (PM), and they mediate cell attachment to the extracellular matrix (ECM) (Takada *et al.* 2007). In addition, integrins transduce signals from the ECM to the cell.

EV1 uses α2β1 integrin as its receptor; however, the viral binding site is different from the normal ligand (collagen and laminin) binding site (Bergelson *et al.* 1992, Bergelson *et al.* 1993, Takada *et al.* 2007). Collagen binds to integrins in open conformation, whereas EV1 seems to favor the closed conformation of integrin in its binding (Jokinen *et al.* 2010). Binding of EV1 causes integrin clustering on the PM and results in EV1–receptor complex internalization (Marjomäki *et al.* 2002, Upla *et al.* 2004). In addition, antibody labeling against β2 microglobulin (β2M) demonstrates its necessity in EV1 infection, although this molecule is not internalized in the cell with EV1 (Ward *et al.* 1998, Marjomäki *et al.* 2002).

In several cell lines, including the lung carcinoma A549 cells, CVA9 has been shown to bind to αVβ3 and αVβ6 integrins (Roivainen *et al.* 1994, Williams

et al. 2004, Heikkilä *et al.* 2009). Typically, αVβ3 integrin acts as a vitronectin, and αVβ6 acts as a fibronectin receptor (Takada *et al.* 2007). CVA9 has been shown to bind to integrin receptors via its Arg-Gly-Asp (RGD)-motif (Roivainen *et al.* 1994, Williams *et al.* 2004). In contrast to EV1, CVA9 does not associate with αV integrins during the internalization process (Heikkilä *et al.* 2009). It has been proposed that besides integrins, other receptor candidates (e.g., glucose-regulated protein 78A and β2M) might be involved in CVA9 entry (Triantafilou *et al.* 1999, Triantafilou *et al.* 2002). It has been reported that in A549 cells, after β2M was silenced with small interfering (si)RNA, CVA9 was arrested at the cell periphery for one hour p.i. (Heikkilä *et al.* 2010). However, after one hour, CVA9 endocytosis continued, leading to an unproductive infection.

2.2 Endocytosis

Endocytosis is a process by which the cell internalizes solutes, macromolecules, cell surface components, and various particles. During endocytosis, the PM invaginates and forms vesicles through membrane fission. Numerous parallel operating internalization routes transfer cargo into the cells (Mayor and Pagano 2007, Doherty and McMahon 2009). Absorption of large (<500 nm) particles typically occurs via triggered processes called phagocytosis or macropinocytosis, whereas smaller particles are often internalized by pinocytic routes, including the well-characterized CME and a set of clathrin-independent pathways.

Invagination (and scission) of the PM forms endosomes, which are responsible for regulating numerous tasks in the cells by sorting, processing, recycling, storing, activating, silencing, and degrading incoming cargo (Huotari and Helenius 2011). The internalized material is routed to various destinations within the cell; the efficient sorting of these molecules is essential for many cellular functions.

The canonical endocytic pathway has a few key elements (Fig. 2): the recycling machinery (the PM, the early endosomes [EEs], the recycling endosomes [REs], and a range of endocytic carrier vesicles [ECVs]), the degradation machinery (lysosomes), and the connecting pathway from the EEs to the degradative system (the multivesicular bodies [MVBs] and the late endosomes [LEs]). The trans-Golgi network (TGN) interacts with the PM, EEs, MVBs, LEs, and lysosomes. Cytosol also has a central role in endocytosis, as it provides proteins needed in sorting, signaling, fusion/fission, and endosome motility processes (Huotari and Helenius 2011).

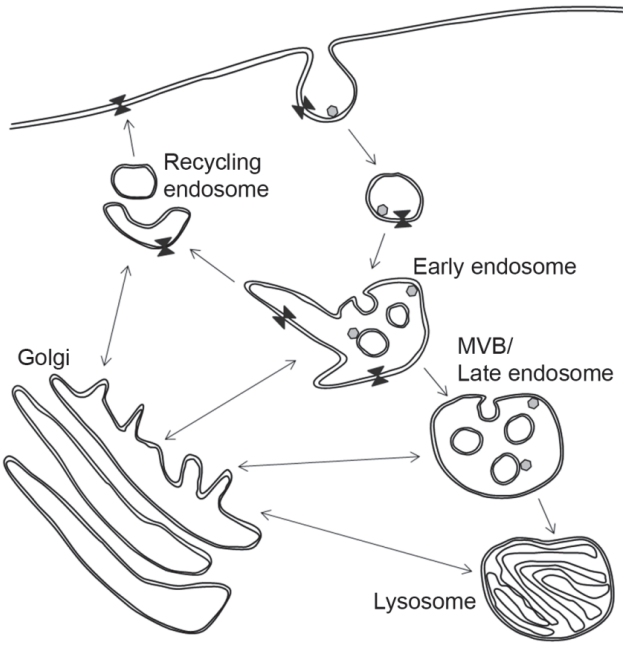

FIGURE 2 Compartments in the canonical endocytic pathway. Early endosomes function as an initial sorting structure, transferring molecules back to the plasma membrane through recycling endosomes, to the trans-Golgi-network by retrograde transport, or to the late endosomes/lysosomes. The late endosomes receive cargo from the endocytic, biosynthetic, and autophagy pathways and further deliver material to the lysosomes and to the Golgi complex. Multivesicular body, MVB.

As mentioned previously, endosomes have important roles in regulating cargo trafficking, storage, and degradation; they are also used as signaling compartments (Miaczynska *et al.* 2004, Platta and Stenmark 2011). Endosome maturation processes allow spatiotemporal regulation of protein trafficking. Endosome maturation is also used in the activation and silencing of signal transduction pathways. Intraluminal vesicle (ILV) formation and endosome acidification are probably two of the most important processes in the maturation of endosomes. ILVs are required for sorting membrane-associated proteins for degradation in lysosomes (Gruenberg 2001, Gruenberg and Stenmark 2004). For instance, signaling receptors are sorted out to ILVs and removed from contact with the cytoplasm, and therefore, are inactivated. On the other hand, acidic endosomes provide a suitable environment for ligand detachment from receptors and hydrolytic reactions; they are also essential for cargo sorting and inactivating internalized pathogens. The gradually decreasing pH in the endocytic pathway provides cargo molecules with a "sense" of their location in the pathway. For example, some viruses have to sense their location accurately in order to be activated in the right endocytic structure (Mercer *et al.* 2010).

2.2.1 Early and recycling endosomes

The EEs, which are the main sorting station in the endocytic pathway, are usually the first structures to receive incoming molecules and solutes. Although EE morphology, localization, composition, and function can be heterogeneous, most EEs are relatively small and located near the PM (Lakadamyali *et al.* 2006). Studies have suggested that there are at least two distinct types of EEs, which differ in their maturation kinetics—dynamic and static (Lakadamyali *et al.* 2006, Leonard *et al*. 2008). The limiting EE membrane contains lipid–protein subdomains; the structure of a single EE is rather complex, including tubular and vacuolar parts (Huotari and Helenius 2011). According to current knowledge, the tubular regions usually recycle back to the PM, whereas the luminal parts of the EE mature onward and develop into ECVs or MVBs, which transport cargo to the LEs (Scott *et al.* 2014).

The EEs receive cargo through several pathways, including the CME, clathrin-independent, and caveolar- and ADP-ribosylation factor 6 (Arf6)-dependent pathways (Mayor and Pagano 2007). A few minutes after arrival in the EEs, the cargo molecules either recycle back to the PM or accumulate in the sorting EEs to be delivered to the LEs and the lysosomes (Maxfield and McGraw 2004). Transferrin (Tf) and its receptor have been widely used as markers of the recycling pathways. After internalization via CME, Tf can be found in EEs, which proceed to traffic Tf to the recycling pathways (Mayle *et al.* 2012). There are two different recycling routes in cells: a fast route traffics Tf directly back to the PM from EEs, whereas a slower route transports Tf to the perinuclear REs first (Ghost *et al*. 1994, Lakadamyali *et al.* 2006).

At the mildly acidic pH (pH 6.8–5.9) of EEs (Maxfield and Yamashiro 1987), many membrane-bound receptors designated to be recycled are uncoupled from their ligands. This is the case, for example, with low-density lipoprotein (LDL)-receptors (Goldstein and Brown 2009). After the ligand–receptor separation, ligands are transported toward the lysosomes, while receptor molecules are recycled back to the PM. On the other hand, EGF and EGFR are a classical example of a ligand–receptor complex that is transported to the ILVs of a maturing LE, and later, to the lysosomes for inactivation and degradation (Wiley *et al.* 1991).

Because endocytosis internalizes massive amounts of membranes into the cells, it is crucial that membrane lipids and proteins are recycled back to the PM in an accurate and efficient manner. Although the EEs and the REs differ in acidification properties and lipid/protein contents (including Rab GTPases) (Zerial and McBride 2001, Hsu and Prekeris 2010), it is difficult to distinguish between these two compartments at the molecular and morphological levels (Tooze and Hollinshead 1991, Stoorvogel *et al.* 1996).

The interactions between cytosolic proteins and the cytosolic surface of the EE membrane are important in many EE-related processes. Various proteins and lipids localize in the tubular regions of EEs (Bonifacino and Rojas 2006), where they contribute to molecular sorting, ECV maturation, and targeting to

other organelles. The membrane subdomains can be enriched, for example, with Rab5, Rab4, Rab11, and early endosome antigen 1 (EEA1) (Sonnichsen *et al.* 2000). The Rab family of small GTPases is frequently associated with membranes of different endocytic structures (Zerial and McBride 2001). Rab5 is a key component of EEs, and it localizes on the EE-limiting membrane from the beginning to the later stages of endosome maturation, where it is the main regulator of the EE conversion to LE. Another Rab protein found in EEs is Rab4. This protein is in charge of the direct and rapid recycling pathway from EEs to the PM, while Rab11 controls another, slower, recycling pathway (via REs) to the PM (Zerial and McBride 2001). The EE compartments exhibit a high capacity to undergo homo- and heterotypic fusion (Foret *et al.* 2012). One of the key players in this fusion process is the Rab5 effector EEA1, a hydrophilic peripheral membrane protein associated with the tubulovesicular parts of EEs (Raiborg *et al.* 2001). In addition to the recycling pathway and the EE to LE maturation processes, the EEs also exchange vesicles with the TGN.

The formation of the ILVs begins already in EEs, when the components of the endosomal sorting complex required for transport (ESCRT) on the limiting membrane of EE (Fig. 3) begin to sort the ubiquitinated membrane proteins into ILVs (Gruenberg and Stenmark 2004).

2.2.2 Endosomal carrier vesicles and multivesicular bodies

While molecules that are recycled back to the PM or destined for the TGN are collected in EE tubules, other proteins and solutes accumulate in the vacuolar parts of the EEs for transport to the lysosomes (Scott *et al.* 2014). During this process, the limiting membrane of an endosome invaginates and forms ILVs. Later, these multivesicular endosomes detach from the EE and continue the maturation process as free ECVs/MVBs (Gruenberg and Stenmark 2004).

In contrast to the EEs and the LEs, the ECVs/MVBs do not display homotypic fusion or heterogeneous morphologies (Gruenberg 2001). At the limiting membrane of an ECV/MVB, a specific phosphoinositide 3-kinase (PI3K), VPS34, generates phosphatidylinositol 3-phosphate (PI3P) from phosphatidylinositol (PI), which in turn initiates the sorting of ubiquitinated receptors into ILVs (Shin *et al.* 2005). VPS34 itself is an effector of the EE GTPase Rab5 (Shin *et al.* 2005). The PI3P serves as a recognition marker for PI3P-binding proteins (e.g., hepatocyte growth factor-regulated tyrosine kinase substrate [Hrs]) already on EEs (Gruenberg and Stenmark 2004). Hrs is a subunit of the ESCRT-0 complex, and when recruited onto the endosome-limiting membrane, it binds to ubiquitinated receptor molecules (Fig. 3) (Henne *et al.* 2011). After this process, with the help of a sequential action of the ESCRT-I, -II, and -III complexes, the receptors are collected into forming ILVs (Fig. 3). ESCRT-0, -I, and –II are involved in cargo sorting and contain ubiquitin-binding domains (Henne *et al.* 2011). In addition, ESCRT-II recruits and activates ESCRT-III, which in turn plays a role in the formation and scission of the ILV. In addition to the four ESCRT complexes (ESCRT-0 to -III), associated proteins help in the ILV formation process. One of those proteins is AAA-ATPase, VPS4, which is

necessary for the release of ESCRT-III from the endosome-limiting membrane, thus promoting ILV formation (Henne *et al.* 2011).

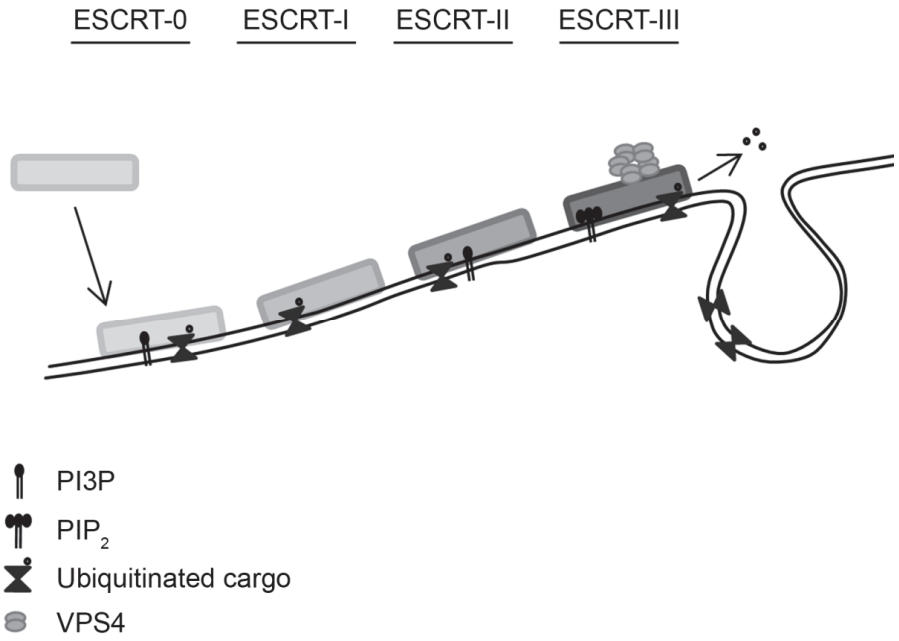

FIGURE 3 The endosomal sorting complexes required for transportation (ESCRT) machinery. Each member of the ESCRT complex is composed of several interacting proteins. ESCRT-0 recruits ubiquitinated cargo to the endosome-limiting membrane. ESCRT-III deubiquitinates and sequesters the cargo to a budding intraluminal vesicle. Phosphatidylinositol-3-phosphate (PI3P), phosphatidylinositol 4,5-bisphosphate (PIP_2). Modified from Williams *et al.* (2007).

If the ESCRT machinery is disturbed (e.g., by component depletion), endosomes typically display an abnormal morphology or fewer ILVs (Doyotte *et al.* 2005, Razi and Futter 2006). For instance, depletion of components of ESCRT-III complex VPS24 reduces the size of LEs (Bache *et al.* 2006). The limiting membrane of endosome VPS24 binds to phosphatidylinositol 4,5-bisphosphate (PIP_2). Furthermore, inhibition of ESCRT-III or VPS4 activity affects ILV formation (Fujita *et al.* 2003, Sachse *et al.* 2004). Before the vesicle closes, the ubiquitin tag is removed from the cargo (Fig. 3) by the action of deubiquitinating enzymes (Clague *et al.* 2012). After forming, the ECVs/MVBs acidify rapidly (pH = 5.5) and continue their microtubule-dependent movement toward the LEs, finally fusing with them (Huotari and Helenius 2011, Bissig and Gruenberg 2013).

The EE-to-MVB-to-LE conversion is driven by the switch from Rab5 to Rab7 (Zerial and McBride 2001). Overexpression of a constitutively active mutant of Rab5 (Q79L) stops the process, but it does not inhibit ILV formation or molecule sorting (Rink *et al.* 2005, Wegner *et al.* 2010). In addition to the

Rab5–Rab7 switch, PI conversion to phosphoinositides plays a role in endosome maturation. Parts of the ESCRT machinery are recruited by both PI3P and PIP_2, which enables ILV formation and cargo sorting (Katzmann *et al.* 2003, Whitley *et al.* 2003).

2.2.3 Late endosomes and lysosomes

Unlike ECVs/MVBs, LE structure is highly pleomorphic and includes multilamellar or mixed multivesicular/multilamellar regions (Huotari and Helenius 2011, Bissig and Gruenberg 2013). During the maturation of LEs, their luminal pH can drop from pH 6 to pH 4.9 (Maxfield and Yamashiro 1987). The PI3P on the limiting membrane of LEs is converted to PIP_2, and at the same time, the LEs lose their capability to fuse with the EEs and to recycle material back to the PM (Huotari and Helenius 2011). Instead, they acquire the necessary tethering complexes to fuse with each other, with lysosomes, and with autophagosomes (Lamb *et al.* 2013). In addition, the lysosomal hydrolases and membrane proteins are transported to LEs from the TGN (Huotari and Helenius 2011), and a new set of microtubule-dependent motors is associated with LEs (Loubery *et al.* 2008). The motor proteins enable the LEs to move deeper into the cell, where they fuse with each other, and eventually, with hybrid organelles (LE/lysosome) and lysosomes (Luzio *et al.* 2007). The fusion with lysosomes is essentially a dead-end pathway for most proteins in LEs. Lysosomes are spherical, electron-dense structures with a heterogeneous composition of vacuoles (Luzio *et al.* 2007). Classical lysosomes have a density that is highly buoyant, and they can be separated from other endosomes by subcellular fractionation.

LE lumens contain acid hydrolases, and highly glycosylated lysosomal membrane proteins, such as Lamp1, protect the limiting membrane of the LE (van Meel and Klumperman 2008). ILV membranes have no protective glycosylated protein coat, but they do contain phospholipid bis(monoacylglycero)phosphate/lysobisphoshatidic acid (BMP/LBPA), which is thought to promote lipid hydrolysis (Huotari and Helenius 2011, Hullin-Matsuda *et al.* 2014). In addition, the ILV membrane contains more cholesterol, sphingolipids, and PI3P than the limiting membrane of LEs. LEs have a central role in cholesterol transport (LDL-derived cholesterol), and they sense the nutrient status of the cell (Settembre *et al.* 2013). Furthermore, mitogen-activated protein kinase (MAPK) signaling on LEs has been found to regulate LE dynamics and cargo degradation (Taub *et al.* 2007).

2.2.4 Endosome acidification

Acidification and its regulation are important parts of endosome maturation in the canonical endosomal pathway. pH values range between 6.8 and 6.1 in EEs, between 6.0 and 4.8 in LEs, and they can drop to around 4.5 in lysosomes (Maxfield and Yamashiro 1987).

Several inhibitors (e.g., NH_4Cl, nigericin, bafilomycins) are used regularly to raise the pH of endosomes (Huotari and Helenius 2011). Bafilomycins inhibit the function of vacuolar ATPase (V-ATPase) and rapidly elevate the pH in acidic cellular structures (Bowman *et al.* 1988). V-ATPases are complex proton pumps that bind and hydrolyze the ATP, pumping protons across the endosomal-limiting membrane at the same time (Marshansky and Futai 2008). V-ATPases are found on the limiting membranes of almost all intracellular organelles.

Transfer of the cargo from the EEs to the LEs (or from the LEs to the lysosomes in some cell lines) is blocked by bafilomycin A1, indicating a defect in endosome maturation. However, bafilomycin A1 seems to have no effect on the recycling pathway (Clague *et al.* 1994, Bayer *et al.* 1998, Baravalle *et al.* 2005).

2.2.5 Endosome motility

Endosome movements are tightly linked to their maturation and function. EEs are formed in the cell periphery, where they perform tiny back-and-forth movements (Huotari and Helenius 2011). As they mature, their net movement along the microtubules is toward the lysosome-rich, perinuclear region of the cell. Two motor protein families, kinesin and dynein, mediate this movement (Loubery *et al.* 2008).

The scattering of LEs and lysosomes all over the cytoplasm, caused by disruption of the microtubules, postpones the maturation of endosomes, as the Rab5/Rab7 switch is not functioning properly (Bayer *et al.* 1998, Vonderheit and Helenius 2005). Interestingly, the depolymerization of microtubules by nocodazole treatment blocks the trafficking of cargo molecules to the LEs and lysosomes, although it does not inhibit endosome acidification (Bayer *et al.* 1998, Mesaki *et al.* 2011).

2.2.6 EV1 and CVA9 endocytosis, uncoating, and replication

Although the structure of enteroviruses is quite simple, the interactions with the host cell proteins can be complex. In the virus life cycle (Fig. 1), the fundamental point is the delivery of a viral genome into the cell cytoplasm for replication. Most viruses take advantage of the host cell's endocytic mechanisms for this purpose (Mercer *et al.* 2010). Viruses have usually evolved to use one or more receptors and entry mechanisms. Endosomes offer an environment that is different from the cytosol, and the endosome maturation process may serve as a trigger that leads to changes in the virus particle and starts the virus uncoating process and/or delivery of the genome into the cytoplasm for replication (Mercer *et al.* 2010).

According to Karjalainen et al. (2008), EV1 is internalized from lipid rafts into tubulovesicular structures that accumulate fluid-phase markers (Fig. 4). These endosomes further mature into MVBs (15 min–2 h p.i.). In an early electron microscopy (EM) study, CVA9 viral particles were seen in vesicles that later matured into large vacuoles (Hecker *et al.* 1974).

In a sucrose gradient ultracentrifugation analysis, native enteroviruses sedimented at 160S, particles that lost the VP4 polypeptides sedimented at 135S, and particles lacking the RNA genome sedimented at 80S (Hogle 2002). In the case of EV1, prior to binding to the cells, the viruses sedimented as the 160S form (Marjomäki *et al.* 2002). After binding to SAOS cells that were stably transfected with an expression construct encoding α2 integrin (SAOS-α2 cells), EV1 sedimented as 160S and 135S particles (Marjomäki *et al.* 2002, Pietiäinen *et al.* 2004), and 80S particles start to form at 30 min p.i. In addition, a neutral red (NR) assay demonstrated that viral uncoating starts at 30 min p.i. and continues to 4 h p.i. (Siljamäki *et al.* 2013). Thus, the data suggest that EV1 uncoating is a slow event that is initiated after virus internalization.

It has been observed that due to the release of viral RNA from the virus capsids, colocalization between the EV1 capsid proteins and genomic RNA decreases after 2 h p.i., (Pietiäinen *et al.* 2004). At 4 h p.i., an increase in the amount of viral RNA staining was observed in the cytoplasm. In conclusion, EV1 uncoating takes place well before the genome is released from the EV1-positive endosome to the cytoplasm. Around the time of the genome release, the replication of EV1 starts in the cytoplasm (Upla *et al.* 2008).

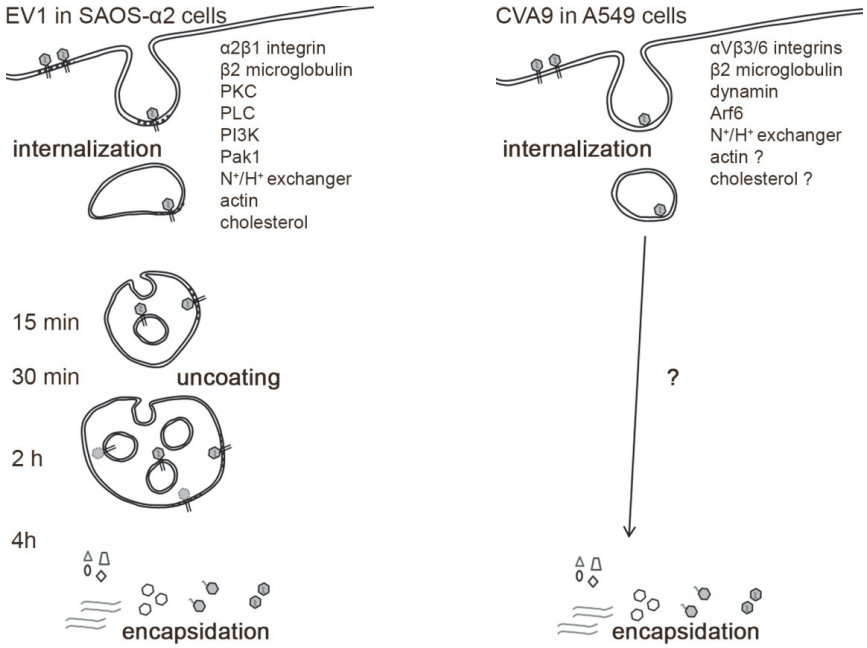

FIGURE 4 Endocytosis of echovirus 1 (EV1) and coxsackievirus A9 (CVA9). EV1 infection is dependent on α2β1 integrin, β2 microglobulin, phosphokinase C (PKC), phospholipase C (PLC), phosphoinositide 3-kinase (PI3K), Pak1, N^+/H^+ exchanger, actin, and cholesterol. EV1 is first internalized into tubulovesicular structures that later (15 min p.i. and onward) mature into multivesicular bodies (MVBs). EV1 uncoating starts 30 min p.i., and at 4 h p.i., new viral proteins start to accumulate in the cytoplasm. CVA9 infection is dependent on αVβ3/6 integrins, β2 microglobulin, dynamin, Arf6, N^+/H^+ exchanger, and possibly, actin and cholesterol.

2.2.6.1 Factors involved in EV1 and CVA9 endocytosis

Although many viruses infect cells via CME (Mercer *et al.* 2010), EV1 and CVA9 do not seem to do so. The transfection of dominant negative (DN) forms of Eps15 (which prevents the formation of clathrin-coated vesicles) or AP180 (which interferes the clathrin route) have been shown to inhibit the internalization of Tf, but not EV1 or CVA9 infections (Benmerah *et al.* 1999, Ford *et al.* 2001, Pietiäinen *et al.* 2004, Upla *et al.* 2004, Heikkilä *et al.* 2010). In addition, CVA9 infection was not inhibited by chlorpromazine (chemical inhibitor of CME) or by siRNAs against genes involved in CME (EEA1, Rab5, clathrin heavy chain) (Heikkilä *et al.* 2010). On the other hand, Krieger et al. (2013) suggested that CME might play a role in EV1 infection in polarized intestinal epithelial cells (Caco2), even though it is not the major route of endocytosis.

The GTPase dynamin was originally thought to participate only in clathrin-coated pit closure, but it was shown later to be important in other endocytic pathways as well (Doherty and McMahon 2009). Expression of the DN mutant of dynamin II, dyn2(K44A), inhibited EV1 infection in green monkey kidney cells (CV-1), but not in SAOS-α2 cells (Pietiäinen *et al.* 2004, Karjalainen *et al.* 2008). In addition, CVA9 infection efficiency was reduced in A549 cells overexpressing the DN form of dynamin 2 (Heikkilä *et al.* 2010). Moreover, dynasore (dynamin inhibitor) inhibited EV1 infection in Caco2 cells and CVA9 infection in A549 cells, arresting the viral particles at the PM (Heikkilä *et al.* 2010, Krieger *et al.* 2013).

It has been suggested that in SAOS-α2 cells, EV1 infection is C-terminal binding protein 1/brefeldin A–ADP-ribosylated substrate (CtBP1/BARS)-dependent (Liberali *et al.* 2008). CtBP1/BARS is a p21-activated kinase 1 (Pak1) substrate required for the closure of macropinosomes. CtBP1/BARS also seems to have a role in the EV1 infection of Caco2 cells (Krieger *et al.* 2013). Based on transfection and colocalization studies, Heikkilä et al. (2010) suggested that Arf6 participates in CVA9 internalization, at least in the early phase of viral entry.

Classically, both non-specific and specific chemical inhibitors of endocytosis have been used to classify endocytosis of the PM proteins. Tables 1 and 2 summarize inhibitors that have been used to study EV1 and CVA9 infections. Factors needed in EV1 and CVA9 infections are shown in Figure 4.

The protein kinase C (PKC) family consists of a number of serine–threonine kinases that controls the functions of other proteins through the phosphorylation process. PKCs are activated by phosphatidylserine, diacylglycerol, and tumor-promoting phorbol esters such as phorbol myristate acetate (PMA) (Mellor and Parker 1998). EV1 infection has been reported to increase the phosphorylation status of PKCα in SAOS-α2 cells (Upla *et al.* 2004). Although short PMA treatments have been suggested to stimulate the PKCs, chronic treatment induces the degradation of PKCs (Srivastava *et al.* 2002), which inhibits the EV1 infection (Upla *et al.* 2004). Upla et al. (2004) delineated the crucial role of PKCα to the first minutes of internalization of EV1 in SAOS-α2 cells. Furthermore, PKC inhibition with rottlerin caused a block in EV1 infection when the drug was added early in Caco2 cells (Krieger *et al.* 2013).

Phospholipase Cs (PLCs) are intracellular enzymes that play an important role in signal transduction processes. They participate in PIP_2 metabolism, generating inositol triphosphate and diacylglycerol. PLCs perform their catalytic function at the PM, where their substrate PIP_2 is present. It has been reported that PLC inhibitor U73122 blocked EV1 infection only during the early entry of EV1, and it inhibited the internalization process of the virus (Karjalainen *et al.* 2008).

PI3Ks are intracellular signal transducer enzymes that phosphorylate the 3 position hydroxyl group of the inositol ring of PIs. Although PI3K inhibitor LY294002 was shown to inhibit EV1 infection, it did not block the viral internalization, and the virus was able to enter the endosomes (Karjalainen *et al.* 2008). In addition, silencing PI3K with siRNA or using an inhibitor (Wortmannin) did not decrease CVA9 infection in A549 cells (Heikkilä *et al.* 2010).

Paks, which are associated with fluid-phase endocytosis and macropinocytosis (Dharmawardhane *et al.* 2000, Liberali *et al.* 2008), are targets of Rho GTPases Rac and Cdc42 (Manser *et al.* 1994). Paks and Rho GTPases are also known to regulate actin dynamics (Ridley 2006). It has been reported that the DN Pak1 construct (Pak AID) totally blocked EV1 infection, whereas the infection efficiency was not affected when cells were transfected with a highly active mutant (Pak1 T423E) or with wild-type (WT) Pak1 (Karjalainen *et al.* 2008). Rac1 transfections (DN and WT forms) and siRNA silencing revealed that malfunctions in Rac1 inhibited the EV1 infection, suggesting that Rac1 may be the upstream regulator of Pak1 (Karjalainen *et al.* 2008). In Caco2 cells, Pak1 inhibitor IPA-3 blocked EV1 infection when it was added 2 h p.i., suggesting that it acts on post-entry events in the infection (Krieger *et al.* 2013). In CAV9 infection, silencing Pak1 or Rac1 with siRNAs had no effect on viral proliferation (Heikkilä *et al.* 2010).

The Na^+/H^+ exchangers are membrane proteins that regulate ion flux across membranes. The PM isoforms of this protein extrude one intracellular proton in exchange for one extracellular sodium. Ethylisopropylamiloride (EIPA) (N+/H+ exchanger inhibitor) inhibited EV1 infection even when added 2 h p.i. (Karjalainen *et al.* 2008, Krieger *et al.* 2013). It also caused an accumulation of EV1 close to the PM and arrested further viral transport. Correspondingly, EIPA also inhibited CVA9 infection in A549 cells and arrested CVA9 particles in vesicle-like structures in the cell periphery (Heikkilä *et al.* 2010).

The actin cytoskeleton plays an essential role in endocytosis. Actin assembly creates protrusions that help the extracellular materials to internalize; actin supports membrane invagination, elongation of the invagination, scission of the new vesicle, and movements of the vesicle away from the membrane (Mooren *et al.* 2012). In SAOS-α2 and Caco2 cells, actin-depolymerizing drugs, such as cytochalasin D, have been shown to inhibit EV1 infection (Karjalainen *et al.* 2008, Krieger *et al.* 2013) and cause EV1 to accumulate on the periphery of SAOS-α2 cells (Karjalainen *et al.* 2008). The stabilizing drug jasplakinolide also inhibited EV1 infection efficiently, and it totally blocked EV1 transportation

from the PM (Karjalainen *et al.* 2008, Krieger *et al.* 2013). Interestingly, in CV-1 cells, an EV1 infection assay with three actin drugs—latrunculin A (an actin monomer–sequestering drug), jasplakinolide, and cytochalasin D—showed no effect on EV1 infection (Pietiäinen *et al.* 2004). Although the actin-stabilizing drug jasplakinolide significantly reduced CVA9 infection, the actin-disrupting agents, cytochalasin D and latrunculin A, did not inhibit CVA9 proliferation (Heikkilä *et al.* 2010).

As endosomes mature, they move toward the perinuclear region along microtubules (Loubery *et al.* 2008). Nocodazole is a microtubule-disrupting agent, but interestingly, it was not shown to have any inhibitory effects on EV1 or CVA9 infections in CV-1 or A549 cells, respectively (Pietiäinen *et al.* 2004, Heikkilä *et al.* 2010).

Membrane cholesterol is important for clathrin- and caveolin-independent virus entry mechanisms (Mercer *et al.* 2010). This seems to be the case for EV1 as well, as nearly all compounds affecting cholesterol synthesis, distribution, or sequestering inhibited viral infection in all of the cell lines studied (Table 1). Siljamäki et al. (2013) concluded that cholesterol contained membranes needed for EV1 internalization and efficient infection, and that the virus is dependent on those cholesterol domains until replication occurs. Interestingly, methyl β-cyclodextrin or a mixture of progesterone and nystatin did not affect the efficiency of CVA9 infection (Heikkilä *et al.* 2010). On the other hand, it has been proposed that CVA9 internalization is lipid microdomain dependent (Triantafilou *et al.* 2002, Triantafilou and Triantafilou 2003).

Calpains are calcium-dependent cysteine proteases that degrade cytoskeletal and cytoplasmic proteins. Calpain 1 is mainly found in cytosol, whereas calpain 2 is associated with detergent-insoluble membrane domains (Upla *et al.* 2004). EV1 internalization has been shown to cause calpain relocalization, and both calpain 1 and calpain 2 were translocated to EV1-positive vesicles during the early phases of viral entry (Upla *et al.* 2008). Furthermore, calpain activity increased during EV1 infection. Because the calpain inhibitor, calpeptin, inhibited EV1 infection even when added at 2.5 h p.i., and because it prevented infection after a microinjection of EV1 genomic RNA into the host cells, Upla et al. (2008) concluded that calpain activation is needed after the release of the EV1 genome into the cytoplasm.

TABLE 1 Pharmacological inhibitors used in echovirus 1 (EV1) infection studies. The plus sign (+) stands for dependence of the target molecule and the minus sign (-) stands for independence of the target molecule in the EV1 infection. Protein kinase C (PKC), phosphoinositide-3-kinase (PI3K), bisindolylmaleimide (BIM), safingol (SAF), phorbol-12-myristate-13-acetate (PMA), ethyl-isopropyl amiloride (EIPA), cytochalasin D (CytD), jasplakinolide (Jas), nocodazole (Noc), methyl-β-cyclodextrin (MβCD), progesterone (Prog), nystatin (Nys).

Target	Dependence	Inhibitor	Cell line	Article
PKC	+	BIM/SAF	SAOS	Upla et al. 2004
PKC	+	BIM/SAF	CV-1	Pietiäinen et al. 2004
PKC	+	PMA	SAOS	Upla et al. 2004
PKC	+	Rottlerin	Caco2	Krieger et al. 2013
PLC	+	U-73122	SAOS	Karjalainen et al. 2008
PI3K	+	LY290042	SAOS	Karjalainen et al. 2008
Pak1	+	IPA-3	Caco2	Krieger et al. 2013
Na^+/H^+ exchanger	+	EIPA	SAOS	Karjalainen et al. 2008
Na^+/H^+ exchanger	+	EIPA	Caco2	Krieger et al. 2013
Actin	+	Cyt D	SAOS	Karjalainen et al. 2008
Actin	-	Cyt D	CV-1	Pietiäinen et al. 2004
Actin	+	Cyt D	Caco2	Krieger et al. 2013
Actin	-	LatA	CV-1	Pietiäinen et al. 2004
Actin	+	Jas	SAOS	Karjalainen et al. 2008
Actin	-	Jas	CV-1	Pietiäinen et al. 2004
Actin	+	Jas	Caco2	Krieger et al. 2013
Microtubules	-	Noc	CV-1	Pietiäinen et al. 2004
Cholesterol	+	MβCD	SAOS	Marjomäki et al. 2002
Cholesterol	+	MβCD	CV-1	Pietiäinen et al. 2004
Cholesterol	+	MβCD	Caco2	Krieger et al. 2013
Cholesterol	+	Filipin	SAOS	Siljamäki et al. 2013
Cholesterol	-	Filipin	Caco2	Krieger et al. 2013
Cholesterol	+	Nystatin	SAOS	Siljamäki et al. 2013
Cholesterol	+	Ketoconazole	SAOS	Siljamäki et al. 2013
Cholesterol	+	Prog+Nys	CV-1	Pietiäinen et al. 2004
Cholesterol	-	U18666A	SAOS	Siljamäki et al. 2013
Sphingolipid	+	Fumonisin B1	SAOS	Siljamäki et al. 2013
Calpain	+	Calpeptin	SAOS	Upla et al. 2008
Calpain	+	Inhibitor1/2	SAOS	Upla et al. 2008

TABLE 2 Pharmacological inhibitors used in coxsackievirus A9 (CVA9) infection studies. The plus sign (+) stands for dependence of the target molecule and the minus sign (-) stands for independence of the target molecule in the CVA9 infection. Phosphoinositide-3-kinase (PI3K), ethyl-isopropyl amiloride (EIPA), cytochalasin D (CytD), latrunculin A (LatA), jasplakinolide (Jas), nocodazole (Noc), methyl-β-cyclodextrin (MβCD), progesterone (Prog), nystatin (Nys).

Target	Dependence	Inhibitor	Cell line	Article
PI3K	-	Wortmannin	A549	Heikkilä et al. 2010
N+/H+ exchanger	+	EIPA	A549	Heikkilä et al. 2010
Actin	-	Cyt D	A549	Heikkilä et al. 2010
Actin	-	LatA	A549	Heikkilä et al. 2010
Actin	+	Jas	A549	Heikkilä et al. 2010
Microtubule	-	Noc	A549	Heikkilä et al. 2010
Cholesterol	-	MβCD	A549	Heikkilä et al. 2010
Cholesterol	-	Prog+Nys	A549	Heikkilä et al. 2010

As discussed previously, endocytic structures accumulate specific molecules (e.g., Rabs, Lamp1) on their limiting (or intraluminal) membranes, which have been used to identify different endocytic structures within cells. Table 3 lists the canonical endosomal markers that have been used to study EV1 location in cells.

In SAOS-α2 and CV-1 cells, EV1 does not colocalize with the EE, RE, LE, lysosomal, ER, or TGN markers (Marjomäki *et al.* 2002, Pietiäinen *et al.* 2004, Karjalainen *et al.* 2008, Rintanen *et al.* 2012). Interestingly, in Caco2 cells, EV1 colocalized with EEA1 and Lamp2 (Krieger *et al.* 2013). Krieger et al. (2013) also found that EV1 infection was inhibited by siRNA-targeting Rab5 and by the expression of dominant negative Rab5. In contrast, Rab7 siRNA and dominant negative Rab7 had only a slight inhibitory effect or no effect at all on EV1 infection. In conclusion, Rab5-positive early endosome structures might play a role in EV1 infection in Caco2 cells. In contrast, silencing Rab5 with siRNA had no effect on CVA9 proliferation in A549 cells (Heikkilä *et al.* 2010).

TABLE 3 The canonical endosomal markers used to study echovirus 1 (EV1) location in cells. Rough/smooth endoplasmic reticulum (r/sER), early endosome antigen 1 (EEA1), cation-independent mannose 6-phosphate receptor (CI-MPR), dil-labeled low-density lipoprotein (Dil-LDL), protein disulfide-isomerase (PDI).

Structure	Colocalization	Protein	Cell line	Article
Early endosome	-	EEA1	SAOS	Marjomäki et al. 2002
Early endosome	-	EEA1	SAOS	Karjalainen et al. 2008
Early endosome	-	EEA1	SAOS	Rintanen et al. 2011
Early endosome	+	EEA1	Caco2	Krieger et al. 2013
Recycling endosome	-	Transferrin	SAOS	Marjomäki et al. 2002
Late endosome	-	CI-MPR	SAOS	Marjomäki et al. 2002
Late endosome	-	CI-MPR	SAOS	Karjalainen et al. 2008
Late endosome	-	CD63	SAOS	Karjalainen et al. 2008
Late endosome	-	CD63	SAOS	Rintanen et al. 2011
Late endosome	-	Lamp1	SAOS	Rintanen et al. 2011
Late endosome	+	Lamp2	Caco2	Krieger et al. 2013
Late endosome	-	Rab7	SAOS	Rintanen et al. 2011
Lysosome	-	LysoTracker	CV-1	Pietiäinen et al. 2004
Lysosome	-	Dil-LDL	SAOS	Rintanen et al. 2011
rER	-	PDI	SAOS	Marjomäki et al. 2002
rER	-	PDI	CV-1	Pietiäinen et al. 2004
sER	-	Syntaxin 17	CV-1	Pietiäinen et al. 2004
Trans-Golgi	-	TNG-46	SAOS	Marjomäki et al. 2002

One of the most important characteristics of the EE-to-LE-to-lysosome maturation process is endosome acidification. Bafilomycin A1, a drug that prevents endosomal acidification by inhibiting the vacuolar proton pump, has been reported to have an inhibitory effect on EV1 infection in SAOS-α2 cells if administered during the early phase of infection (Rintanen *et al.* 2012). On the other hand, it had only a slight effect on EV1 infection in Caco2 cells (Krieger *et al.* 2013), and CVA9 infection was not inhibited by NH_4Cl (inhibitor of endosomal acidification) (Heikkilä *et al.* 2010).

2.3 Epidermal growth factor receptor

EGFR, a transmembrane cell–surface receptor, plays an important role in essential cellular functions, such as proliferation and migration. Its activity also has an important role in the pathogenesis of human cancers. EGFR belongs to the ErbB family of receptor tyrosine kinases. The ErbB protein family consists of four members (Erb1–4), which bind multiple ligands: EGF, transforming growth factor-α, heparin-binding EGF, betacellulin, amphiregulin, epiregulin,

epigen, and neuregulins 1–4 (Olayioye *et al.* 2000). In this thesis, we focus on Erb-1, the "typical" EGFR.

2.3.1 EGFR endocytosis

Although EGFR can be activated by ligand-independent mechanisms as well as by multiple ligands, in this thesis we focus on the receptor activation caused by its primary ligand, EGF. Ligand binding produces a conformational change in the extracellular domain of the receptor, which activates EGFR and leads to receptor dimerization and internalization (Ogiso *et al.* 2002). Under normal cell culture conditions, the majority of EGFRs are located on the PM, where the receptors are constitutively internalized at the rate of basal membrane recycling (Wiley *et al.* 1991).

While inactive EGFR is mainly recycled back to the cell surface (Wiley 2003), the activation of EGFR leads to accelerated internalization and degradation of the receptor (Wiley *et al.* 1991). This downregulation and degradation is the major negative feedback regulatory mechanism that controls the intensity and duration of receptor signaling. On the other hand, EGF–receptor complexes remain active in endosomes and continue to signal even after internalization (Wiley 2003, Platta and Stenmark 2011).

When EGFR is activated with a low concentration of EGF (1–2 ng/ml or lower), the receptor is internalized at a high rate (Wiley 1988). The mechanism of endocytosis is clathrin-dependent (Sorkin and Goh 2008), but soon after internalization, clathrin-coated vesicles release their coats and fuse with EEs (Hopkins *et al.* 1985) (Fig. 5). This process occurs minutes after endocytosis. Instead of dissociating from its ligand at mildly acidic EE conditions, EGFR remains to be dimerized, phosphorylated, and ubiquitinated (Sorkin and Carpenter 1991, Sigismund *et al.* 2013).

When cells are stimulated with high concentrations of EGF, clathrin-independent internalization takes over (Sorkin and Goh 2008), and most of the EGF–receptor complexes are internalized with slower kinetics (Lund *et al.* 1990). Liberali et al. (2008) showed that in epidermoid carcinoma cells (A431), stimulation with high concentrations of EGF leads to CtBP1/BARS-dependent macropinocytic internalization of EGFR.

From EEs, there are two major destinations for EGFR—recycling or degradation (Fig. 5)—and the equilibrium between them balances receptor signaling. Recycling of the EGF–receptor complex occurs through two kinetically and mechanistically distinct pathways (Grant and Donaldson 2009). The rapid pathway involves early endosomes and Rab4- and Rab35-regulated structures, whereas the second recycling pathway exhibits slower kinetics and probably originates from a pool of EGF–receptor complexes located in the limiting membrane of MVBs. These structures are Rab11-positive. Increased recycling is predicted to prolong signaling of the EGFR (Platta and Stenmark 2011).

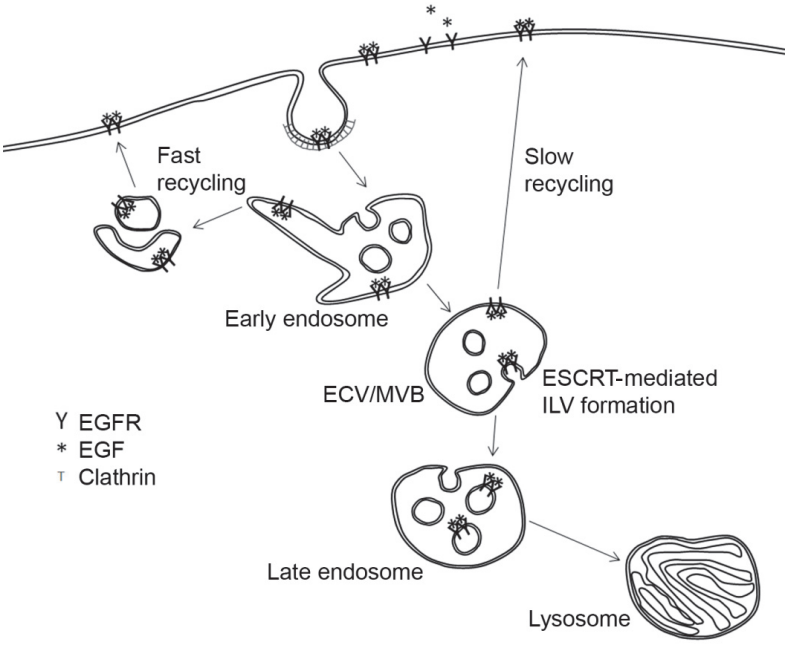

FIGURE 5 Model of EGFR endocytosis and intracellular sorting (low EGF stimulation concentration). EGF binding leads to receptor dimerization, phosphorylation, and ubiquitination. Ubiquitinated EGFRs are recognized at the plasma membrane by clathrin-mediated endocytosis machinery. After internalization, the EGF–receptor complex either recycles back to the plasma membrane or remains in early endosomes, which later mature into multivesicular bodies (MVB). Ubiquitinated EGFRs are recognized by the ESCRT machinery, and intraluminal vesicles (ILVs) are formed. Receptors that are not ubiquitinated can be recycled back to the plasma membrane via the slow recycling pathway. Later, MVBs fuse with lysosomes, resulting in degradation of both EGF and EGFR.

After 15–20 min of EGF stimulation, ubiquitinated EGF-receptor complexes, destined for degradation, begin to accumulate in the intraluminal membranes of MVBs with the help of the ESCRT machinery (Fig. 3) (Sorkin and Goh 2008). After this process, the receptors cannot be recycled back to the PM. Ubiquitinated receptors are recognized by several proteins (e.g., the ESCRT-0 component Hrs and the ESCRT-I component tumor susceptibility gene 101 (TSG101)) (Williams and Urbe 2007). The interaction of Hrs with TSG101 promotes the recruitment of subsequent ESCRT complexes following the ESCRT-III-dependent ILV scission (Henne *et al.* 2011). Loss of TSG101 induces the formation of multicisternal endosomes (Doyotte *et al.* 2005) and inhibits the degradation of EGFR (Razi and Futter 2006). ESCRT-III complex component VPS24 is also necessary for EGFR degradation (Bache *et al.* 2006). Before sorting to ILVs, ubiquitin is removed from the EGFR by deubiquitinating enzymes, and free ubiquitin is recycled back to the cytosolic pool of ubiquitin.

2.3.2 Ligand-mediated EGFR activation and receptor signaling

EGFR is known to dimerize and autophosphorylate upon EGF binding (Ogiso *et al.* 2002, Sorkin and Goh 2008). Consequently, phosphotyrosine-binding proteins and other cytoplasmic substrates are recruited to the site, activating multiple signaling pathways, including the MAPK, PI3K, and PLC pathways. PI3K is known to recruit Akt/protein kinase B to the plasma membrane, whereas PLC directly interacts with EGFR, leading to PKC activation (Lill and Sever 2012). Although signaling from activated EGFRs occurs mostly from the plasma membrane, it is now known that receptors are able to activate specific signaling pathways from intracellular structures as well (Wiley 2003).

3 AIMS OF THE PRESENT STUDY

The detailed aims of the present study were as follows:

1 To define the infectious entry pathway of CVA9 and the endocytic structures along the pathway (II)

2 To study the nature and importance of multivesicular structures along the EV1 and CVA9 infection pathways (I, II)

3 To study the effect of EV1 entry on the receptor recycling pathways: detailed study of EGFR sorting and downregulation (III)

4 OVERVIEW OF THE METHODS

Detailed descriptions of the materials and methods used can be found in the original publications, indicated by Roman numerals. The methods used in this study are summarized in Table 4.

TABLE 4 Methods used in the original publications included in the thesis.

Method	Publication
Cell culture	I, II, III
Virus (EV1 or CVA9) production and purification	I, II, III
Transfections	I, II
siRNA experiments	I
Quantitative real-time PCR analysis	I, II
Viral (EV1 or CVA9) infections	I, II, III
Integrin clustering experiments	I
Endosomal pH measurement	I, II
Immunofluorescence and confocal microscopy	I, II, III
Data analysis and processing of the microscopic data	I, II, III
Electron microscopy	I, II
Statistical testing	I, II, III
Live cell microscopy	I, II
SDS-PAGE and immunoblotting	III

5 RESULTS AND DISCUSSION

5.1 CVA9 endocytosis and uncoating

As earlier studies have suggested that there are some similarities in internalization pathways (e.g., integrins as cellular receptors, independent of CME or microtubule polymerization) between EV1 and CVA9, we wanted to investigate the nature of CVA9 endocytosis in further detail. We started by using chemical inhibitors that have been widely used to downregulate endocytosis (Table 5).

TABLE 5 Pharmacological inhibitors used in coxsackievirus A9 (CVA9) infection. The plus sign (+) stands for dependence of the target molecule and the minus sign (-) stands for independence of the target molecule in the CVA9 infection. Phospholipase C (PLC), phosphoinositide-3-kinase (PI3K), ethyl-isopropyl amiloride (EIPA), nocodazole (Noc), bafilomycin A1 (Baf).

Target	Dependence	Inhibitor	Cell line	Article
PLC	+	U-73122	A549	II
Rac1	+	NSC23766	A549	II
Na^+/H^+ exchanger	+	EIPA	A549	II
PI3K	-	Wortmannin	A549	II
PI3K	-	LY290042	A549	II
Pak1	-	IPA-3	A549	II
Microtubule	-	Noc	A549	II
Acidification	-	Baf	A549	II

In both the CAV9 infection and RT-PCR assays, U-73122, NSC23766, and EIPA caused a statistically significant decrease in infection or genomic strand production, while Wortmannin, LY290042, and IPA-3 had no significant effect (II, Fig. 2). Thus, the results suggested that PLC, Rac1, and Na^+/H^+ exchanger

inhibitors decrease CVA9 infection, whereas PI3K or Pak1 do not seem to play a role in the CVA9 infection process.

When we investigated the temporal effects of PLC on Rac1 and Na^+/H^+ exchanger inhibitors more closely, we found that the inhibitory effect of U-73122 is limited to the early stages of infection (before 1 h p.i.) (II, Fig. 2). This finding was expected, as we also found that PLC acts early in EV1 infection (Karjalainen *et al.* 2008). In addition, the previous control assays for U-73122 action showed that it blocks the entry of dextran completely, further proving that PLC activity is needed in the very first uptake step of fluid-phase endocytosis (Karjalainen *et al.* 2008). In the case of NSC23766, the inhibitory effect on CVA9 infection was restricted to time points between 1 and 3 h p.i., whereas EIPA disrupted the infection from early time points to later ones (II, Fig. 2). Rac1 plays a vital role in a range of cellular processes (actin reorganization, cell transformation, initiation of DNA synthesis, cell migration) (Bosco *et al.* 2009), and we found that Rac1 inhibitor did not interrupt the viral uncoating process, but rather, acted after uncoating (II, Fig. 2). Although the exact role of Rac1 in CVA9 infection remains to be studied, we suggest that in CVA9 infection, Rac1 acts in membrane remodeling through the activation of actin (Morel *et al.* 2009). Earlier results suggested that EIPA causes the accumulation of EV1 and CVA9 close to the PM, arresting further transport (Karjalainen *et al.* 2008, Heikkilä *et al.* 2010, Krieger *et al.* 2013). EIPA has also been shown to inhibit the intracellular replication of at least two other enteroviruses (human rhinovirus 2 and coxsackievirus B3) (Gazina *et al.* 2005, Harrison *et al.* 2008). In addition, it has been suggested that EIPA inhibits Rac1 and Cdc42 activation (Koivusalo *et al.* 2010). In conclusion, EIPA seems to have several inhibitory effects along the enterovirus endocytosis pathways.

In order to determine the time course of CVA9 uncoating, replication, and formation of new infective particles, we performed various assays. The NR assays revealed that while CVA9 uncoating starts at 30 min p.i., the majority of the process takes place at around 2 h p.i (II, Fig. 1). This timing is rather similar to what we observed earlier with EV1 (Pietiäinen *et al.* 2004, Siljamäki *et al.* 2013). The immunolabeling of double-stranded RNA, as well as $TCID_{50}$ assays, suggested that both active replication of CVA9 (visible dsRNA structures) and infectious particle formation occurred after 3 h p.i. Again, this result is very similar to earlier observations of EV1 (Pietiäinen *et al.* 2004, Upla *et al.* 2008) and other enteroviruses, although there are cell-line-dependent differences. For example, in HeLa cells, poliovirus releases its genome rapidly after 10 min p.i. (Brandenburg *et al.* 2007), but in polarized human brain microvascular endothelial cells, poliovirus remains on the PM and enters the cytoplasm after 2.5 h (Coyne *et al.* 2007), and uncoating takes place after 4 h.

Viewed together, the results show that the entry of CVA9 is very similar to that of EV1; the only clear difference is the lack of effect of Pak1. However, that effect might be cell-type dependent, as all of the CVA9 experiments were conducted in A549 cells; EV1 and CVA9 were not tested in similar cell lines.

5.2 CVA9 and EV1 do not enter the canonical endocytosis pathway, and the infections are independent of acidification

As earlier results suggested that EV1 does not colocalize with the EE, RE, LE or lysosome markers in SAOS-α2 or CV-1 cells (Table 3) (Marjomäki *et al.* 2002, Pietiäinen *et al.* 2004, Karjalainen *et al.* 2008, Rintanen *et al.* 2012), we wanted to investigate whether CVA9 also evades these classical endocytic structures. As with EV1, CVA9 colocalization with EEA1, Rab7, and Lamp1 was low during virus internalization (II, Fig. 4). Moreover, Coyne et al. (2007) showed that yet another enterovirus, poliovirus, did not colocalize with EEA1, Rab7, or Lamp2.

In our experiments, the DN–Rab5 (Rab5-S34N–GFP) construct inhibited CVA9 infection in a statistically significant manner, whereas the constitutively active mutant had a minor inhibitory effect on CVA9 infection (II, Fig. 4). Heikkilä et al. (2010) previously suggested that Rab5 does not play a role in CVA9 infection in A549 cells. As this result was based on a siRNA assay, where the total silencing of Rab5 was somewhat uncertain, we cannot say for sure whether Rab5 is needed for CVA9 infection. On the other hand, Krieger et al. (2013) concluded that Rab5 has a role in EV1 infection in Caco2 cells. Although Rab5 is strongly associated with EEs, Krzyzaniak et al. (2013) suggested that Rab5 is also active in macropinocytosis.

A strong piece of evidence for EV1 and CVA9 not choosing the lysosomal pathway comes from functional endocytosis studies using Dil–LDL. Dil–LDL has been shown to be targeted via the sorting early endosomes to the lysosomes and to colocalize with Lamp1 (Humphries *et al.* 2010, II, Fig. 4). When Dil–LDL was internalized into SAOS-α2 and A549 cells together with clustered α2β1 integrin/EV1 and CVA9, respectively, no colocalization between virus particles and Dil–LDL was detected (Rintanen *et al.* 2012, I, Fig. 2, II, Fig. 4), strongly suggesting that both of these viruses avoid lysosomes.

Because the microtubule-depolymerizing agent nocodazole blocks the transport of cargo from EEs to LEs (Bayer *et al.* 1998, Mesaki *et al.* 2011) and does not have an effect in EV1 or CVA9 infection (Pietiäinen *et al.* 2004, Heikkilä *et al.* 2010, II, Fig. 5), we wanted to test whether virus transfer to LEs is important for CVA9 infection. The results showed that nocodazole treatment did not increase CVA9 colocalization with EEA1 or decrease the measured background colocalization with Lamp1 (II, Fig. 5). Thus, these results further confirmed that CVA9 internalization is not dependent on the canonical entry pathway (from early to late endosome and lysosome).

Endosomes acidify as they mature in the canonical endocytosis pathway. Our earlier studies suggested that EV1 does not colocalize with acidic vesicles (Pietiäinen *et al.* 2004) and that CVA9 infection is not inhibited by NH_4Cl (Heikkilä *et al.* 2010). Therefore, we studied whether CVA9 was also independent of acidification for its infectious pathway. Although the V-ATPase inhibitor bafilomycin A1 slightly decreased CVA9 infection, the RT-PCR assay revealed no decrease in genomic or complementary strand production (II, Fig.

8). Because bafilomycin A1 has been shown to arrest transport in EEs (Bayer *et al.* 1998), we tested whether bafilomycin A1 treatment causes an accumulation of CVA9 particles in EEs, and we found that such an accumulation did not occur (II, Fig. 8). As with EV1 (Karjalainen *et al.* 2008), CVA9 did not colocalize with LysoTracker during the 3.5h live imaging period (II, Fig. 9). Lastly, an intra-endosomal pH measurement assay was performed in order to gain more accurate information regarding the internal pH of the endosomes along the EV1 internalization and CVA9 pathways. In these assays, the intra-endosomal pH of α2β1 integrin structures (during EV1 infection) and CVA9-positive vesicles stayed neutral at time points 1, 2, and 3 h p.i (I, Fig. 2, II, Fig. 8).

In conclusion, the results demonstrated that EV1 and CVA9 do not accumulate in canonical, acidic endosomes or need endosome acidification for successful infection. Various studies have shown that at least poliovirus and coxsackievirus B3 infections are independent of acidic environment (Gromeier and Wetz 1990, Perez and Carrasco 1993, Brandenburg *et al.* 2007, Patel *et al.* 2009). Although it was already known that enteroviruses are acid stable, these results provide evidence that endosome acidification may not be needed at all in enterovirus infection.

5.3 EV1 and CVA9 accumulate in MVBs, and ESCRT machinery is needed in the infections

According to our earlier results, EV1 is internalized into tubulovesicular structures that later mature into MVBs (Fig. 4) (Karjalainen *et al.* 2008). Next, we wanted to investigate whether MVBs play a role in CVA9 infection as well. From EM images and quantitative analyses conducted from them, it can be seen that CVA9 particles are mostly on the PM at 5 min p.i., whereas after 30 min, approximately one-third of the CVA9 particles were internalized and could be found inside endosomes (II, Fig. 3). Moreover, approximately half of these structures were identified as MVBs. Later, at 2 h p.i., CVA9 particles were mostly found in MVBs, suggesting that MVBs are truly important for infectious entry of CVA9. As the ESCRT machinery catalyzes the progressive involution of the endosomal-limiting membrane and formation of MVBs (Gruenberg and Stenmark 2004, Henne *et al.* 2011), we tested the importance of the ESCRT machinery for EV1 and CVA9 infection by perturbing the function of selected ESCRT proteins.

VPS4 is essential for the dissociation of ESCRT-III from the endosomal membrane (Babst *et al.* 1998). We transfected SAOS-α2 and A549 cells with a DN-VPS4 (VPS4-E235Q–GFP) or control GFP plasmid, and after 48h of expression, we infected the same cells with EV1 or CVA9, respectively. The overexpression of DN-VPS4 had a clear inhibitory effect on both infections (I, Fig. 3, II, Fig. 6). In the case of CVA9, double-stranded RNA production had also clearly decreased in DN-VPS4-transfected cells (II, Fig. 6).

As VPS4-E235Q–GFP seemed to prevent the infection of EV1 and CVA9, we further studied the morphology of α2-, EV1-, and CVA9-MVBs by confocal microscopy and by EM. The confocal microscopy findings indicated that both EV1 and α2-integrin colocalized with VPS4-E235Q–GFP-endosomes that were CI-MPR- and Tf-negative (I, Fig. 4 and S4). The EM studies revealed that most of the clustered α2-integrin in VPS4-E235Q–GFP-expressing cells was found in small endosomes; however, integrin was occasionally trapped on the limiting membrane of enlarged VPS4-E235Q–GFP-positive structures (I, Fig. 3). In the control cells, α2-MVBs were larger and contained ILVs with integrin both on the limiting membrane and in internal membranes. Furthermore, the EM assay revealed that considerably less integrin was found in the MVBs of VPS4-E235Q–GFP-expressing cells than in those of control cells. Similarly, the electron micrographs showed that in VPS4-E235Q–GFP-transfected cells, CVA9 was found in small vesicles with no ILVs (II, Fig. 7).

The ESCRT-0 protein Hrs binds to the endosome-limiting membrane and recruits other ESCRT components to this ILV formation site (Henne *et al.* 2011). As overexpression of WT-Hrs blocks EGFR transport (Urbe *et al.* 2003), we were interested to see whether Hrs overexpression had an effect on CVA9 infection or on the internalization of EV1 receptor α2β1 integrin. We transfected A549 and SAOS-α2 cells with Hrs-WT–GFP or a control GFP plasmid. In A549 cells transfected with the control GFP plasmid, the CVA9 infection proceeded normally (II, Fig. 6). In contrast, the overexpression of WT-Hrs–GFP had a strong inhibitory effect on the production of CVA9 capsid protein. In WT-Hrs–GFP-expressing SAOS-α2 cells, the association of α2β1 integrin clusters with Hrs was studied by live cell microscopy. Time-lapse imaging showed that colocalization of α2 integrin and Hrs gradually increased during integrin internalization (up to 2 h) (I, Fig. 6). The same process was seen in a colocalization analysis between endogenous Hrs and clustered α2 integrin using confocal microscopy and cryo-EM (I, Fig. 7 and S4). The cryo-EM assay also revealed that CVA9 was not found in the MVBs of WT-Hrs-transfecteed cells (II, Fig. 7).

The importance of the ESCRT-I proteins TSG101 and VPS37A and the ESCRT-III protein VPS24 were studied in EV1 infection by siRNA, immunofluorescence, and cryo-EM assays. SAOS-α2 cells were co-transfected with siRNA and an indicator of successful transfection (siGLO marker). The siRNAs against VPS37A and VPS24 decreased EV1 infection efficiently, whereas siRNA knock-down of TSG101 had a minor inhibitory effect on the infection (I, Fig. 5). Fluorescent images of SAOS-α2 cells with downregulated VPS37A revealed that virus capsids were frequently trapped in small cytoplasmic vesicles, while control siRNA-transfected cells were infected normally (I, Fig 5). In electron micrographs, VPS37A and VPS24 colocalized with clustered α2 integrin (I, Fig. 7).

In conclusion, both EV1 and CVA9 accumulate in MVBs during their internalization. We studied the role of ESCRT machinery comprehensively in both EV1 and CVA9 infections, and the results suggest that all of the ESCRT proteins studied were needed in EV1 and CVA9 infections. This finding further

confirms the importance of MVBs and ILVs in both EV1 and CVA9 infections. Although MVBs are generally thought to lead to degradative lysosomes, not all of the material in the ILV membrane ends up in lysosomes. For example, class II major histocompatibility complex (MHC) and tetraspanins form class II MHC compartments that are not degradative (van Niel *et al.* 2006). Another example of non-degradative MVBs are melanosomes (Theos *et al.* 2006). Although the results show the importance of ESCRT machinery and MVBs in both virus infections, the mechanistic reason for the need for MVBs remains unclear.

In summary, EV1 and CVA9 internalization resemble each other closely: 1) the effects of endocytosis inhibitors and the uncoating and replication time courses were similar; 2) both viruses avoid canonical endocytic structures but accumulate in non-acidic MVBs; 3) acidification is not needed for successful EV1 or CVA9 infection; and 4) functional ESCRT machinery is essential for both viruses. Because other enteroviruses are also known to be independent of endosome acidification, one can speculate whether there are also further similarities with other enteroviruses. If so, this knowledge might help in antiviral and vaccine development.

5.4 EGFR and EV1 are closely associated during virus infection

On the PM, EGFR has been shown to reside close to α2β1 integrin and to co-immunoprecipitate with it (Yu *et al.* 2000, Moro *et al.* 2002). Furthermore, EGF stimulation has been shown to cause internalization of α2β1 integrin (Ning *et al.* 2005). However, our results here suggest that in SAOS-α2 and A549 cells, neither EV1 nor α2 integrin colocalize with EGFR after their stimulated internalization (I, Fig. 8, III, Fig. 1). Furthermore, EGF stimulation has no effect on EV1 infection or the internalization efficiency of clustered α2 integrin (I, Fig. 8). This may be due to the fact that EV1 causes the formation of a novel entry pathway for the virus–integrin complex that is separate from the continuous recycling pathway of α2β1 integrin along the CME (Rintanen *et al.* 2012). Thus, it seems that the virus-induced pathway is not sensitive to EGF stimulation. In contrast, we wanted to study whether EV1 internalization had an effect on EGFR endocytosis.

In A549 cells, α2 integrin and EGFR colocalized on the PM in the absence of EGF stimulation, but after EGF stimulation and integrin clustering, the internalized receptors no longer colocalized (I, Fig. 8). The internalization of EV1 (and clustered α2 integrin) and biotinylated EGF in SAOS-α2 and A549 cells was followed using fluorescence microscopy. Although the structures resided very close to each other, the confocal images showed no apparent colocalization between biotin-EGF and EV1 or its receptor (I, Fig. 8 III, Fig. 1). This finding was confirmed by quantifying the colocalization between endogenous EGFR and EV1/clustered α2 integrin in both SAOS-α2 and A549 cells (I, Fig. 8). The live imaging showed that the biotin–EGF and clustered α2

integrin structures were very close to each other, but still separate (III, Movies 1 and 2).

Finally, we depolymerized the microtubules with nocodazole and tested whether doing so had any effect on EGFR or EV1 targeting. Nocodazole-treated, EGF-stimulated SAOS-α2 cells were infected with EV1, and internalization of EGFR and EV1 was followed using confocal microscopy. In the nocodazole-treated cells, EGFR-positive vesicles accumulated in the cell periphery, and EGFR degradation was inhibited (I, Fig. 8). Moreover, the data showed no apparent colocalization of EGFR with EV1, which would be the case if they followed the same internalization pathway.

Collectively, these results indicate that although EGFR and EV1 are closely associated during their internalization, they still traffic through separate pathways. EGFR is degraded in lysosomes, while clustered α2 integrin and EV1 accumulate in cytoplasmic vesicles.

5.5 EV1 infection slows down the degradation of EGFR

Although we had observed that the α2 integrin signal turns over at a higher pace after viral infection (Rintanen *et al.* 2012), this downregulation is much slower than what has been typically observed for EGFR in numerous studies (Burke *et al.* 2001, Salazar and Gonzalez 2002, Sigismund *et al.* 2008). In addition, after EGF stimulation in SAOS-α2 cells, the signal from clustered α2 integrins stayed strong during 2 h of imaging, whereas the EGFR signal was reduced (I, Fig. 8). Although this was the case with clustered α2 integrins, we observed that the EV1 infection caused higher surface and internalized EGFR signals compared to the control cells without EV1 (III, Fig. 2). The same result was seen in SDS-PAGE samples for the total pool of endogenous EGFR. These results clearly showed that EV1 infection had an inhibitory effect on the overall downregulation of EGFR.

As EV1 infection may affect cellular function in a more general manner, we studied the role of EV1 infection in the receptor recycling pathways. Tf is one of the most studied molecular cargoes that are directed to the recycling pathway after entering into EEs (Mayle *et al.* 2012). If there is a defect in recycling caused by EV1 infection, there should be an increase in the colocalization of Tf with EEA1. The colocalization analyses showed that there was no apparent difference in Tf and EEA1 colocalization in cells with or without EV1 (III, Fig. 3). Another well-studied cargo molecule is the fluid phase marker IgG, which is destined for either recycling or degradation (Ward *et al.* 2003). The quantifications from confocal images revealed no differences in the number of IgG-positive objects between samples with or without EV1, meaning that EV1 does not have an effect on overall fluid phase uptake efficiency in A549 cells (III, Fig 3).

In conclusion, EV1 infection seems to accumulate EGFR on the PM and slow down the downregulation of EGFR without affecting other endocytosis

pathways. Whether the PM accumulation is due to a deceleration of EGFR internalization or an increase in EGFR recycling back to the PM is still unclear.

5.6 Changes in EGFR sorting and signaling during EV1 infection

Because EV1 infection decelerates the degradation of EGFR, we wanted to study whether this is reflected in EGFR colocalization with EEs, REs, LEs, or lysosomes. Reduced EGFR degradation could be due to 1) EGFR accumulation on the PM, 2) EGFR accumulation in EEs or LEs (before lysosomal degradation), 3) EGFR accumulation in macropinosomes, or 4) increased trafficking of EGFR to the recycling pathway. The quantifications from the confocal images revealed no statistically significant differences in EGFR colocalization with EEA1 or Rab7 during EV1 infection (III, Fig. 4). On the other hand, EGFR colocalization with recycling Tf was slightly increased at 15 min p.i. and decreased with Lamp1 at 1 h p.i., suggesting that EV1 infection might increase the recycling of EGFR back to the PM and decrease its targeting to lysosomes. Our previous studies showed macropinocytic uptake of both EV1 and EGFR (Karjalainen *et al*. 2008, Liberali *et al*. 2008). Both pathways used a similar regulator, CtBP1/BARS, which is needed to close the macropinocytic cup during uptake (Liberali *et al*. 2008). Hence, when activated by high concentrations of EGF, EV1 and EGFR may use a similar uptake pathway and accumulate in rather large macropinosome-like structures, depending on the cell type studied. It seems possible that EGFR accumulates in macropinosomes before entering degradative lysosomes; therefore, its accumulation does not result in colocalization with canonical endocytic markers.

Our previous studies revealed that EV1 infection activates PKC (Pietiäinen *et al.* 2004). We also know that EGFR phosphorylation by PKC targets EGFR to recycling structures (Bao *et al.* 2000). We therefore wanted to study whether phosphoPKCα (pPKCα) status was increased in EGF+EV1 treated cells. While EGF and EV1 were each already able to induce the cellular phosphorylation status of PKCα, treatment with a combination of EGF and EV1 increased the pPKCα activity even further (III, Fig. 5). In EGF+EV1 treated cells, an enhanced pPKCα signal could direct the EGFR pathway towards recycling; however, this aspect and the specific phosphorylation of EGFR still need to be studied. As EV1 alone also caused an accumulation of surface EGFR, it seems possible that the increase in PKCα phosphorylation by EV1 is sufficient to increase recycling and accumulate the EGFR at the PM.

The phosphorylation status of two signaling proteins, Akt and p44/42 MAPK, were followed to evaluate the activity of EGFR signaling in cells during EV1 infection. After a 15-min EGF stimulation, Akt was already active, but the activity level was much lower after 2 h (III, Fig. 5). EV1 treatment alone resulted in a lower level of phosphorylated Akt, suggesting that it could not induce EGFR phosphorylation to a great extent. In contrast, after the treatment with both EGF and EV1, the cells displayed much higher phosphorylation of Akt

after 15 min, 2 h, and 4 h, suggesting that EGFR signaling was higher due to accumulation in cytoplasmic endosomes. Similarly, the p44/42 MAPK phosphorylation status was clearly increased at all tested time points in the EGF+EV1 samples (III, Fig. 5), which provides further evidence that EGFR signaling was increased due to EV1 infection.

6 CONCLUDING REMARKS

The main conclusions of this thesis are as follows:

I The EV1 internalization pathway involves a novel MVB population (Fig. 6), which is separate from canonical acidic endosomes (e.g., the EGFR degradation pathway). Although the two pathways are separate, the same ESCRT mechanisms partially regulate the EV1–MVB formation, and ESCRT machinery is needed for successful EV1 infection.

II The infectious entry pathways of EV1 and CVA9 follow very similar characteristics (Fig. 6), which may be the case for other closely related enteroviruses as well. Similar to EV1, the majority of CVA9 uncoating occurs in non-acidic MVBs around 2 h p.i., and CVA9 infection is independent of endosome acidification. Genome replication begins around 3 h p.i., and later, newly synthesized viral capsid proteins and infectious viral particles accumulate in the cytoplasm.

III EV1 entry has a specific effect on EGFR sorting and downregulation without affecting transferrin recycling or default sorting to the lysosomal pathway. EV1 causes accumulation of EGFR endosomes in the cytoplasm and allows for more recycling, whereas sorting to lysosomes is reduced. This leads to prolonged signaling in endosomes and reduced downregulation of EGFR.

Despite their significance, there are no common drugs or vaccines against enterovirus infections other than for polio. Because EV1 and CVA9 internalization pathways resemble each other greatly and there are similarities with other enteroviruses as well, this knowledge could be used in future antiviral and vaccine development.

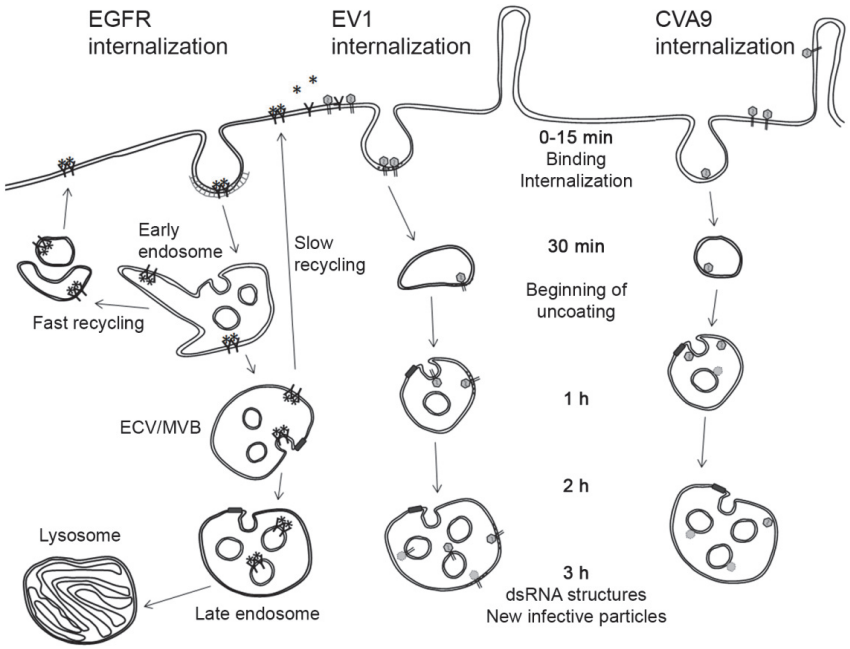

FIGURE 6 Epidermal growth factor (EGF) binding leads to EGF receptor (EGFR) internalization via clathrin-mediated (shown here) and possibly other pathways. After internalization, the EGF–receptor complex is either recycled back to the plasma membrane or transferred to acidic multivesicular bodies (MVBs), and later, to late endosomes and lysosomes for degradation. Intraluminal vesicles of EGFR-MVBs are formed by the ESCRT machinery. At the cell surface, echovirus 1 (EV1) receptor α2β1 integrin colocalizes with EGFR; however, after receptor clustering by EV1 and virus–receptor complex internalization, the EV1 and EGFR pathways are separated. EV1-positive tubulovesicular structures mature into non-acidic MVBs. As in EGFR-MVB maturation, the ESCRT machinery here is also responsible for intraluminal vesicle formation, and functional ESCRT machinery is needed in EV1 infection. As with EV1, coxsackievirus A9 (CVA9) is also internalized into endosomes, which gradually form ESCRT-driven intraluminal vesicles, leading to non-acidic MVBs. The uncoating and replication time courses of EV1 and CVA9 are similar. The majority of uncoating occurs around 2 h p.i. (when the virus is found in MVBs), although it starts as early as around 30 min p.i. The double-stranded RNA (dsRNA) structures appear in cells after 3 h, and later, the newly synthetized capsid proteins and infectious virus particles fill the cell cytoplasm.

Acknowledgements

This work was carried out during 2011-2014 at the University of Jyväskylä, at the Department of Biological and Environmental Sciences/Nanoscience Center, Division of Cell and Molecular Biology.

I am extremely grateful to my supervisor Docent Varpu Marjomäki for all the support she has given me since the very first day being in her group. The skills I have gained under her supervision are truly invaluable and with these skills I am more confident in starting my researcher career.

I also wish to thank my second supervisor Professor Timo Hyypiä for the opportunity to start my PhD studies with the CVA9 project. I would like to thank the reviewers of this thesis, Docent Tero Ahola and Docent Vesa Olkkonen, for their constructive and valuable comments. I am grateful to Professor Renate Fuchs who kindly accepted the invitation to serve as an opponent in the public examination of my dissertation. My support group members, Professor James M. Hogle, Dr. Sarah Butcher and Dr. Merja Roivainen are greatly acknowledged for guidance and advice during last couple of years of my PhD studies.

Next, I thank the former members of the group Marjomäki. Nina, Mikko K, Elina S, Lassi and Katri K: we are more than co-workers, we are friends. Thank you for our conversations and laughter; good times and many more to come. In addition, thank you Anita, Pasi, Pekka and Paula U for many joyful moments. I also want to express my gratitude to the present group Marjomäki, especially Mari, Maria, Paula T, Artur and Marie. Thank you for refreshing conversations in the office. Altogether, I have been blessed with the best colleagues in the whole wide world! Heikki, Mikko Y, Salla, Jarkko, Elisa, Ritika, Jonne, Leona, Leena, Laura, Kai, Elina D, Sanna, Elina M and Jori: What can I say… Thank you for all those enjoyable moments at corridors, scientific meetings, cruise ships, summer cottages, karonkkas, parties, toilettes… Quite many memorable moments!

I also want to thank my parents and my LITTLE brother for all their support over the years. My family, relatives and friends have given me a nice counterbalance to my work. A special thanks goes to Katri A, my best friend, who has stood by me although things were quite rough at times. And Anssi: although our paths got separated, I really want to thank you for your love, support, care and friendship over the 12.5 years together.

Warmest thanks to Olli, Hanna, Kristian, Nico, AP, Aaro and rest of the gang from Sukelluskeskus. Your support and care helped me back to the surface (!?) when I needed it most. There are no words to describe my gratitude. Finally, I want to express my deepest gratitude to Eetu who made me smile again. Thank You.

YHTEENVETO (RÉSUMÉ IN FINNISH)

Enterovirusten indusoima, neutraali sisäänmenoreitti ja sen vuorovaikutukset epidermaalisen kasvutekijäreseptorireitin kanssa

Virukset ovat itsenäiseen elämään kykenemättömiä biologisia järjestelmiä, jotka tarvitsevat isäntäsolun proteiineja ja energiantuottoa lisääntyäkseen. Virukset rakentuvat genomista (DNA tai RNA) ja sitä ympäröivästä proteiinikuoresta eli kapsidista. Tämän lisäksi joillain viruksilla kapsidia ympäröi lipidikalvosta ja siihen uponneista proteiineista ja hiilihydraateista koostuva vaippa. Viruksen elinkierto koostuu neljästä perusvaiheesta: (1) isäntäsolun tunnistaminen ja siihen kiinnittyminen; (2) perintöaineksen siirtäminen isäntäsoluun; (3) uusien virusrakenneosien tuottaminen isäntäsolussa ja (4) uusien viruspartikkeleiden vapautuminen isäntäsolusta. Enterovirukset ovat pieniä, pyöreitä vaipattomia RNA-viruksia, jotka lisääntyvät pääasiassa suolistossa. Ne eivät kuitenkaan tavallisesti aiheuta suolistotauteja vaan esimerkiksi nuhakuumetta, aivokalvotulehdusta, sydänlihastulehdusta, enterorokkoa ja muita ihottumatauteja. Enterovirusten ryhmään kuuluvat muun muassa poliovirus, echovirukset, coxsackievirukset sekä muut enterovirukset.

Yksi viruksen elinkierron tärkeimmistä tapahtumista on perintöaineksen siirtäminen isäntäsoluun. RNA-virusten genomin monistuminen (replikaatio) tapahtuu isäntäsolun solulimassa, ja sinne pääsemiseksi viruksen on ohitettava monia esteitä (solukalvo, isäntäsolun immuunipuolustus jne.). Endosytoosi on kaikille soluille tyypillinen tapahtuma, jonka avulla solu ottaa sisäänsä nestettä ja siihen liuenneita molekyylejä (esimerkiksi ravinteet ja kasvutekijät). Endosytoosissa solukalvolle muodostuu kuoppa, joka myöhemmin kuroutuu irti kalvosta. Näin muodostuneet kalvopäällysteiset rakkulat (endosomit) kuljettavat kalvon lipidit ja proteiinit sekä endosomin sisällön eteenpäin solulimassa. Solut käyttävät erilaisia endosytoosireittejä erilaisten molekyylien kuljettamiseen. Tunnetuimmat reiteistä ovat klatriinivälitteinen endosytoosi sekä makropinosytoosi. Solulimassa endosomit kypsyvät edelleen. Yleensä kypsymisen aikana endosomin kalvon proteiinikoostumus muuttuu ja endosomin sisältö happamoituu.

Tässä väitöskirjatyössä tutkitut enterovirukset, echovirus 1 (EV1) ja coxsackievirus A9 (CVA9), käyttävät endosytoosia genominsa toimittamiseen isäntäsolun solulimaan. Aiemmat tutkimukset ovat osoittaneet, että esimerkiksi EV1 tunkeutuu solun sisään makropinosytoosia muistuttavan reitin avulla, ja noin kahden tunnin jälkeen viruksen sisäänmenosta viruspartikkelit kertyvät monirakkulaisiin endosomeihin.

Tämän väitöskirjan ensimmäisessä ja toisessa osatyössä tutkittiin tarkemmin EV1:n ja CVA9:n sisäänmenoreittejä sekä solunsisäisiä rakenteita, joihin viruspartikkelit sisäänmenonsa jälkeen kertyvät. Osatyössä I osoitettiin, että EV1-rikkaat monirakkulaendosomit eroavat happamista rakenteista, joihin esimerkiksi epidermaalinen kasvutekijäreseptori (EGFR) kertyy klatriinivälitteisen endosytoosin jälkeen. Neutraalien EV1-monirakkulaendosomien muodostumi-

sessa kuitenkin toimii samat proteiinit (ESCRT-koneisto) kuin happamien EGFR-rakenteiden muodostumisessa. Osatyössä I todettiin myös, että toimiva ESCRT-koneisto ja monirakkulaiset rakenteet ovat välttämättömiä onnistuneessa EV1-infektiossa.

Osatyössä II keskityttiin toisen enteroviruksen, CVA9:n, endosytoosireittiin ja infektion aikaisiin virusrikkaisiin rakenteisiin. CVA9:n käyttämän endosytoosireitin ja viruksen elinkierron aikataulun havaittiin muistuttavan todella paljon EV1:n vastaavia. Kuten EV1, myös CVA9 kertyi infektion aikana monirakkulaisiin, neutraaleihin rakenteisiin, joiden muodostuminen ESCRT-koneiston avulla oli välttämätöntä infektion onnistumisen kannalta.

Väitöskirjan viimeisen osatyön tulokset paljastivat, että EV1-infektiolla on spesifinen vaikutus EGFR:n lajitteluun ja hajotukseen. Normaalisti kasvutekijällä stimuloitu EGFR ohjautuu nopeasti entsymaattiseen hajotukseen, mutta EV1:llä infektoiduissa soluissa tämä hajotus on hitaampaa ja EGFR näyttäisi kertyvän sekä solukalvolle että solunsisäisiin rakenteisiin. Tämä johtaa EGFR:n välittämän signaloinnin pidentymiseen, minkä voi ajatella olevan hyödyksi EV1-infektion kannalta.

Virusten avulla tehtävällä solu- ja molekyylibiologisella perustutkimuksella on pitkät perinteet. Samaan aikaan nykylääketieteestä löytyy sovelluksia viruksille muun muassa rokotetuotannossa ja syöpähoidoissa. Tämän lisäksi nykyinen globaaliyhteiskunta, helpottunut tavaroiden ja ihmisten liikkuminen sekä viime vuosina ilmaantuneet uudet ja mahdollisesti erittäin vaaralliset virustaudit nostavat jatkuvasti esille virustutkimuksen ja viruslääkkeiden kehityksen tärkeyden.

REFERENCES

Babst M., Wendland B., Estepa E.J. & Emr S.D. 1998. The Vps4p AAA ATPase regulates membrane association of a Vps protein complex required for normal endosome function. *EMBO J* 17: 2982-2993.

Bache K.G., Stuffers S., Malerod L., Slagsvold T., Raiborg C., Lechardeur D., Walchli S., Lukacs G.L., Brech A. & Stenmark H. 2006. The ESCRT-III subunit hVps24 is required for degradation but not silencing of the epidermal growth factor receptor. *Mol Biol Cell* 17: 2513-2523.

Bao J., Alroy I., Waterman H., Schejter E.D., Brodie C., Gruenberg J. & Yarden Y. 2000. Threonine phosphorylation diverts internalized epidermal growth factor receptors from a degradative pathway to the recycling endosome. *J Biol Chem* 275: 26178-26186.

Baravalle G., Schober D., Huber M., Bayer N., Murphy R.F. & Fuchs R. 2005. Transferrin recycling and dextran transport to lysosomes is differentially affected by bafilomycin, nocodazole, and low temperature. *Cell Tissue Res* 320: 99-113.

Bayer N., Schober D., Prchla E., Murphy R.F., Blaas D. & Fuchs R. 1998. Effect of bafilomycin A1 and nocodazole on endocytic transport in HeLa cells: implications for viral uncoating and infection. *J Virol* 72: 9645-9655.

Benmerah A., Bayrou M., Cerf-Bensussan N. & Dautry-Varsat A. 1999. Inhibition of clathrin-coated pit assembly by an Eps15 mutant. *J Cell Sci* 112 (Pt 9): 1303-1311.

Bergelson J.M., Chan B.M., Finberg R.W. & Hemler M.E. 1993. The integrin VLA-2 binds echovirus 1 and extracellular matrix ligands by different mechanisms. *J Clin Invest* 92: 232-239.

Bergelson J.M., Shepley M.P., Chan B.M., Hemler M.E. & Finberg R.W. 1992. Identification of the integrin VLA-2 as a receptor for echovirus 1. *Science* 255: 1718-1720.

Bissig C. & Gruenberg J. 2013. Lipid sorting and multivesicular endosome biogenesis. *Cold Spring Harb Perspect Biol* 5: a016816.

Bonifacino J.S. & Rojas R. 2006. Retrograde transport from endosomes to the trans-Golgi network. *Nat Rev Mol Cell Biol* 7: 568-579.

Bosco E.E., Mulloy J.C. & Zheng Y. 2009. Rac1 GTPase: a "Rac" of all trades. *Cell Mol Life Sci* 66: 370-374.

Bowman E.J., Siebers A. & Altendorf K. 1988. Bafilomycins: a class of inhibitors of membrane ATPases from microorganisms, animal cells, and plant cells. *Proc Natl Acad Sci U S A* 85: 7972-7976.

Brandenburg B., Lee L.Y., Lakadamyali M., Rust M.J., Zhuang X. & Hogle J.M. 2007. Imaging poliovirus entry in live cells. *PLoS Biol* 5: e183.

Burke P., Schooler K. & Wiley H.S. 2001. Regulation of epidermal growth factor receptor signaling by endocytosis and intracellular trafficking. *Mol Biol Cell* 12: 1897-1910.

Clague M.J., Coulson J.M. & Urbe S. 2012. Cellular functions of the DUBs. *J Cell Sci* 125: 277-286.

Clague M.J., Urbe S., Aniento F. & Gruenberg J. 1994. Vacuolar ATPase activity is required for endosomal carrier vesicle formation. *J Biol Chem* 269: 21-24.

Coyne C.B., Kim K.S. & Bergelson J.M. 2007. Poliovirus entry into human brain microvascular cells requires receptor-induced activation of SHP-2. *EMBO J* 26: 4016-4028.

Dharmawardhane S., Schurmann A., Sells M.A., Chernoff J., Schmid S.L. & Bokoch G.M. 2000. Regulation of macropinocytosis by p21-activated kinase-1. *Mol Biol Cell* 11: 3341-3352.

Doherty G.J. & McMahon H.T. 2009. Mechanisms of endocytosis. *Annu Rev Biochem* 78: 857-902.

Doyotte A., Russell M.R., Hopkins C.R. & Woodman P.G. 2005. Depletion of TSG101 forms a mammalian "Class E" compartment: a multicisternal early endosome with multiple sorting defects. *J Cell Sci* 118: 3003-3017.

Ford M.G., Pearse B.M., Higgins M.K., Vallis Y., Owen D.J., Gibson A., Hopkins C.R., Evans P.R. & McMahon H.T. 2001. Simultaneous binding of PtdIns(4,5)P2 and clathrin by AP180 in the nucleation of clathrin lattices on membranes. *Science* 291: 1051-1055.

Foret L., Dawson J.E., Villasenor R., Collinet C., Deutsch A., Brusch L., Zerial M., Kalaidzidis Y. & Julicher F. 2012. A general theoretical framework to infer endosomal network dynamics from quantitative image analysis. *Curr Biol* 22: 1381-1390.

Fujita H., Yamanaka M., Imamura K., Tanaka Y., Nara A., Yoshimori T., Yokota S. & Himeno M. 2003. A dominant negative form of the AAA ATPase SKD1/VPS4 impairs membrane trafficking out of endosomal/lysosomal compartments: class E vps phenotype in mammalian cells. *J Cell Sci* 116: 401-414.

Gazina E.V., Harrison D.N., Jefferies M., Tan H., Williams D., Anderson D.A. & Petrou S. 2005. Ion transport blockers inhibit human rhinovirus 2 release. *Antiviral Res* 67: 98-106.

Goldstein J.L. & Brown M.S. 2009. The LDL receptor. *Arterioscler Thromb Vasc Biol* 29: 431-438.

Grant B.D. & Donaldson J.G. 2009. Pathways and mechanisms of endocytic recycling. *Nat Rev Mol Cell Biol* 10: 597-608.

Gromeier M. & Wetz K. 1990. Kinetics of poliovirus uncoating in HeLa cells in a nonacidic environment. *J Virol* 64: 3590-3597.

Gruenberg J. 2001. The endocytic pathway: a mosaic of domains. *Nat Rev Mol Cell Biol* 2: 721-730.

Gruenberg J. & Stenmark H. 2004. The biogenesis of multivesicular endosomes. *Nat Rev Mol Cell Biol* 5: 317-323.

Harrison D.N., Gazina E.V., Purcell D.F., Anderson D.A. & Petrou S. 2008. Amiloride derivatives inhibit coxsackievirus B3 RNA replication. *J Virol* 82: 1465-1473.

Hecker W., Meyer J., Boeni R. & Bienz K. 1974. Pinocytotic uptake and intralysosomal crystal formation of coxsackievirus A9 in monkey kidney cells. An electron microscopic autoradiographic study. *Arch Gesamte Virusforsch* 46: 167-174.

Heikkila O., Susi P., Stanway G. & Hyypia T. 2009. Integrin alphaVbeta6 is a high-affinity receptor for coxsackievirus A9. *J Gen Virol* 90: 197-204.

Heikkila O., Susi P., Tevaluoto T., Harma H., Marjomaki V., Hyypia T. & Kiljunen S. 2010. Internalization of coxsackievirus A9 is mediated by {beta}2-microglobulin, dynamin, and Arf6 but not by caveolin-1 or clathrin. *J Virol* 84: 3666-3681.

Henne W.M., Buchkovich N.J. & Emr S.D. 2011. The ESCRT pathway. *Dev Cell* 21: 77-91.

Hogle J.M. 2002. Poliovirus cell entry: common structural themes in viral cell entry pathways. *Annu Rev Microbiol* 56: 677-702.

Hopkins C.R., Miller K. & Beardmore J.M. 1985. Receptor-mediated endocytosis of transferrin and epidermal growth factor receptors: a comparison of constitutive and ligand-induced uptake. *J Cell Sci Suppl* 3: 173-186.

Hsu V.W. & Prekeris R. 2010. Transport at the recycling endosome. *Curr Opin Cell Biol* 22: 528-534.

Hullin-Matsuda F., Taguchi T., Greimel P. & Kobayashi T. 2014. Lipid compartmentalization in the endosome system. *Semin Cell Dev Biol* 31: 48-56.

Humphries W.H.,4th, Fay N.C. & Payne C.K. 2010. Intracellular degradation of low-density lipoprotein probed with two-color fluorescence microscopy. *Integr Biol (Camb)* 2: 536-544.

Huotari J. & Helenius A. 2011. Endosome maturation. *EMBO J* 30: 3481-3500.

Hyypia T., Hovi T., Knowles N.J. & Stanway G. 1997. Classification of enteroviruses based on molecular and biological properties. *J Gen Virol* 78 (Pt 1): 1-11.

Jokinen J., White D.J., Salmela M., Huhtala M., Kapyla J., Sipila K., Puranen J.S., Nissinen L., Kankaanpaa P., Marjomaki V., Hyypia T., Johnson M.S. & Heino J. 2010. Molecular mechanism of alpha2beta1 integrin interaction with human echovirus 1. *EMBO J* 29: 196-208.

Karjalainen M., Kakkonen E., Upla P., Paloranta H., Kankaanpaa P., Liberali P., Renkema G.H., Hyypia T., Heino J. & Marjomaki V. 2008. A Raft-derived, Pak1-regulated entry participates in alpha2beta1 integrin-dependent sorting to caveosomes. *Mol Biol Cell* 19: 2857-2869.

Katzmann D.J., Stefan C.J., Babst M. & Emr S.D. 2003. Vps27 recruits ESCRT machinery to endosomes during MVB sorting. *J Cell Biol* 162: 413-423.

Koivusalo M., Welch C., Hayashi H., Scott C.C., Kim M., Alexander T., Touret N., Hahn K.M. & Grinstein S. 2010. Amiloride inhibits macropinocytosis by lowering submembranous pH and preventing Rac1 and Cdc42 signaling. *J Cell Biol* 188: 547-563.

Krieger S.E., Kim C., Zhang L., Marjomaki V. & Bergelson J.M. 2013. Echovirus 1 entry into polarized Caco-2 cells depends on dynamin, cholesterol, and cellular factors associated with macropinocytosis. *J Virol* 87: 8884-8895.

Krzyzaniak M.A., Zumstein M.T., Gerez J.A., Picotti P. & Helenius A. 2013. Host cell entry of respiratory syncytial virus involves macropinocytosis followed by proteolytic activation of the F protein. *PLoS Pathog* 9: e1003309.

Lakadamyali M., Rust M.J. & Zhuang X. 2006. Ligands for clathrin-mediated endocytosis are differentially sorted into distinct populations of early endosomes. *Cell* 124: 997-1009.

Lamb C.A., Yoshimori T. & Tooze S.A. 2013. The autophagosome: origins unknown, biogenesis complex. *Nat Rev Mol Cell Biol* 14: 759-774.

Liberali P., Kakkonen E., Turacchio G., Valente C., Spaar A., Perinetti G., Bockmann R.A., Corda D., Colanzi A., Marjomaki V. & Luini A. 2008. The closure of Pak1-dependent macropinosomes requires the phosphorylation of CtBP1/BARS. *EMBO J* 27: 970-981.

Lill N.L. & Sever N.I. 2012. Where EGF receptors transmit their signals. *Sci Signal* 5: pe41.

Loubery S., Wilhelm C., Hurbain I., Neveu S., Louvard D. & Coudrier E. 2008. Different microtubule motors move early and late endocytic compartments. *Traffic* 9: 492-509.

Lund K.A., Lazar C.S., Chen W.S., Walsh B.J., Welsh J.B., Herbst J.J., Walton G.M., Rosenfeld M.G., Gill G.N. & Wiley H.S. 1990. Phosphorylation of the epidermal growth factor receptor at threonine 654 inhibits ligand-induced internalization and down-regulation. *J Biol Chem* 265: 20517-20523.

Luzio J.P., Pryor P.R. & Bright N.A. 2007. Lysosomes: fusion and function. *Nat Rev Mol Cell Biol* 8: 622-632.

Manser E., Leung T., Salihuddin H., Zhao Z.S. & Lim L. 1994. A brain serine/threonine protein kinase activated by Cdc42 and Rac1. *Nature* 367: 40-46.

Marjomaki V., Pietiainen V., Matilainen H., Upla P., Ivaska J., Nissinen L., Reunanen H., Huttunen P., Hyypia T. & Heino J. 2002. Internalization of echovirus 1 in caveolae. *J Virol* 76: 1856-1865.

Marshansky V. & Futai M. 2008. The V-type H+-ATPase in vesicular trafficking: targeting, regulation and function. *Curr Opin Cell Biol* 20: 415-426.

Maxfield F.R. & McGraw T.E. 2004. Endocytic recycling. *Nat Rev Mol Cell Biol* 5: 121-132.

Maxfield F.R. & Yamashiro D.J. 1987. Endosome acidification and the pathways of receptor-mediated endocytosis. *Adv Exp Med Biol* 225: 189-198.

Mayle K.M., Le A.M. & Kamei D.T. 2012. The intracellular trafficking pathway of transferrin. *Biochim Biophys Acta* 1820: 264-281.

Mayor S. & Pagano R.E. 2007. Pathways of clathrin-independent endocytosis. *Nat Rev Mol Cell Biol* 8: 603-612.

Mellor H. & Parker P.J. 1998. The extended protein kinase C superfamily. *Biochem J* 332 (Pt 2): 281-292.

Mercer J., Schelhaas M. & Helenius A. 2010. Virus entry by endocytosis. *Annu Rev Biochem* 79: 803-833.

Mesaki K., Tanabe K., Obayashi M., Oe N. & Takei K. 2011. Fission of tubular endosomes triggers endosomal acidification and movement. *PLoS One* 6: e19764.

Miaczynska M., Pelkmans L. & Zerial M. 2004. Not just a sink: endosomes in control of signal transduction. *Curr Opin Cell Biol* 16: 400-406.

Mooren O.L., Galletta B.J. & Cooper J.A. 2012. Roles for actin assembly in endocytosis. *Annu Rev Biochem* 81: 661-686.

Morel E., Parton R.G. & Gruenberg J. 2009. Annexin A2-dependent polymerization of actin mediates endosome biogenesis. *Dev Cell* 16: 445-457.

Moro L., Dolce L., Cabodi S., Bergatto E., Boeri Erba E., Smeriglio M., Turco E., Retta S.F., Giuffrida M.G., Venturino M., Godovac-Zimmermann J., Conti A., Schaefer E., Beguinot L., Tacchetti C., Gaggini P., Silengo L., Tarone G. & Defilippi P. 2002. Integrin-induced epidermal growth factor (EGF) receptor activation requires c-Src and p130Cas and leads to phosphorylation of specific EGF receptor tyrosines. *J Biol Chem* 277: 9405-9414.

Ning Y., Zeineldin R., Liu Y., Rosenberg M., Stack M.S. & Hudson L.G. 2005. Down-regulation of integrin alpha2 surface expression by mutant epidermal growth factor receptor (EGFRvIII) induces aberrant cell spreading and focal adhesion formation. *Cancer Res* 65: 9280-9286.

Oberste M.S., Maher K., Kilpatrick D.R. & Pallansch M.A. 1999. Molecular evolution of the human enteroviruses: correlation of serotype with VP1 sequence and application to picornavirus classification. *J Virol* 73: 1941-1948.

Ogiso H., Ishitani R., Nureki O., Fukai S., Yamanaka M., Kim J.H., Saito K., Sakamoto A., Inoue M., Shirouzu M. & Yokoyama S. 2002. Crystal structure of the complex of human epidermal growth factor and receptor extracellular domains. *Cell* 110: 775-787.

Ohkuma S. & Poole B. 1978. Fluorescence probe measurement of the intralysosomal pH in living cells and the perturbation of pH by various agents. *Proc Natl Acad Sci U S A* 75: 3327-3331.

Olayioye M.A., Neve R.M., Lane H.A. & Hynes N.E. 2000. The ErbB signaling network: receptor heterodimerization in development and cancer. *EMBO J* 19: 3159-3167.

Patel K.P., Coyne C.B. & Bergelson J.M. 2009. Dynamin- and lipid raft-dependent entry of decay-accelerating factor (DAF)-binding and non-DAF-binding coxsackieviruses into nonpolarized cells. *J Virol* 83: 11064-11077.

Perez L. & Carrasco L. 1993. Entry of poliovirus into cells does not require a low-pH step. *J Virol* 67: 4543-4548.

Pietiainen V., Marjomaki V., Upla P., Pelkmans L., Helenius A. & Hyypia T. 2004. Echovirus 1 endocytosis into caveosomes requires lipid rafts, dynamin II, and signaling events. *Mol Biol Cell* 15: 4911-4925.

Platta H.W. & Stenmark H. 2011. Endocytosis and signaling. *Curr Opin Cell Biol* 23: 393-403.

Raiborg C., Bache K.G., Mehlum A., Stang E. & Stenmark H. 2001. Hrs recruits clathrin to early endosomes. *EMBO J* 20: 5008-5021.

Razi M. & Futter C.E. 2006. Distinct roles for Tsg101 and Hrs in multivesicular body formation and inward vesiculation. *Mol Biol Cell* 17: 3469-3483.

Reijngoud D.J., Oud P.S. & Tager J.M. 1976. Effect of ionophores on intralysosomal pH. *Biochim Biophys Acta* 448: 303-313.

Ridley A.J. 2006. Rho GTPases and actin dynamics in membrane protrusions and vesicle trafficking. *Trends Cell Biol* 16: 522-529.

Rink J., Ghigo E., Kalaidzidis Y. & Zerial M. 2005. Rab conversion as a mechanism of progression from early to late endosomes. *Cell* 122: 735-749.

Rintanen N., Karjalainen M., Alanko J., Paavolainen L., Maki A., Nissinen L., Lehkonen M., Kallio K., Cheng R.H., Upla P., Ivaska J. & Marjomaki V. 2012. Calpains promote alpha2beta1 integrin turnover in nonrecycling integrin pathway. *Mol Biol Cell* 23: 448-463.

Roivainen M., Piirainen L., Hovi T., Virtanen I., Riikonen T., Heino J. & Hyypia T. 1994. Entry of coxsackievirus A9 into host cells: specific interactions with alpha v beta 3 integrin, the vitronectin receptor. *Virology* 203: 357-365.

Sachse M., Strous G.J. & Klumperman J. 2004. ATPase-deficient hVPS4 impairs formation of internal endosomal vesicles and stabilizes bilayered clathrin coats on endosomal vacuoles. *J Cell Sci* 117: 1699-1708.

Salazar G. & Gonzalez A. 2002. Novel mechanism for regulation of epidermal growth factor receptor endocytosis revealed by protein kinase A inhibition. *Mol Biol Cell* 13: 1677-1693.

Scott C.C., Vacca F. & Gruenberg J. 2014. Endosome maturation, transport and functions. *Semin Cell Dev Biol* 31: 2-10.

Settembre C., Fraldi A., Medina D.L. & Ballabio A. 2013. Signals from the lysosome: a control centre for cellular clearance and energy metabolism. *Nat Rev Mol Cell Biol* 14: 283-296.

Shin H.W., Hayashi M., Christoforidis S., Lacas-Gervais S., Hoepfner S., Wenk M.R., Modregger J., Uttenweiler-Joseph S., Wilm M., Nystuen A., Frankel W.N., Solimena M., De Camilli P. & Zerial M. 2005. An enzymatic cascade of Rab5 effectors regulates phosphoinositide turnover in the endocytic pathway. *J Cell Biol* 170: 607-618.

Sigismund S., Argenzio E., Tosoni D., Cavallaro E., Polo S. & Di Fiore P.P. 2008. Clathrin-mediated internalization is essential for sustained EGFR signaling but dispensable for degradation. *Dev Cell* 15: 209-219.

Sigismund S., Algisi V., Nappo G., Conte A., Pascolutti R., Cuomo A., Bonaldi T., Argenzio E., Verhoef L.G., Maspero E., Bianchi F., Capuani F., Ciliberto A., Polo S. & Di Fiore P.P. 2013. Threshold-controlled ubiquitination of the EGFR directs receptor fate. *EMBO J* 32: 2140-2157.

Siljamaki E., Rintanen N., Kirsi M., Upla P., Wang W., Karjalainen M., Ikonen E. & Marjomaki V. 2013. Cholesterol dependence of collagen and echovirus 1 trafficking along the novel alpha2beta1 integrin internalization pathway. *PLoS One* 8: e55465.

Sonnichsen B., De Renzis S., Nielsen E., Rietdorf J. & Zerial M. 2000. Distinct membrane domains on endosomes in the recycling pathway visualized by multicolor imaging of Rab4, Rab5, and Rab11. *J Cell Biol* 149: 901-914.

Sorkin A. & Goh L.K. 2008. Endocytosis and intracellular trafficking of ErbBs. *Exp Cell Res* 314: 3093-3106.

Sorkin A. & Carpenter G. 1991. Dimerization of internalized epidermal growth factor receptors. *J Biol Chem* 266: 23453-23460.

Srivastava J., Procyk K.J., Iturrioz X. & Parker P.J. 2002. Phosphorylation is required for PMA- and cell-cycle-induced degradation of protein kinase Cdelta. *Biochem J* 368: 349-355.

Stoorvogel W., Oorschot V. & Geuze H.J. 1996. A novel class of clathrin-coated vesicles budding from endosomes. *J Cell Biol* 132: 21-33.

Takada Y., Ye X. & Simon S. 2007. The integrins. *Genome Biol* 8: 215.

Taub N., Teis D., Ebner H.L., Hess M.W. & Huber L.A. 2007. Late endosomal traffic of the epidermal growth factor receptor ensures spatial and temporal fidelity of mitogen-activated protein kinase signaling. *Mol Biol Cell* 18: 4698-4710.

Theos A.C., Truschel S.T., Tenza D., Hurbain I., Harper D.C., Berson J.F., Thomas P.C., Raposo G. & Marks M.S. 2006. A lumenal domain-dependent pathway for sorting to intralumenal vesicles of multivesicular endosomes involved in organelle morphogenesis. *Dev Cell* 10: 343-354.

Tooze J. & Hollinshead M. 1991. Tubular early endosomal networks in AtT20 and other cells. *J Cell Biol* 115: 635-653.

Triantafilou K. & Triantafilou M. 2003. Lipid raft microdomains: key sites for Coxsackievirus A9 infectious cycle. *Virology* 317: 128-135.

Triantafilou K., Fradelizi D., Wilson K. & Triantafilou M. 2002. GRP78, a coreceptor for coxsackievirus A9, interacts with major histocompatibility complex class I molecules which mediate virus internalization. *J Virol* 76: 633-643.

Triantafilou M., Triantafilou K., Wilson K.M., Takada Y., Fernandez N. & Stanway G. 1999. Involvement of beta2-microglobulin and integrin alphavbeta3 molecules in the coxsackievirus A9 infectious cycle. *J Gen Virol* 80 (Pt 10): 2591-2600.

Upla P., Marjomaki V., Nissinen L., Nylund C., Waris M., Hyypia T. & Heino J. 2008. Calpain 1 and 2 are required for RNA replication of echovirus 1. *J Virol* 82: 1581-1590.

Upla P., Marjomaki V., Kankaanpaa P., Ivaska J., Hyypia T., Van Der Goot F.G. & Heino J. 2004. Clustering induces a lateral redistribution of alpha 2 beta 1 integrin from membrane rafts to caveolae and subsequent protein kinase C-dependent internalization. *Mol Biol Cell* 15: 625-636.

Urbe S., Sachse M., Row P.E., Preisinger C., Barr F.A., Strous G., Klumperman J. & Clague M.J. 2003. The UIM domain of Hrs couples receptor sorting to vesicle formation. *J Cell Sci* 116: 4169-4179.

van Meel E. & Klumperman J. 2008. Imaging and imagination: understanding the endo-lysosomal system. *Histochem Cell Biol* 129: 253-266.

van Niel G., Wubbolts R., Ten Broeke T., Buschow S.I., Ossendorp F.A., Melief C.J., Raposo G., van Balkom B.W. & Stoorvogel W. 2006. Dendritic cells regulate exposure of MHC class II at their plasma membrane by oligoubiquitination. *Immunity* 25: 885-894.

Vonderheit A. & Helenius A. 2005. Rab7 associates with early endosomes to mediate sorting and transport of Semliki forest virus to late endosomes. *PLoS Biol* 3: e233.

Ward E.S., Zhou J., Ghetie V. & Ober R.J. 2003. Evidence to support the cellular mechanism involved in serum IgG homeostasis in humans. *Int Immunol* 15: 187-195.

Ward T., Powell R.M., Pipkin P.A., Evans D.J., Minor P.D. & Almond J.W. 1998. Role for beta2-microglobulin in echovirus infection of rhabdomyosarcoma cells. *J Virol* 72: 5360-5365.

Wegner C.S., Malerod L., Pedersen N.M., Progida C., Bakke O., Stenmark H. & Brech A. 2010. Ultrastructural characterization of giant endosomes induced by GTPase-deficient Rab5. *Histochem Cell Biol* 133: 41-55.

Whitley P., Reaves B.J., Hashimoto M., Riley A.M., Potter B.V. & Holman G.D. 2003. Identification of mammalian Vps24p as an effector of phosphatidylinositol 3,5-bisphosphate-dependent endosome compartmentalization. *J Biol Chem* 278: 38786-38795.

Wiley H.S. 2003. Trafficking of the ErbB receptors and its influence on signaling. *Exp Cell Res* 284: 78-88.

Wiley H.S. 1988. Anomalous binding of epidermal growth factor to A431 cells is due to the effect of high receptor densities and a saturable endocytic system. *J Cell Biol* 107: 801-810.

Wiley H.S., Herbst J.J., Walsh B.J., Lauffenburger D.A., Rosenfeld M.G. & Gill G.N. 1991. The role of tyrosine kinase activity in endocytosis, compartmentation, and down-regulation of the epidermal growth factor receptor. *J Biol Chem* 266: 11083-11094.

Williams C.H., Kajander T., Hyypia T., Jackson T., Sheppard D. & Stanway G. 2004. Integrin alpha v beta 6 is an RGD-dependent receptor for coxsackievirus A9. *J Virol* 78: 6967-6973.

Williams R.L. & Urbe S. 2007. The emerging shape of the ESCRT machinery. *Nat Rev Mol Cell Biol* 8: 355-368.

Yu X., Miyamoto S. & Mekada E. 2000. Integrin alpha 2 beta 1-dependent EGF receptor activation at cell-cell contact sites. *J Cell Sci* 113 (Pt 12): 2139-2147.

Zerial M. & McBride H. 2001. Rab proteins as membrane organizers. *Nat Rev Mol Cell Biol* 2: 107-117.

ORIGINAL PAPERS

I

ECHOVIRUS 1 INFECTION DEPENDS ON BIOGENESIS OF NOVEL MULTIVESICULAR BODIES

by

Mikko Karjalainen, Nina Rintanen, Moona Lehkonen, Katri Kallio, Anita Mäki, Kirsi Hellström, Valtteri Siljamäki, Paula Upla & Varpu Marjomäki 2011

Cellular Microbiology 13: 1975–1995.

Reprinted with kind permission of
© Jonh Wiley & Sons, Inc

II

COXSACKIEVIRUS A9 INFECTS CELLS VIA NONACIDIC MULTIVESICULAR BODIES

by

Moona Huttunen, Matti Waris, Ritva Kajander, Timo Hyypiä & Varpu Marjomäki 2014

Journal of Virology 88: 5138–5151.

Reprinted with kind permission of
© American Society for Microbiology

JVI
Journals.ASM.org

Coxsackievirus A9 Infects Cells via Nonacidic Multivesicular Bodies

Moona Huttunen,[a] Matti Waris,[b] Ritva Kajander,[b] Timo Hyypiä,[b] Varpu Marjomäki[a]

Department of Biological and Environmental Science and NanoScience Center, University of Jyväskylä, Jyväskylä, Finland[a]; Department of Virology, University of Turku, Turku, Finland[b]

ABSTRACT

***Coxsackievirus* A9 (CVA9) is a member of the human enterovirus B species in the *Enterovirus* genus of the family *Picornaviridae*. According to earlier studies, CVA9 binds to αVβ3 and αVβ6 integrins on the cell surface and utilizes β2-microglobulin, dynamin, and Arf6 for internalization. However, the structures utilized by the virus for internalization and uncoating are less well understood. We show here, based on electron microscopy, that CVA9 is found in multivesicular structures 2 h postinfection (p.i.). A neutral red labeling assay revealed that uncoating occurs mainly around 2 h p.i., while double-stranded RNA is found in the cytoplasm after 3 h p.i. The biogenesis of multivesicular bodies (MVBs) is crucial for promoting infection, as judged by the strong inhibitory effect of the wild-type form of Hrs and dominant negative form of VPS4 in CVA9 infection. CVA9 infection is dependent on phospholipase C at the start of infection, whereas Rac1 is especially important between 1 and 3 h p.i., when the virus is in endosomes. Several lines of evidence implicate that low pH does not play a role in CVA9 infection. The infection is not affected by Bafilomycin A1. In addition, CVA9 is not targeted to acidic late endosomes or lysosomes, and the MVBs accumulating CVA9 have a neutral pH. Thus, CVA9 is the second enterovirus demonstrated so far, after echovirus 1, that can trigger neutral MVBs, which are important for virus infection.**

IMPORTANCE

We demonstrate here that the enterovirus coxsackievirus A9 (CVA9) uses a nonclathrin and nonacidic pathway to infect cells. CVA9 does not accumulate in conventional late endosomes or lysosomes. We found that inhibitors of phospholipase C (PLC), Rac1, and the Na^+/H^+ exchanger decreased CVA9 infection. The PLC inhibitor acts on early entry, the Rac1 inhibitor acts between 1 and 3 h, when the virus is in endosomes, and the Na^+/H^+ exchange inhibitor acts during various steps during the virus life cycle. The infection depends on the formation of novel neutral multivesicular bodies (MVBs), which accumulate CVA9 during the first hours of entry. Thus, CVA9 is the second enterovirus demonstrated so far, after echovirus 1, that can trigger formation of neutral MVBs. The data show that these enteroviruses favor nonacidic conditions and complex MVBs to promote virus infection.

Human enteroviruses (HEVs) belong to the *Picornaviridae* family and have an approximately 7.5-kb-long single-stranded RNA genome with positive polarity. The genome is enclosed in an icosahedral protein capsid (30 nm in diameter), consisting of 60 copies of each of the four different structural proteins (VP1 to -4). HEVs are important human pathogens and cause illnesses ranging from the common cold to paralysis and other infections of the central nervous system, carditis, and severe disease syndromes in newborns. HEVs are classified into four species (A to D) on the basis of sequence analysis (1). Of the coxsackie A viruses (CVAs), type 9 is the only one that belongs to the HEV-B species (2). CVA9 particle has an extension containing an RGD (arginine-glycine-aspartic acid) motif at the C terminus of the VP1 protein that is not found in other HEVs except for echovirus 9 strain Barty (3).

CVA9 has been studied quite extensively by using molecular biology methods and in animal models. It has been shown that the virus attaches to αV integrins on the cell surface in several cell lines (4–6), including the lung carcinoma A549 cells used in this study. Other receptor candidates, such as glucose-regulated protein 78 A and a subunit of major histocompatibility complex class I (MHC-I) antigen (7), as well as β2-microglobulin (8), have also been proposed to be involved in CVA9 entry. After primary attachment, CVA9 does not appear to be bound to αV integrins during internalization (4), in contrast to another enterovirus, echovirus 1 (EV1), which is internalized in complex with its receptor, α2β1 integrin (9).

Most animal viruses take advantage of the host cell's endocytic mechanisms for internalization, and viruses have evolved to use one or more receptors and entry mechanisms (10). After arrival in the endosome lumen, viruses can be, for example, exposed to changes in pH and ions and proteolytic events that may initiate the uncoating process (11, 12). These events trigger changes in the virus particle that lead to the delivery of the genome into the cell for further replication.

From our previous studies, we know that β2-microglobulin, dynamin, and Arf6 play roles in the entry process of CVA9 (13). Recent structural studies also revealed details about the uncoating process of CVA9 (14). However, the cellular structures used by CVA9 for internalization and uncoating are still poorly known. Recently, we showed that another enterovirus, EV1, does not enter the host cell in acidic endosomes (15, 16). Instead, EV1 enters multivesicular bodies (MVBs) that morphologically resemble

Received 7 November 2013 **Accepted** 17 February 2014
Published ahead of print 26 February 2014
Editor: A. Simon
Address correspondence to Varpu Marjomäki, varpu.s.marjomaki@jyu.fi.
T.H. and V.M. contributed equally to this work.
Copyright © 2014, American Society for Microbiology. All Rights Reserved.
doi:10.1128/JVI.03275-13

acidic endosomes, even though they are biochemically different structures. This was a striking finding, as the MVBs are supposed to exhibit low pH, and acidity has been suggested to contribute to their biogenesis (17, 18). As both EV1 and CVA9 are acid-stable enteroviruses, we wanted to see if these viruses exhibit similarities in their internalization processes and, more importantly, if CVA9 could also induce the biogenesis of neutral MVBs. We show here that after uptake from the plasma membrane, CVA9 accumulates in nonacidic MVBs and that those structures are needed in CVA9 infection.

MATERIALS AND METHODS

Cells, viruses, and antibodies. The human lung carcinoma A549 cell line was obtained from the American Type Culture Collection (ATCC). The cells were maintained in Dulbecco's modified Eagle's medium (DMEM) containing 5% fetal bovine serum (FBS) supplemented with penicillin and streptomycin. CVA9 (Griggs strain) (2, 19) was propagated in A549 cells and purified in sucrose gradients as described previously (20). Culture medium for virus infections was supplemented with 1% FBS. For all infection studies, a multiplicity of infection (MOI) of 10 was used. Typically, this MOI leads to 50 to 70% infection in A549 cells.

Polyclonal rabbit antiserum against CVA9 was produced as described earlier (21), and mouse monoclonal antibody (MAb) K6 against the virus (22) was obtained from Lucia Fiore (Instituto Superiore di Sanita, Rome, Italy). Alexa Fluor 488 (AF-488)- and AF-555-labeled anti-mouse and anti-rabbit secondary antibodies and the ProLong Gold antifade reagent were obtained from Invitrogen. In addition, the following antibodies were used: J2, recognizing double-stranded RNA (dsRNA; MAb; catalog number 10010500; English & Scientific Consulting Kft.); early endosome antigen 1 (EEA1; MAb; catalog number 610457; BD Transduction Laboratories); Lamp1, to identify late endosomes and lysosomes (MAb; sc-20011; Santa Cruz Biotechnology); Rab7, to identify a member of the Rab family of small guanosine triphosphatases (GTPases) Rab7 (polyclonal antibody produced in rabbit; catalog number R4779; Sigma-Aldrich); phalloidin-tetramethylrhodamine B isothiocynate for labeling filamentous actin (catalog number P1951; Sigma); anti-green fluorescent protein (GFP; IgG fraction produced in rabbit) and LysoTracker Green for labeling acidic structures (product numbers A11122 and L7526, respectively; Invitrogen). 1,1′-Dioctadecyl-3,3,3′,3′-tetramethyl-indocarbocyanine perchlorate–low-density lipoprotein (DiI-LDL) was obtained from Seppo Ylä-Herttuala (University of Eastern Finland, Kuopio, Finland).

Immunofluorescence and confocal microscopy. A549 cells were grown on coverslips to subconfluency. CVA9 was first bound to the cells for 45 min on ice in DMEM containing 1% FBS, then the cells were washed, and after incubation at 37°C (in 1% DMEM) they were fixed with 4% paraformaldehyde (PFA) for 20 min, permeabilized with 0.2% Triton X-100 for 5 min, and stained with antibodies (dilutions made in 3% bovine serum albumin [BSA]-phosphate-buffered saline [PBS]). In the preinternalization labeling assays, CVA9 capsids were labeled with primary and secondary antibodies prior to the incubation. The cells were mounted using ProLong Gold antifade reagent with 4′,6-diamidino-2-phenylindole and examined with an Olympus microscope IX81 with a FluoView-1000 confocal setup or a Zeiss Cell Observer wide-field microscope.

Neutral red-CVA9 assay. A Neutral red-CVA9 (NR-CVA9) assay was conducted in A549 cells that were infected in the presence of 10 μg/ml of NR (catalog number 101369; Merck). The virus was released after overnight infection by freeze-thawing the cells three times and harvesting by centrifugation. NR-CVA9 was used without further purification. A549 cells were incubated with NR-CVA9 for 45 min on ice, washed, and incubated at 37°C in the darkness. At the indicated time points, the cells were exposed to light for 10 min at room temperature and subsequently transferred back to 37°C. The control cells were not exposed to the light reaction. At 6 h postinfection (p.i.), the cells were labeled for immunofluorescence (see "Immunofluorescence and confocal microscopy," above). The proportion of infected cells that reacted with the anti-CVA9 antibody was then calculated. In a subsequent NR-CVA9 assay, the Rac1 inhibitor NSC23766 (see "Chemical inhibitors," below, and Table 1) or dimethyl sulfoxide (DMSO) was added to A459 cells prior to incubation. At the indicated time points, the cells were exposed to light for 10 min at room temperature, after which the medium was changed back to 1% DMEM and the cells were transferred back to 37°C.

TABLE 1 Pharmacological inhibitors used in this study

Inhibitor	Effect	Concn used
U-73122	Phospholipase C inhibition	10 μM
Wortmannin	Phosphoinositide-3-kinase inhibition	100 nM
NSC23766	Rac1 inhibition	100 μM
IPA-3	Pak1 inhibition	5 μM
EIPA	Na^+/H^+ exchange inhibition	100 μM
Nocodazole	Microtubule depolymerization	33 μM
Bafilomycin A1	Vacuolar ATPase inhibition	50 nM
LY290042	Phosphoinositide-3-kinase inhibition	50 μM

$TCID_{50}$ assay. For the 50% tissue culture infective dose ($TCID_{50}$) assay, first the A549 cells were grown on 24-well plates to subconfluency. CVA9 was bound to cells for 45 min on ice in DMEM containing 1% FBS. Then, the cells were washed and incubated at 37°C for the indicated times, after which they were scraped and pelleted. The cell-virus pellets were stored at −20°C and later dissolved in PBS (containing 0.5 mM $MgCl_2$). For the $TCID_{50}$ assay, A549 cells were seeded in a 96-well plate and after overnight incubation the earlier-prepared cell-virus extracts were added to the first well and then serially diluted using 1:4 dilutions. The plates were incubated at 37°C for 2 days. To fix and label the extract mixtures in the plates, a 0.2% crystal violet stain (containing 5% formalin and 10% ethanol) was added to the wells. After incubation at room temperature, the wells were washed with H_2O and air dried. The $TCID_{50}$/ml values were calculated by using the Reed-Muench formula.

Chemical inhibitors. A549 cells were incubated at 37°C in DMEM supplemented with 1% FBS and 10 μM U-73122 (product number 662035; Calbiochem), 100 nM Wortmannin (product number 681675; Calbiochem), 100 μM NSC 23766 (product number 2161; Tocris Bioscience), 5 μM IPA 3 (product number 3622; Tocris Bioscience), 100 μM 5-(*N*-ethyl-*N*-isopropyl) amiloride (EIPA; product number A3085; Sigma), 33 μM Nocodazole (product number M1404; Sigma), 50 nM Bafilomycin A1 (product number 196000; Calbiochem), or 50 μM LY294002 (product number 440202; Calbiochem). The inhibitors were added to cells 30 min before the infection assay or at the indicated time points postinfection, depending on the assay. After 6 h, the proportion of the cells containing virus capsid protein were calculated. The cell viability after the drug treatments was tested in a 3-(4,5-dimethyl-2-thiazolyl)-2,5-diphenyl-2H-tetrazolium bromide (MTT) cell growth assay (product number CT02; Millipore) according to the manufacturer's instructions.

RT-PCR. The control and CVA9-infected A549 cells were collected from the plates 6 h p.i., pelleted, and stored at −70°C until analyzed. Methods for the RNA quantification have been described earlier (23). The cell pellets were subjected to automatic nucleic acid extraction in a MagNA Pure 96 instrument (product item 06541089001; Roche Applied Science). An aliquot of each extract was reverse transcribed with 1.2 μM antisense primer (5′-GAAACACGGACACCCAAAGTA) or sense primer (5′-CGGCCCCTGAATGCGGCTAA) or without a primer, using 20 U RevertAid H Minus Moloney murine leukemia virus reverse transcriptase (RT) and 4 U RiboLock RNase inhibitor (Fermentas). From the 20-μl RT reaction mixture, a 5-μl sample was used in a PCR with 600 nM each primer and Maxima SYBR master mix (Fermentas). Amplifications were run on a Rotor-Gene 6000 (Corbett Research) with the following cycling conditions: 95°C for 10 min; 40 cycles of 95°C for 15 s, 64 to 55°C (touchdown 1°C/cycle for the first 10 s) for 30 s, 72°C for 40 s; and final melt at 72 to 95°C, 1°C/5 s. A dilution series of a plasmid containing CVA9 cDNA (2)

was used to generate a standard curve. The copy numbers of the genomic and complementary strands were obtained by PCR after the RT reaction with the antisense primer and with the sense primer, respectively. The copy number observed after PCR of the RT reaction mixture without a primer was deducted from the assay values to correct for the primer-independent signal.

EM. For visualization of the internalized CVA9 particles (see Fig. 3B and D, below), prior to the incubation at 37°C A549 cells were labeled with anti-CVA9 rabbit polyclonal antibody against the viral capsid proteins and, subsequently, with protein A (PA)-gold (diameter, 10 nm; Cell Microscopy Center, Utrecht, Netherlands). The samples were processed for electron microscopy (EM) as described previously (24). Briefly, the cells were fixed in 4% PFA containing 0.1% glutaraldehyde in 50 mM Tris buffer, pH 7.6, at room temperature for 1 h or at 4°C overnight. After 1% osmiumtetroxide (in H_2O) treatment, the cells were dehydrated, stained with 2% uranylacetate, and embedded in LX-112 Epon (product number 21210; Ladd Research).

In addition to this monolayer preparation, EM samples were also prepared by cell pelleting. A549 cells, grown on plates, were washed with 0.1 M phosphate buffer and fixed with 2.5% glutaraldehyde in the buffer at room temperature for 10 min. The samples were centrifuged (6,000 rpm, 30 min) and washed three times with 0.1 M phosphate buffer and two times with H_2O. The pellets were then embedded into 2.5% agarose in H_2O at 37°C. The pelleted samples in agarose were fixed again and stained with 1% osmium tetroxide in H_2O at room temperature for 30 min. After three washes, the samples were stained with 1% uranyl acetate in H_2O at room temperature for 30 min, washed again, and dehydrated with acetone (two times with 30%, 50%, 70%, and 100% for 10 min). Before proceeding to the 100% LX-112 Epon embedding step, the samples were preembedded with a mixture of Epon in 100% acetone (equal volumes) at room temperature for 45 min. The monolayer and pellet samples were cut, and the section images were observed by using a Jeol 1400 microscope.

For cryo-immuno-EM (see Fig. 7A to C, below), cells were treated as described by Slot and Geuze (25). Briefly, nontransfected and transfected A549 cells were infected with CVA9. The cells were then fixed in 4% PFA in 0.1 M phosphate buffer at room temperature, after which the cells were scraped from the substrate and further fixed for 1 h. After pelleting, the cells were immersed in 12% gelatin in PBS, cut into small pieces, placed in 2.3 M sucrose in PBS at 4°C, and frozen in liquid nitrogen. Thin cryosections were cut with a Leica Ultracut UCT microtome. For double immunolabeling, the sections were first incubated in 5% BSA, 0.1% gelatin in PBS. Antibodies and gold conjugates were diluted in 0.1% BSA in PBS. All washings were performed in 0.1% BSA-C in PBS. After blocking as described above, sections were exposed to the primary antibodies (rabbit anti-CVA9 and rabbit anti-GFP) for 60 min each (with a blocking step in between). After washing, mixtures with PA-gold complex (diameters, 5 and 10 nm, respectively) were incubated. The controls were prepared by carrying out the labeling procedure without primary antibody. The sections were embedded in methylcellulose and examined with a Jeol 1400 microscope.

Transfections. FuGENE HD transfection reagent (product number E2311; Promega) was used for transfections of subconfluent A549 cells according to the manufacturer's instructions. The cells were used for experiments after an expression time of 48 h. The Hrs-WT–GFP fusion was obtained from Sylvie Urbé (Cellular and Molecular Physiology, University of Liverpool, Liverpool, United Kingdom), the VPS4-E235Q–GFP plasmid was obtained from Harald Stenmark (Department of Biochemistry, Institute for Cancer Research, The Norwegian Radium Hospital, Oslo, Norway), the Rab5-Q79L–yellow fluorescent protein (YFP) and Rab5-S34N–enhanced green fluorescent protein (EGFP) fusions were obtained from Lucas Pelkmans (Institute of Molecular Life Sciences, University of Zurich, Zurich, Switzerland), and the Rab5-WT–GFP fusion was obtained from Miguel Seabra (Faculty of Medicine, National Heart and Lung Institute, Imperial College, London, United Kingdom).

DiI-LDL assay. A549 cells were grown on coverslips to subconfluency. CVA9 was first bound to the cells for 45 min on ice in DMEM containing 1% FBS. After removing the excess virus, the cells were incubated in 1% DMEM complemented with 30 μg/ml of DiI-LDL for 2 h. After fixation and permeabilization, the cells were stained with CVA9 anti-capsid, anti-Lamp1, and fluorescent secondary antibodies.

LysoTracker green assay. One hour after CVA9 inoculation, LysoTracker Green was added to the A549 cells and the mixture was incubated for 1 h at 37°C. CVA9 was labeled prior to internalization, which was initiated by moving A549 cells to a preheated (37°C) microscope sample stage. Localization of LysoTracker Green and CVA9 capsid proteins was followed during the infection in live cells by using the Zeiss LSM510 confocal setup with CO_2-independent medium (Life Technologies) containing 1% FBS.

Intraendosomal pH measurements. Intraendosomal pH measurements were conducted as previously described (15). Briefly, CVA9 was first bound to A549 cells on ice, followed by incubation with rabbit polyclonal anti-CVA9 antibody. Then, equal amounts of goat anti-rabbit–fluorescein and goat anti-rabbit AF-555 conjugates were bound to the cells on ice, and the cells were moved to 37°C for 4 h. The cells were kept at 37°C in the Zeiss LSM510 confocal setup under CO_2-independent medium containing 1% FBS. Confocal sections were taken 1, 2, and 3 h p.i. To construct a pH titration curve, cell membranes were permeabilized with 20 μM nigericin in pH standard buffer solutions [150 mM KCl, 5 mM glucose, and 15 mM Tris (pH 7.5 and 7.0) or 15 mM 2-(*N*-morpholino)ethanesulfonic acid (pH 6.5)]. Altogether, 30 cells in each case from two independent experiments were scanned, and the ratio of fluorescein/AF-555 fluorescence was determined for each section with the program BioImageXD (26).

Data analysis and processing of the microscopy data. An open source software package, BioImageXD (26), was used for the confocal image quantifications. Levels for the laser power, detector amplification, and optical sections were optimized for each channel before starting the imaging. In the dsRNA assay, altogether 20 cells from two independent experiments, 10 cells from each, and from all different time points were randomly selected and optically sectioned using a confocal microscope. For measuring of the number, size, and intensities of dsRNA objects, the following BioImageXD protocol was used. First, volumes were filtered with a difference-of-Gaussians filter to suppress noise and enhance regions of interest. Next, a manually selected threshold level was applied to produce binary image data. Finally, individual objects were found for analysis by computing a Euclidean distance transform on binary data, inverting the result, and applying the watershed transform from local minimal positions. Depending on the experiment, objects smaller than 0, 6, or 10 voxels were removed.

To quantify the level of colocalization, altogether 20 cells from two independent experiments, 10 cells from each, were randomly selected and optically sectioned by using a confocal microscope. Colocalization was evaluated from the center slice images or from the projection of the cell by examination of the merged images, and further analysis was performed with the BioImageXD program. The images were preprocessed with a difference-of-Gaussians filter to remove noise and enhance regions of interest before the colocalization analysis. Thresholds for the analysis were adjusted manually to eliminate fluorescence originating from the background and from diffuse staining. Signal overlap was expressed separately for both of the channels, as a proportion of the intensity colocalizing with the other channel. Statistical significance of observed colocalization was calculated by using Costes algorithm (27), embedded within the software, and only colocalizations with zero coincidence probabilities were taken into account (i.e., $P = 1.00$).

For measuring the intensities of the vesicles in the pH experiment, a multistep segmentation protocol implemented within BioImageXD software was used. Images were first smoothed with the Gaussian filter and binary by using an adaptively calculated threshold value (mean + 5) from 10 lateral pixel size radius regions. Objects were defined using the Euclid-

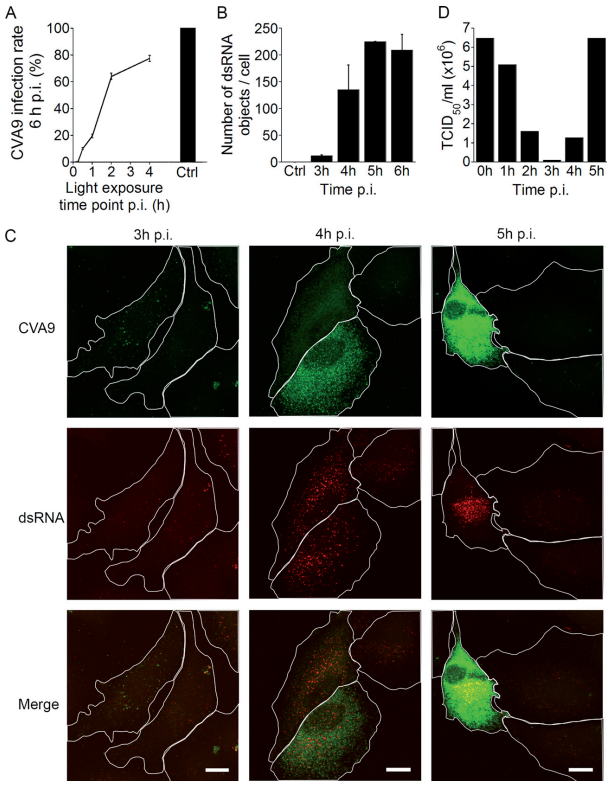

FIG 1 Uncoating and replication of CVA9 in A549 cells. (A) The infection rate (the proportion of cells producing viral capsid protein 6 h p.i.) after incubation with Neutral Red (NR)-labeled CVA9. The cells were exposed to light treatment at different time points, and the infection was continued to 6 h p.i. The control cells (Ctrl) were infected and incubated in the darkness. The results are averages of two independent experiments (± standard errors [SE]) for 600 cells counted. (B) The number of dsRNA structures in cells. A549 cells were infected with CVA9; samples were fixed at different time points and labeled with anti-dsRNA and anti-CVA9 capsid antibodies. The results are averages of two independent experiments (± SE). At each time point, 20 cells were imaged. (C) Representative confocal images of CVA9-infected A549 cells at 3, 4, and 5 h p.i., labeled with anti-CVA9 capsid (green) and anti-dsRNA (red) antibodies. Bars, 10 μm. (D) The $TCID_{50}$/ml values at different time points p.i. A549 cells were infected with CVA9, collected at different time points, and serially diluted on top of A549 monolayers. After 2 days of incubation, $TCID_{50}$/ml values were calculated.

ean distance transform and watershed transform as explained above. Finally, all objects of sizes smaller than 5 voxels were removed from the analysis to remove noise and small debris.

Statistical testing. A *t* test was used for pairwise statistical comparison between samples. For proportions or ratios, a *t* test was applied after an arcsine square root transformation of the original variable to convert the binomial distribution of the data to follow a normal distribution. For testing the means between samples from EM, a binomial *t* test was applied.

RESULTS

Uncoating and replication of CVA9. In order to determine the time course of CVA9 uncoating in A549 cells, we used a Neutral red-labeled virus (NR-CVA9) (28). Light exposure causes irreversible cross-linking of the labeled viral genome, thus inhibiting the viral uncoating process. If the viruses have not undergone uncoating before the light reaction, no new virus will be synthesized, whereas uncoated viruses will initiate a replication cycle that includes expression of VP1. If the light exposure was performed 0 or 15 min p.i., the cells did not produce VP1 at 6 h p.i. When the light exposure was performed at 30 min or 1 h p.i., less than 20% of the cells were infected at 6 h p.i., suggesting that the uncoating process had started but was not yet at its peak (Fig. 1A). When the light treatment was carried out at 2 and 4 h p.i., around 60 to 75% of the cells expressed VP1 at 6 h after infection. The results suggest that the majority of CVA9 capsid uncoating takes place around 2 h after virus attachment.

To investigate the timing of active replication, we fixed the infected cells at different time points and labeled them with both a CVA9 (anti-capsid) antibody and a J2 antibody. The J2 antibody

recognizes dsRNA that is the primary element in the infection cycle. The mock-infected cells were negative for J2 labeling (Fig. 1B). The first visible dsRNA-containing structures appeared in cells at 3 h p.i. (Fig. 1B and C), and they appeared in scattered locations near but not colocalizing with the structures positive for CVA9 capsid protein (Fig. 1C). The number of dsRNA structures (Fig. 1B and C) in addition to the volume and intensity increased as the infection progressed (data not shown).

Furthermore, we performed a $TCID_{50}$ assay to evaluate the timing of infective particle formation. Infected A549 cells were collected at different time points, fragmented, serially diluted, and cultured on top of a new monolayer of A549 cells. After 2 days of incubation, the cells were fixed and labeled with crystal violet dye, and $TCID_{50}$/ml values were calculated. The results showed that as the entry and uncoating processes begin, the CVA9 particles start to lose their infectivity after 1 h (Fig. 1A and D). After the 3-h time point, at the same time when dsRNA structures appear in the cytoplasm (Fig. 1B and C), the $TCID_{50}$/ml values correspondingly increased (Fig. 1D). Taken together, we conclude that the uncoating of the majority of CVA9 particles takes place around 2 h p.i., and active replication (visible dsRNA structures) of the virus and new infective particle formation occur after 3 h p.i.

Effects of chemical inhibitors of endocytosis on CVA9 infection. Earlier studies suggested that components belonging to the clathrin pathway are not involved in CVA9 entry (13). However, there is still very little understanding of CVA9 internalization, and we wanted to investigate in further detail some players that have effects on EV1 entry, e.g., phospholipase C (PLC), Pak1, Rac1, and the Na^+/H^+ exchanger (29). We decided to use chemical inhibitors that have been widely used to downregulate the action of these proteins. The inhibitors used in this study and their mode of action are shown in Table 1. First, we determined which inhibitors affected CVA9 infection. We treated the A549 cells with the chemical inhibitors for 30 min prior to CVA9 binding on ice. After removing the unbound virus, the cells were incubated at 37°C with the inhibitors. At 6 h p.i., the cells were fixed and labeled with the primary anti-CVA9 antibody and fluorescent secondary antibody. The proportion of A549 cells full of virus capsid proteins was calculated in different situations (Fig. 2A). U-73122, NSC23766, and EIPA caused statistically highly significant ($P = 0.0$, 0.0004, and 0.0, respectively) decreased in infection, whereas Wortmannin and IPA-3 had no significant effects. To evaluate the cell viability after the drug treatments, a colorimetric MTT assay (Millipore) was performed. The drug treatments did not cause significant cell death (data not shown), indicating that the observed changes in virus proliferation were due to inhibitory effects of the drugs.

Next, we carried out an RT-PCR assay to find out whether the drugs affected new viral RNA production. In correspondence with the immunofluorescent (IF) assay results described above, U-73122, NSC23766, and EIPA caused statistically significant decreases ($P = 0.006$, 0.01, and 0.006, respectively) in genomic strand production (Fig. 2B). The same inhibitors seemed to decrease the production of the complementary strand also, although the reductions were not statistically significant. As in the IF assay (Fig. 2A), Wortmannin and IPA-3 had no statistically significant effects on virus RNA production (Fig. 2B). To verify the Wortmannin result, we also used the drug LY290042, another inhibitor of phosphatidylinositol 3-kinase (PI3-kinase), which gave similar results (data not shown). The results from both the IF and RT-PCR assays thus suggested that PLC, Rac1, and Na^+/H^+ exchanger inhibitors decrease CVA9 infection in A549 cells.

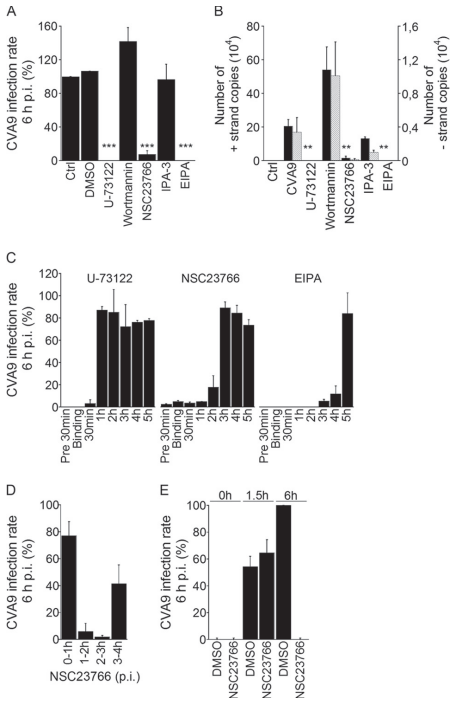

FIG 2 Effects of endocytosis inhibitors on CVA9 infection. (A and B) A549 cells were preincubated with inhibitors (Table 1) that were also present throughout the experiment. After virus binding, the cells were incubated for 6 h. (A) The infection percentages (cells producing high amounts of CVA9 capsid protein at 6 h p.i.) of control (Ctrl and DMSO) and inhibitor-treated cells were quantified. The experiment was performed three times, and the means are shown (± standard errors [SE]). Statistical significance was calculated with a paired-sample *t* test (after arcsine square root transformation). ***, $P < 0.001$. (B) The presence of genomic (+) and complementary (−) RNA strands was analyzed with RT-PCR. The results are averages of three parallel samples (± SE). Statistical significance was calculated with a paired-sample *t* test. **, $P < 0.01$. (C) The inhibitors were introduced to the cells at different time points postinfection, and the incubation with the inhibitors was carried out until 6 h p.i., after which the infection percentages were quantified. The experiment was performed two times, and the means are shown (± SE). (D) The Rac1 inhibitor (NSC23766) was introduced to the cells at different time points. After the 1-h treatment, the medium was replaced with fresh 1% DMEM and the incubation was carried out until 6 h p.i., after which the infection percentages were quantified. The experiment was performed two times, and the means are shown (± SE). (E) The NR-CVA9 was bound to A549 cells in the darkness. The Rac1 inhibitor (NSC23766) or DMSO (a control) were introduced to the cells, and cells were incubated in the darkness for 0, 1.5, or 6 h. At these time points, the 10-min light reactions were carried out, the drug was replaced with fresh medium, and cells were transferred back into the incubator for the remaining incubation time (6 h). The infection percentages were quantified at each time point. The experiment was performed two times, and the means are shown (± SE).

In order to clarify more carefully the temporal regulation of PLC, Rac1, and Na^+/H^+ exchanger inhibitors in CVA9 infection,

we performed a more detailed time course inhibitory assay. In this assay, the drugs were introduced to the cells at different time points postinfection, and incubation with the inhibitors was carried out until 6 h p.i. After fixation, the VP1 protein was labeled with fluorescent antibody and the proportions of A549 cells containing newly synthesized virus proteins were calculated under different conditions. As shown in Fig. 2C, the inhibitory effect of U-73122 was limited to early stages of infection (before 1 h p.i.). In the case of NSC23766, the inhibitory effect seemed to be limited to time points before 3 h p.i. (Fig. 2C). EIPA, on the other hand, disrupted the infection more or less throughout the experiment (Fig. 2C).

To better elucidate the time point when the Rac1 inhibitor affects CVA9 infection, the 1-h interval treatments with NSC23766 were carried out over 6 h of infection. The virus bound onto the cells without the inhibitor. If the Rac1 inhibitor treatment were performed at 0 to 1 h p.i. or later, NSC23766 was replaced with fresh 1% DMEM; at the 6-h time point, only a 20% decrease in the infection rate was observed, relative to the DMSO control (set as 100%) (Fig. 2D). This result also confirmed the known fact that the inhibitory effect of NSC23766 is reversible. If the NSC23766 treatment were carried out between the 1- to 2-h or 2- to 3-h time points, CVA9 infection rates were dramatically decreased (Fig. 2D). The drug treatment at 3 to 4 h p.i. (Fig. 2D) confirmed the previous results (Fig. 2C; NSC23766 chart), indicating that after the 3-h time point NSC23766 lost its inhibitory effect. These results suggested to us that Rac1 is somehow involved in the CVA9 infection process at time points between 1 and 3 h.

As the inhibitory effect of NSC23766 seemed to coincide with the time points most important for the CVA9 uncoating process, we carried out a variation of the NR assay with this drug. In this experiment, NR-CVA9 bound to A549 cells on ice in the dark. After removing the unbound virus, the Rac1 inhibitor (NSC23766) or DMSO (control) was introduced to the cells, and cells were incubated in the dark for 0, 1.5, or 6 h. At these time points, the 10-min light reactions were carried out, the drug was replaced with fresh 1% DMEM without the inhibitor, and cells were put back into the incubator for the remaining time (total incubation time, 6 h). After fixation, the cells were labeled with the primary anti-CVA9 antibody and fluorescent secondary antibody, and the proportions of A549 cells containing newly synthesized virus proteins were calculated. As shown in Fig. 2E, if the light reaction was executed at the 0-h time point, no newly synthetized VP1 proteins were observed after 6 h of incubation in either DMSO- or NSC23766-treated cells, as expected (control experiments). In addition, if the NSC23766 was kept on the cells throughout the assay, the virus infection was totally inhibited (Fig. 2E, NSC23766 at 6 h), as already shown in Fig. 2A and B for the other assays. Furthermore, DMSO-treated cells were infected after 6 h, as expected (Fig. 2D). Interestingly, if the light reaction was executed at the 1.5-h time point, both DMSO- and NSC23766-treated cells were infected with similarly lower efficiencies at 6 h p.i. The magnitude of infection was in good agreement with the uncoating results obtained and illustrated in Fig. 1A. The results therefore suggest that the Rac1 inhibitor NSC23766 does not affect the uncoating of CVA9, and this leaves us with an interesting suggestion, that Rac1 may exert its effect through other means than uncoating when the virus resides in endosomes.

CVA9 accumulates in MVBs. In order to investigate CVA9 infection at the ultrastructural level, we used EM methods. CVA9 was first bound onto the surface of A549 cells on ice, and the virus particles were labeled with an anti-capsid antibody and PA-gold particles (diameter, 10 nm). Cell-bound CVA9, attached to antibody and PA-gold, was then internalized at 37°C, and the cells were fixed at various time points. We confirmed by fluorescence microscopy methods that this preinternalization labeling of the virus maintained to a large extent its infectivity (Fig. 3A). At 5 min, CVA9 particles were found mostly on the plasma membrane, usually near membrane extensions (Fig. 3B). After 15 min, the virus was still found mainly attached to these ruffles in several areas (data not shown). When the CVA9 particles and cellular actin were labeled with fluorescent dyes, these ruffles were typically actin positive (Fig. 3C).

We were interested in the nature of the structures where CVA9 accumulated during the entry process. The EM assay indicated that at 30 min, around 28% of CVA9 particles were internalized and could be found in vesicles close to the plasma membrane (Fig. 3D) and that about half of the vesicular structures had visible intraluminal vesicles (ILVs) (Fig. 3E). At the 30-min time point, the colocalization of CVA9 capsid protein, labeled with IF methods before virus internalization, with early endosome (EEA1) antibody, was negligible (Fig. 3F). EM images taken at 2 h p.i. revealed that internalized CVA9 was then mostly found in MVBs (Fig. 3D and E). The MVBs resembled typical multivesicular structures, with several small ILVs and occasional larger vesicles. Strikingly, at the 2-h time point, the preinternalization labeled CVA9 did not colocalize with the lysosomal marker Lamp1 (Fig. 3G). Quantification of the proportions of the CVA9-containing endosomes with or without ILVs showed that the number of multivesicular structures containing CVA9 increased significantly ($P < 0.001$) between 30 min and 2 h (Fig. 3E). Uninfected cells, treated with primary and secondary antibodies in the EM assay, showed negligible PA-gold background. These results demonstrated that during the internalization process, CVA9 accumulates in MVBs, which interestingly seems to be distinct from EEA1- and Lamp1-positive structures.

CVA9 is not targeted to EEA1- or Lamp1/Rab7-positive structures, and the infection is microtubule independent. Although the CVA9-MVBs in the EM images closely resembled the acidic early and late endosomes, they did not seem to colocalize with the canonical endosomes in the IF images (Fig. 3D, F, and G). Therefore, the role of early and late endosomes in CVA9 infection was studied further, and the presence of the virus particles in these structures was quantified. The A549 cells were infected with CVA9, and between 15 to 120 min of incubation, cells were fixed and labeled with CVA9 anticapsid antibody and early endosome (EEA1) or late endosome/lysosome (Lamp1 and Rab7) antibodies. In addition, multiple transfections were prepared to investigate the role of Rab5 in CVA9 infection, and the colocalization between CVA9 and DiI-LDL during the internalization process was determined.

During 15 to 60 min of incubation, a low amount of the CVA9 particles (labeled after fixation) colocalized with EEA1-positive structures (Fig. 4A). Only a few vesicles showed colocalization in the IF images, and it seemed that even the low amount of colocalization was somewhat exaggerated, due to close apposition of the separate vesicles and limited resolution of the confocal microscopy images, leading to some false colocalization. In addition to EEA1 labeling, we were interested in the role of Rab5 in CVA9 infection. The A549 cells were transfected with wild-type (WT)-Rab5–GFP, constitutively active Rab5 (Rab5-Q79L–GFP), or dominant negative (DN)-Rab5 (Rab5-S34N–GFP); after 48 h of

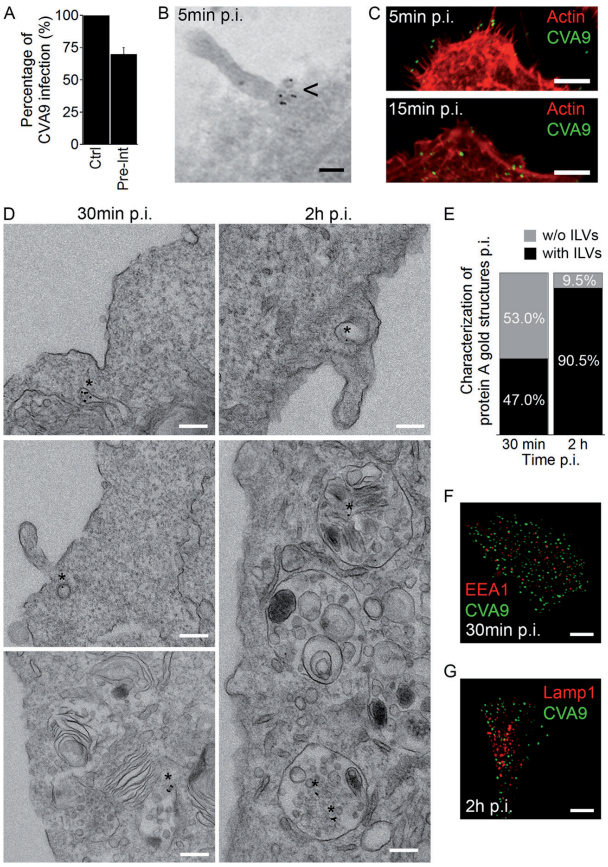

FIG 3 CVA9 accumulates in MVBs. (A) After CVA9 binding onto A549 cells, the virus was labeled with primary anti-CVA9 capsid antibody followed by fluorescent secondary label (Pre-Int). The 6-h infection was carried out, and the infection rates (cells producing CVA9 capsid protein at 6 h p.i.) were quantified. The experiment was performed three times, and the means are shown (± standard errors [SE]). (B) For EM, the virus and antibody binding was as performed as described for panel A, except that the fluorescent secondary label was replaced with protein A (PA)-gold particles (diameter, 10 nm). After 5 min of incubation at 37°C, the samples were prepared for EM (epon embedding). The arrowhead indicates the presence of CVA9 label in sections. Bar, 100 nm. (C) A549 cells were infected with CVA9, and after 5 and 15 min at 37°C, the samples were fixed and labeled with anti-CVA9 capsid antibody (green) and tetramethyl rhodamine isothiocyanate phalloidin (red). Bars, 5 μm. (D) Sample preparations were prepared as described for panel B. The asterisks indicate the presence of CVA9 label in the sections after 30 min and 2 h of incubation. Bars, 200 nm. (E) The ratio of CVA9-positive structures with (black bars) or without (gray bars) ILVs was quantified from more than 300 cells. (F and G) Prior to the 30 min or 2 h of incubation at 37°C, A549 cells were labeled with anti-CVA9 antibody (green). After the incubations, samples were fixed and labeled with EEA1 or Lamp1 antibodies (red). Bars, 10 μm.

expression the cells were infected with CVA9 for 6 h, and virus capsid protein production in transfected A549 cells was determined. The constitutively active mutant had little effect on CVA9 infection, whereas the DN Rab5 (Rab5-S34N–GFP) construct inhibited CVA9 infection in a statistically significant manner ($P = 0.009$) (Fig. 4B).

Colocalization of virus particles with Lamp1-positive structures was quite low, reaching a maximum 25% at the 2-h time point (Fig. 4C), suggesting that CVA9 mainly associates with structures other than Lamp1-positive endosomes. Furthermore, the colocalization of CVA9 with Rab7 was even lower (<10%) during the 30- to 120-min incubation periods, indicating that CVA9 does not traffic through late endosomes (Fig. 4D). According to our previous observations, and as stated above, close apposition of the endosomal vesicles between virus signal with Lamp1 may cause a false-positive signal due to limited resolution under confocal microscopy (16). As seen in Fig. 4C and D, Lamp1 vesicles were more crowded in the perinuclear region than Rab7-positive structures, which may be the reason why CVA9

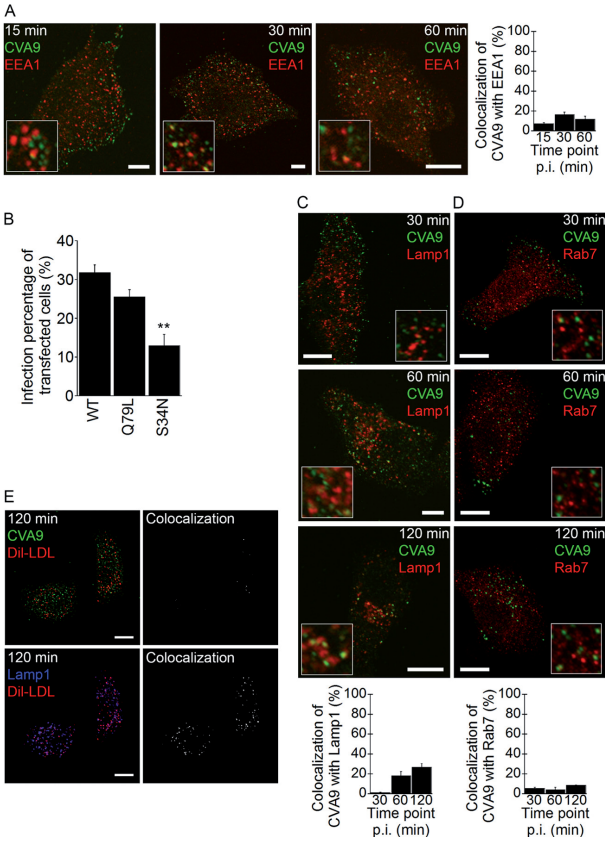

FIG 4 CVA9 infection is not associated with the lysosomal pathway. (A) A549 cells were infected with CVA9, and after 15, 30, or 60 min of incubation, the samples were fixed and labeled with anti-CVA9 capsid antibody (green) and EEA1 antibody (red). Quantification of colocalization of CVA9 with EEA1 was done from projection stacks of single cells by using the BioImageXD software (see Materials and Methods). Altogether, 30 cells from three independent experiments were analyzed. The results are shown as mean values (± standard errors [SE]). Bars, 10 μm. (B) A549 cells were transfected with a wild-type Rab5 (Rab5-WT–GFP; WT in the chart), constantly active Rab5 construct (Rab5-Q79L–GFP; Q79L in the chart), or a dominant negative Rab5 construct (Rab5-S34N–GFP; S34N in the chart). After 48 h for expression, the cells were infected with CVA9 and the infection percentage (cells producing CVA9 capsid protein at 6 h p.i.) of transfected cells was quantified. The results are mean values of two independent experiments (± SE), and statistical significance was calculated with a paired-sample *t* test (after arcsine square root transformation). **, $P < 0.01$. (C and D) A549 cells were treated and analyzed as described for panel A. After 30, 60, and 120 min of incubation, the samples were fixed and labeled with anti-CVA9 capsid antibody (green) and Lamp1 or Rab7 antibodies (red). Altogether, 30 cells from three independent experiments were analyzed. The results are shown as mean values (± SE). Bars, 10 μm. (E) CVA9 was internalized into A549 cells with DiI-LDL (30 μg/ml) for 2 h. The samples were fixed and labeled with anti-CVA9 capsid (green) and Lamp1 antibodies (blue); DiI-LDL is seen in red. The colocalized voxels between CVA9 and DiI-LDL or Lamp1 and DiI-LDL were done from projection stacks and using the BioImageXD software.

colocalization with Lamp1 seems to be higher than with Rab7. In order to verify the negligible use of the clathrin pathway, we examined simultaneous entry of CVA9 with DiI-LDL, which is the canonical marker of the clathrin pathway, which ends eventually in lysosomes. Co-uptake of DiI-LDL and CVA9 resulted in clearly distinct endosomes in the cytoplasm after 2 h (Fig. 4E). Several DiI-LDL vesicles costained with Lamp1, whereas CVA9 stayed separate, further demonstrating that CVA9 acts separate from the clathrin-dependent pathway.

The microtubule-depolymerizing agent Nocodazole (Noc) blocks transport of the cargo from early to late endosomes, resulting in the accumulation of cargo in earlier structures in the acidic pathway (30). We thus decided to use this drug to inhibit CVA9 entry to late endosomes in order to evaluate whether the virus transfer to late endosomes is important for CVA9 infection. We treated A549 cells similarly as in the chemical inhibitor assay above (see Materials and Methods). The results showed that Noc treatment did not inhibit infection during the 6 h of incubation

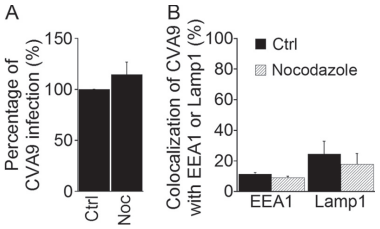

FIG 5 Microtubules are not needed in CVA9 infection. (A) A549 cells were preincubated with nocodazole (Noc) (see Table 1). After CVA9 binding, cells were incubated for 6 h. The inhibitor was present throughout the experiment. The proportions of infected cells (cells producing CVA9 capsid protein 6 h p.i.) among control (Ctrl) and inhibitor-treated cells were quantified. The experiment was repeated three times, and the mean values are shown (± standard errors [SE]). Statistical significance was calculated with a paired-sample *t* test (after arcsine square root transformation). (B) A549 cells were preincubated with Noc, and the cells were infected with CVA9. After a 1-h (EEA1) or 2-h (Lamp1) incubation, the samples were fixed and labeled with anti-CVA9 and EEA1 or Lamp1 antibodies, respectively. Quantification of colocalization of CVA9 with EEA1 and Lamp1 was done from confocal projection stacks of single cells by using BioImageXD software. Thirty cells from each of the three independent experiments were analyzed. The results are shown as mean values (± SE).

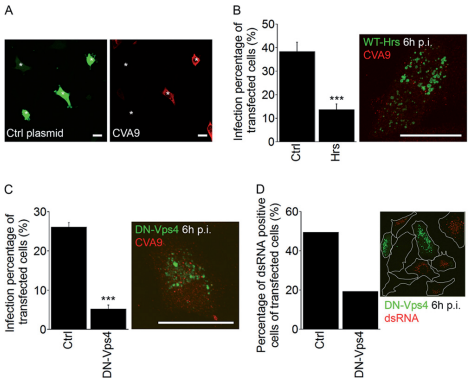

FIG 6 The ESCRT complex is needed for successful CVA9 infection. (A) Fluorescent images of GFP-transfected cells (Ctrl plasmid, green) and CVA9-infected cells (red) at 6 h p.i. The asterisks represent transfected cells. Bars, 30 μm. (B) A549 cells were transfected with a wild-type plasmid of Hrs (Hrs-WT–GFP; Hrs in the chart) or the control GFP construct (Ctrl). After 48 h for expression, cells were infected with CVA9, and the infection percentages (cells producing CVA9 capsid protein 6 h p.i.) of transfected cells were quantified 6 h p.i. The results are mean values of two independent experiments (± standard errors [SE]), and statistical significance was calculated with a paired-sample *t* test (after arcsine square root transformation). ***, $P < 0.001$. In the maximum intensity projection of confocal sections (time point, 6 h p.i.), the Hrs-WT–GFP was visualized in green and CVA9 was visualized in red. Bar, 30 μm. (C) The dominant negative mutant of Vps4 (VPS4-E235Q–GFP; DN-Vps4 in the chart) and the control GFP construct (Ctrl) were transfected in cells. Sample preparation and analysis were performed as described for Fig. 6B. The results are mean values of two independent experiments (± SE), and statistical significance was calculated with a paired-sample *t* test (after arcsine square root transformation). ***, $P < 0.001$. Maximum intensity projection of confocal sections of a cell expressing VPS4-E235Q–GFP (DN-VPS4, green) at 6 h p.i. CVA9 is shown in red. Bar, 30 μm. (D) The transfection was performed as for panel C. After CVA9 infection (6 h), the samples were labeled with anti-dsRNA antibody, and the percentages of dsRNA-positive cells within the transfected cells were calculated. In both cases, more than 50 cells were quantified.

(Fig. 5A). We confirmed the breakdown of the microtubule network after Noc treatment based on diffuse cytoplasmic labeling of tubulin monomers when we used IF labeling (data not shown). The cell viability after the drug treatments was verified by the colorimetric MTT assay (Millipore) (data not shown). Next, we tested whether Noc treatment caused an accumulation of CVA9 label in early endosomes, which would be expected if late endosomes were used in the viral infectious pathway. A549 cells were treated with Noc for 30 min prior to CVA9 binding, and after 1 h of incubation the cells were fixed and labeled with CVA9 anticapsid antibody and EEA1 antibody. As Fig. 5B shows, such accumulation did not occur. In addition, we studied whether Noc treatment affected CVA9 colocalization with Lamp1. The results showed that Noc treatment did not statistically significantly decrease CVA9 colocalization with Lamp1 ($P = 0.62$) (Fig. 5B). In conclusion, since Noc treatment did not inhibit CVA9 infection or affect colocalization with EEA1, the results further confirmed that CVA9 internalization is not dependent on the canonical entry pathway (from early to late endosome and lysosome).

MVBs are important for CVA9 infection. In mammalian cells, MVBs are form via progressive involution of the endosomal limiting membrane in a process catalyzed by the endosomal sorting complex required for transport (ESCRT) (31, 32). One of the first components that acts in the complex set of events leading to protein sorting to MVBs is ESCRT 0, the hepatocyte growth factor-regulated tyrosine kinase substrate (Hrs) (33). Hrs binds directly to the limiting membrane of the endosome and recruits other ESCRT components to the site. Since earlier results suggested that overexpression of WT-Hrs causes a block of epidermal growth factor receptor (EGFr) transport, possibly by titration of interacting factors required downstream of Hrs (e.g., ESCRTs) or due to problems in the release of Hrs from endosomal membranes (34), we were interested in whether Hrs overexpression had an effect on CVA9 infection. We transfected A549 cells with Hrs-WT–GFP or a control GFP plasmid, and after 48 h of expression the cells were infected with CVA9 for 6 h and virus capsid protein was labeled. In control cells, transfected with the control GFP plasmid, the cytoplasm contained large amounts of virus capsid proteins after 6 h p.i. (Fig. 6A). In contrast, the overexpression of WT-Hrs–GFP had a strong and statistically significant ($P = 0.0007$) inhibitory effect on VP1 production (Fig. 6B). In WT-Hrs-transfected cells, CVA9 label was found in vesicle-like structures, whereas in normally infected cells (Fig. 6A) the whole cytoplasm was full of newly synthesized capsid protein and we could not identify vesicle-like structures. For visualization purposes when using the confocal microscope, the imaging thresholds were set differently to visualize the low amount of input virus after transfection (Fig. 6B and C) and to visualize the much higher amount of newly synthetized capsid protein in infected cells (Fig. 6A).

We previously showed that the last component of ESCRTs, the ATPase Vps4 (35), inhibits EV1 infection and EV1-MVB function (15). Therefore, we also wanted to examine the role of Vps4 in CVA9 infection. A549 cells were transfected with DN-Vps4 (VPS4-E235Q–GFP) or a control GFP plasmid. As with the Hrs transfection experiment mentioned above, after 48 h of expres-

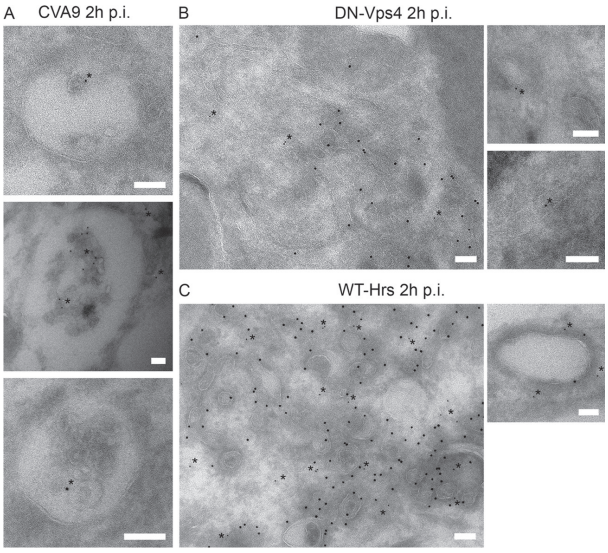

FIG 7 WT-Hrs and DN-Vps4 transfections restrict CVA9-MVB formation. (A) A549 cells were infected with CVA9 for 2 h after which the cells were prepared for cryo-immuno-EM. Thin frozen sections were then labeled for CVA9 capsid protein (PA-gold; diameter, 5 nm; asterisks) and GFP (PA-gold; diameter, 10 nm). Bars, 100 nm. (B and C) A549 cells were transfected with the DN mutant of Vps4 (VPS4-E235Q–GFP; DN-Vps4 (B) or WT-Hrs (C). After 48 h for expression, the cells were infected with CVA9 for 2 h and then prepared for cryo-immuno-EM. Thin frozen sections were then labeled for CVA9 capsid protein (PA-gold; diameter, 5 nm; asterisks) and GFP (PA-gold; diameter, 10 nm). Bars, 100 nm.

sion, the cells were processed for CVA9 infection and capsid protein labeling by IF methods. The overexpression of VPS4-E235Q–GFP had a strong and statistically significant ($P = 2.3E{-}05$) inhibitory effect on VP1 production (Fig. 6C). As with the WT-Hrs transfection described above, CVA9 label in DN-Vps4-transfected cells was found in vesicle-like structures. Besides the VP1 labeling, we also labeled the dsRNA in cells transfected with VPS4-E235Q–GFP or control plasmid. The confocal images and analyses based on those images indicated that in VPS4-E235Q-GFP-expressing cells, the amount of dsRNA structures was clearly decreased (Fig. 6D).

In addition to the infectivity assays descripted above, we used cryo-immuno-EM to verify whether virus label was present in MVBs during normal infection versus after overexpression of WT-Hrs or transfection with DN-Vps4 (VPS4-E235Q–GFP). Nontransfected and transfected A549 cells were infected with CVA9, and cryo-immuno-EM-samples were prepared. From thin sections, CVA9 capsid protein and GFP were labeled with PA-gold (diameter, 5 and 10 nm, respectively). In nontransfected cells, MVBs positive for CVA9 label were frequently found after 2 h (Fig. 7A). In contrast, in cells transfected with DN-Vps4 (VPS4-E235Q–GFP; verified by GFP labeling), CVA9 was observed in small vesicles with no clear accumulation of ILVs (Fig. 7B). Likewise, after overexpression of WT-Hrs, the transfected cells showed high amounts of smaller vesicles in the cytoplasm, and in those cells CVA9 was not observed in MVBs (Fig. 7C). Together with the infectivity assay results (Fig. 6A to D), these results showed that at least two players (Hrs and Vps4) are involved in the MVB formation process during CVA9 infection and thus directly indicated that ESCRTs are needed for formation of virus-driven MVBs.

Endosomes accumulating CVA9 are neutral. In order to study in more detail the relations of CVA9 to acidic structures and whether acidity is at all needed for CVA9 infection, we used several approaches that exploited chemical inhibitors and direct intraendosomal measurements of acidity. A vacuolar proton ATPase (v-ATPase) is known to establish an acidic pH in the lumen of endocytic organelles, and the pH gradually proceeds to lower values from early endosomes to late endosomes and lysosomes (36). Bafilomycin A1 (Baf) is a specific v-ATPase inhibitor, and it has been shown to inhibit vesicle budding from early endosomes (37) and the transport from late endosomes to lysosomes (38). We thus decided to use this drug to inhibit acidification of endosomes during CVA9 entry. We treated A549 cells similarly as for the first chemical inhibitor assay (see Materials and methods) and observed that, although the Baf treatment slightly decreased the infection rate of CVA9, the virus maintained its level of infectivity to a large extent (Fig. 8A). In addition, we performed an RT-PCR assay for the Baf-treated cells, and no decrease in the genomic or complementary strand production was observed (Fig. 8B). To verify that Baf treatment elevated the pH in endocytic compartments, an intraendosomal measurement assay was carried out for the control protein EGFr, which is known to accumulate in late endosomes and lysosomes (16). The cell viability after the drug treatments was verified by the colorimetric MTT assay (Millipore).

In HeLa cells, Baf arrests the transport of markers in early endosomes, in the canonical early endosomes-to-late endosomes-

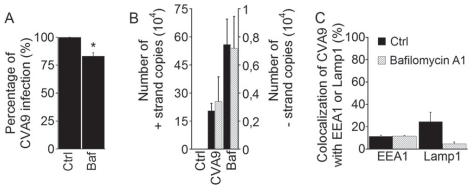

FIG 8 Bafilomycin A1 does not inhibit CVA9 infection. (A) A549 cells were preincubated with Baf (see Table 1). After CVA9 binding, the cells were incubated for 6 h in the presence of inhibitor. The proportions of infected cells (cells producing CVA9 capsid protein at 6 h p.i.) of control (Ctrl) and inhibitor-treated (Baf) cells were quantified. The experiment was repeated three times, and the mean values are shown (± standard errors [SE]). Statistical significance was calculated with a paired-sample *t* test (after arcsine square root transformation). *, $P < 0.05$. (B) A549 cells were preincubated with Baf, and the cells were infected with CVA9. After 6 h, samples were prepared for RT-PCR. The presence of genomic (+) and complementary (−) RNA strands was analyzed with RT-PCR. The RT-PCR results are averages of three parallel samples (± SE). Statistical significance was calculated with a paired-sample *t* test. (C) A549 cells were pre-incubated with Baf, after which the A549 cells were infected with CVA9 and after incubation for 1 h (for EEA1 labeling) or 2 h (for Lamp1 labeling), cells were fixed and labeled with anti-CVA9 and EEA1 or Lamp1 antibodies. Quantification of colocalization of CVA9 with EEA1 and Lamp1 was done from confocal projection stacks of single cells by using BioImageXD software. Thirty cells from each of the three independent experiments were analyzed. The results are shown as mean values (± SE).

to-lysosomes route (39). Thus, we next tested whether Baf treatment caused an accumulation of CVA9 label in early endosomes. A549 cells were treated with Baf for 30 min prior to CVA9 binding, after which the cells were infected with the virus; after 60 min of incubation, the cells were fixed and labeled with CVA9 anticapsid antibody and EEA1 antibody. As shown in Fig. 8C (EEA1 bars), such accumulation did not occur. In addition, we studied whether Baf treatment affected CVA9 colocalization with Lamp1. The results showed that the colocalization between CVA9 capsid protein and Lamp1 labels decreased, although not in a statistically significant manner ($P = 0.06$).

As the Baf result described above suggested that the CVA9 entry pathway is not dependent on vesicle acidification, we wanted to determine directly whether the endosomes used by CVA9 are at all acidic. We started by live imaging of CVA9 with LysoTracker green, which is used as a live probe that accumulates in acidic structures. After CVA9 binding, capsid protein labeling, and internalization for 1 h at 37°C, LysoTracker green was added to the cells for 1 h at 37°C. Our earlier results (Fig. 3A) already demonstrated that this kind of preinternalization labeling of the virus does not inhibit the CVA9 infection rate significantly. LysoTracker green labeling showed a bright signal in a high number of endosomes, probably representing both late endosomes and lysosomes (Fig. 9A). Despite the high number of acidic endosomes, there was no apparent colocalization with CVA9-positive endosomes (Fig. 9B). These results thus further confirmed that CVA9 does not accumulate in acidic structures during a 3.5-h live imaging period.

In order to gain more accurate information of the pHs of the endosomes along the infectious CVA9 pathway, we performed an intraendosomal pH measurement assay (15, 16). In the assay, a pH-stable AF-555 conjugate and a pH-sensitive fluorescein isothiocyanate (FITC) conjugate were introduced to forming CVA9-

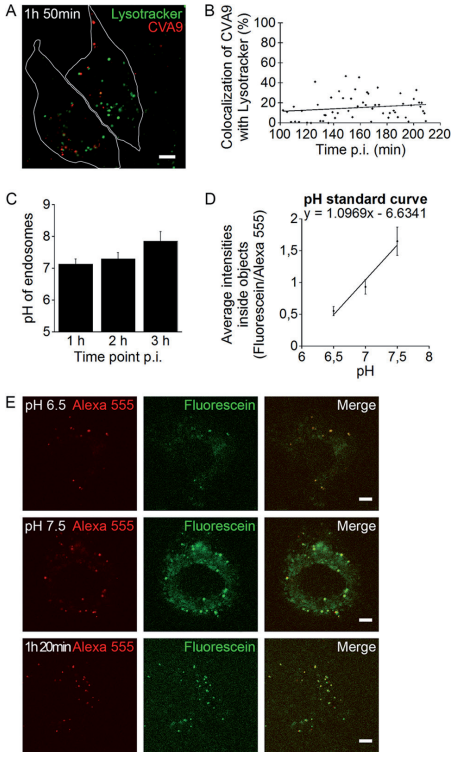

FIG 9 CVA9 structures are nonacidic. (A and B) After CVA9 binding, the virus capsid was labeled (red) and the internalization was initiated by moving A549 cells to a preheated (37°C) microscope sample stage. After 1 h, LysoTracker green was added to the cells for 1 h. Localization of LysoTracker green- and CVA9-positive structures was followed during CVA9 infection in live cells. Bar, 5 μm. (A) A representative confocal projection stack image taken at 1 h 50 min p.i. Bar, 10 μm. (B) Quantifications of colocalization of CVA9 with LysoTracker green were done from projection stacks of single cells by using the BioImageXD software. Altogether, 60 individual cells were analyzed. (C, D, and E) A549 cells were sequentially incubated on ice with primary and secondary antibodies to label plasma membrane-bound CVA9. The secondary antibody was conjugated with pH-sensitive FITC (fluorescein; green) and pH-resistant AF-555 (red). The internalization was started by moving the cells to 37°C, and the cells were imaged live with a confocal microscope. (C) The ratios between FITC and AF-555 signals with or without CVA9 were measured from each time point and compared with the pH standard curve. Error bars represent standard errors of three independent experiments (30 cells measured from each). (D) The pH standard curve was acquired by measuring ratios of virus-bound dyes in the presence of different pH buffer solutions supplemented with nigericin. Error bars represent standard errors of three independent experiments (30 cells measured from each). (E) Images represent single confocal sections of cells, showing the two dyes in endosomes at pH 6.5 and 7.5 and after 1 h 20 min p.i. Bars, 5 μm.

positive endosomes. The fluorescence intensity ratio between FITC and AF-555 was measured from internalized CVA9 vesicles at different time points and compared against a pH standard curve (Fig. 9D) that was prepared in the same live assay. The assay

showed in three consecutive assays that the pH of CVA9 vesicles stayed remarkably neutral at time points 1, 2, and 3 h p.i. (Fig. 9C). As shown in Fig. 9E, the fluorescence signal for the fluorescein conjugate was remarkably lower at pH 6.5 than pH 7.5. The results thus demonstrated altogether that CVA9 does not accumulate in acidic endosomes.

DISCUSSION

In spite of extensive molecular studies of CVA9, the structures involved in the infectious entry and uncoating processes have remained unclear. We recently reported that CVA9 does not use clathrin- or caveolin1-associated pathways to infect A549 cells (13). Here we have shown that CVA9 enters endosomes that gradually develop into nonacidic multivesicular endosomes. These results are remarkably similar to those we observed with another enterovirus, EV1 (15, 16), and thus suggest that these two acid-stable enteroviruses may also bear other similarities in theur mechanisms of internalization, uncoating, and genome release from endosomes.

According to the results presented here, uncoating of CVA9 in A549 cells is initiated at 30 min p.i. The major part of uncoating takes place around 2 h, when the virus is found in MVBs, which was confirmed by EM. The first signs of active replication (dsRNA) were observed at 3 h p.i., and the formation of new, infective CVA9 particles occurred after the 3-h time point. The uncoating and replication time schedule is very similar to what we found for EV1. In SAOS-α2 cells, the majority of EV1 uncoating took place after 1 h (9, 40), and the increase of positive- and negative-strand viral RNA was detectable around 2 to 3 h (15, 23, 41). Inspections of the data accumulated from other enteroviruses suggest some further similarities, although there are clearly cell-line-dependent differences as well. In HeLa cells, poliovirus (PV) RNA release is rapid and efficient and begins already after 10 min p.i. (28). On the other hand, in polarized human brain microvascular endothelial cells, PV remains on the cell surface longer, as it starts to enter the cytoplasm at 2.5 h p.i., and the uncoating takes place after 4 h (42).

The effects of inhibitory drugs on infection showed clear similarities with EV1 but also some interesting differences. Similar to EV1, CVA9 infection was affected by inhibitors of PLC, Rac1, and an Na^+/H^+ exchanger but, in contrast, was not affected by the inhibitors of PI3K and Pak1. As with EV1, the effect of PLC inhibition was restricted to early time points of infection (before 1 h). We showed previously that PLC inhibition causes an arrest of EV1 and fluid-phase uptake on the plasma membrane (29). Most probably, this is the case also with CVA9, considering that PLC inhibition was without effect during uncoating of the virus. EIPA has been used as one major indicator of macropinocytosis in numerous virus studies. It exerts its effect already during early entry, leaving many viruses and ligands undergoing macropinocytosis on the plasma membrane or, as it was shown for CVA9 and EV1, in peripheral early-type vesicles (13, 29). However, as seen from our detailed time course studies, EIPA seems to have several inhibitory effects all the way through virus infection and not only during virus entry, which makes it difficult pinpoint the point of action. It has been shown that EIPA inhibits the intracellular replication of human rhinovirus 2 and coxsackievirus B3 (43, 44), and in the case of human rhinovirus 2, the viral release process is also inhibited in EIPA-treated cells. EIPA was recently shown to cause local changes in the Na^+ and H^+ gradients in vesicles and prevent Rac1 and Cdc42 activation (45).

The effects on Rac1 signaling by EIPA may actually explain some of the unexpected results that we observed with the Rac1 inhibitor at a later step for both the EIPA and Rac1 inhibitors. Our previous results with EV1 suggested that Rac1 is involved during early entry, leading to downstream Pak1 activation and use of CtBP/BARS for macropinocytic entry on the plasma membrane (29, 46). Now, with CVA9, it is clear that Rac1 inhibition was most effective in the postentry, endosomal step. Furthermore, CVA9 infection was not dependent on Pak1, suggesting that early downstream activation of Pak1 via Rac1 is not needed. What could be the role of Rac1 in the endosomal structures? Unexpectedly, the Rac1 inhibitor did not disturb the viral uncoating process, which was verified in an NR-based uncoating assay. Rac1 is a small GTPase, which plays a fundamental role in a variety of cellular processes: actin cytoskeletal reorganization, cell transformation, the introduction of DNA synthesis, and cell migration, to name a few (47). Actin nucleation and polymerization have been shown to control endosome biogenesis, even beyond the first entry step, indicating that actin may have direct effects on cytoplasmic endosomes, presumably driving membrane remodeling (48). Here, our results suggest that Rac1 activation is needed after the viral uncoating process. The exact role of Rac1 in the endosomes during CVA9 infection is a subject for further studies.

We were especially interested in the endosomes that accumulated CVA9 during the first 2 h of infection, because the majority of CVA9 uncoating takes place during that time period and because the production of dsRNA has not yet started in the cytoplasm. Several lines of evidence demonstrated that MVBs are important structures in CVA9 infection. First of all, the EM analysis showed the majority of the CVA9-positive structures were multivesicular at 2 h p.i. Furthermore, between 30 min and 2 h, the proportion of CVA9 vesicles with ILVs increased. The most direct evidence for the importance of the MVBs to CVA9 infection comes from the studies with the ESCRT machinery. Both the overexpression of the first component of this machinery, Hrs, as well as expression of the DN mutant of the last component (Vps4) had a strong effect on CVA9 infectivity, indicating that infection does not occur without MVBs. This is similar to what we found for EV1 previously (15). In addition, cryo-immuno-EM showed that in cells transfected with either WT-Hrs or DN-Vps4 (VPS4-E235Q–GFP), CVA9 was found in endosomes without ILVs. The mechanistic understanding of the possible role of ILVs in EV1 and CVA9 infections remains a subject for further studies.

Since the most studied pathway leading to MVBs is the acidic canonical endosomal pathway (early to late endosomes and lysosomes), the dogma has been that the MVBs are mostly acidic. However, we showed previously and extensively for EV1 that acidity did not play a role for EV1 infection and that the MVBs used by EV1 were close to neutral in acidity (15, 16, 29). We demonstrated here that CVA9 does not enter the conventional acidic endosomes and, further, that it does not require an acidic environment for initiation of infection: (i) Baf treatment did not decrease viral RNA or protein production, (ii) CVA9 did not colocalize with EEA1, Lamp1, internalized DiI-LDL, or Rab7, and (iii) the extents of colocalization with these structures were not changed after the Baf or Noc treatment. The findings are similar to what we obtained for EV1 infection (16, 29, 41) but, interestingly, these results bear similarities also with PV infection. Coyne et al. (42)

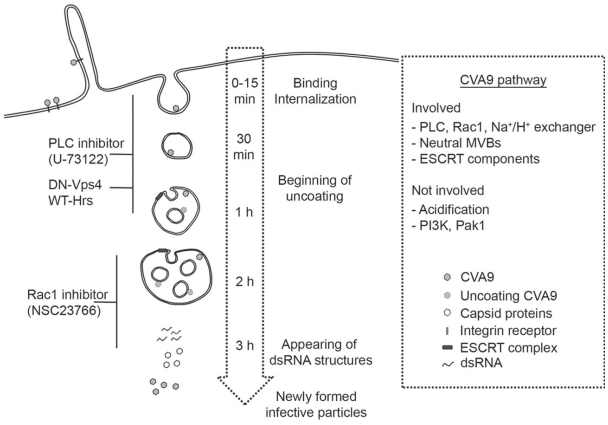

FIG 10 Model of the CVA9 internalization pathway. CVA9 infection starts with virus uptake associated with plasma membrane ruffles. Inhibition of PLC activity prevents early entry of CVA9. CVA9 is internalized to endosomes, which gradually form ESCRT-driven intraluminal vesicles, leading to neutral MVBs. The majority of uncoating occurs around 2 h p.i., when CVA9 is in MVBs. Rac1 inhibition affects CVA9 infection in the endosomal step, after which the replication starts in the cytoplasm and leads to accumulation of dsRNA structures and later the newly synthetized viral capsid proteins and infective virus particles.

showed that vesicles containing PV, VP1, or the PV receptor did not colocalize with EEA1, Rab7, or the late endosome marker LAMP-II. In addition, the productive RNA release and infectivity of PV were not dependent on the acidic environment of late endosomes (28, 49–51). Moreover, endocytosis of yet another enterovirus, coxsackievirus B3, and its infectivity are suggested to be independent of clathrin, caveolin, and endosomal acidification in HeLa cells (52). Thus, it is becoming more evident that some enteroviruses have similarities in their entry and that acidity may not play a role in their infectious cycle.

In conclusion, based on the findings in this report, we generated a model for CVA9 internalization and intracellular CVA9 structures that are important in the infection process (Fig. 10). CVA9 infection starts by virus uptake associated with plasma membrane ruffles. Inhibition of PLC activity is most effective during the earlier time points of virus uptake. Internalized CVA9 is found in endosomes that gradually form ESCRT-driven intraluminal vesicles, leading to neutral MVBs. The majority of uncoating occurs around 2 h p.i., when the bulk of CVA9 is in MVBs. Rac1 inhibition affects CVA9 infection in the endosomal step, after which replication starts in the cytoplasm and leads to accumulation of dsRNA structures and later newly synthesized viral capsid proteins and infective virus particles.

ACKNOWLEDGMENTS

We thank Lucia Fiore (Instituto Superiore di Sanita, Rome, Italy), Sylvie Urbé (Cellular and Molecular Physiology, University of Liverpool, Liverpool, United Kingdom), Harald Stenmark (The Norwegian Radium Hospital, Oslo, Norway), Lucas Pelkmans (Institute of Molecular Life Sciences, University of Zurich, Zurich, Switzerland), and Miguel Seabra (Faculty of Medicine, National Heart and Lung Institute, Imperial College, London, United Kingdom) for providing us with K6 CVA9 antibody, Hrs-WT–GFP, VPS4-E235Q–GFP, Rab5-Q79L–YFP, and Rab5-S34N–EGFP and Rab5-WT–GFP, respectively. We thank the Biocenter Oulu EM Core Facility for cutting and labeling thin frozen sections and Epon samples.

The work was supported by grants from the Academy of Finland (grants 119354 and 257125), Sigrid Juselius Foundation, National Graduate School on Nanoscience, and Ellen and Artturi Nyyssönen Foundation.

REFERENCES

1. **Hyypiä T, Hovi T, Knowles NJ, Stanway G.** 1997. Classification of enteroviruses based on molecular and biological properties. J. Gen. Virol. **78:**1–11.
2. **Chang KH, Auvinen P, Hyypiä T, Stanway G.** 1989. The nucleotide sequence of coxsackievirus A9; implications for receptor binding and enterovirus classification. J. Gen. Virol. **70:**3269–3280.
3. **Nelsen-Salz B, Eggers HJ, Zimmermann H.** 1999. Integrin αvβ3 (vitronectin receptor) is a candidate receptor for the virulent echovirus 9 strain Barty. J. Gen. Virol. **80:**2311–2313.
4. **Heikkilä O, Susi P, Stanway G, Hyypiä T.** 2009. Integrin αVβ6 is a high-affinity receptor for coxsackievirus A9. J. Gen. Virol. **90:**197–204. http://dx.doi.org/10.1099/vir.0.004838-0.
5. **Roivainen M, Piirainen L, Hovi T, Virtanen I, Riikonen T, Heino J, Hyypiä T.** 1994. Entry of coxsackievirus A9 into host cells: specific interactions with alpha v beta 3 integrin, the vitronectin receptor. Virology **203:**357–365. http://dx.doi.org/10.1006/viro.1994.1494.
6. **Williams CH, Kajander T, Hyypiä T, Jackson T, Sheppard D, Stanway G.** 2004. Integrin alpha v beta 6 is an RGD-dependent receptor for coxsackievirus A9. J. Virol. **78:**6967–6973. http://dx.doi.org/10.1128/JVI.78.13.6967-6973.2004.
7. **Triantafilou K, Fradelizi D, Wilson K, Triantafilou M.** 2002. GRP78, a coreceptor for coxsackievirus A9, interacts with major histocompatibility complex class I molecules which mediate virus internalization. J. Virol. **76:**633–643. http://dx.doi.org/10.1128/JVI.76.2.633-643.2002.
8. **Triantafilou M, Triantafilou K, Wilson KM, Takada Y, Fernandez N, Stanway G.** 1999. Involvement of β2-microglobulin and integrin $\alpha_v\beta_3$ molecules in the coxsackievirus A9 infectious cycle. J. Gen. Virol. **80:**2591–2600.
9. **Marjomäki V, Pietiäinen V, Matilainen H, Upla P, Ivaska J, Nissinen L, Reunanen H, Huttunen P, Hyypiä T, Heino J.** 2002. Internalization of echovirus 1 in caveolae. J. Virol. **76:**1856–1865. http://dx.doi.org/10.1128/JVI.76.4.1856-1865.2002.
10. **Mercer J, Schelhaas M, Helenius A.** 2010. Virus entry by endocytosis. Annu. Rev. Biochem. **79:**803–833. http://dx.doi.org/10.1146/annurev-biochem-060208-104626.

11. **Fuchs R, Blaas D.** 2010. Uncoating of human rhinoviruses. Rev. Med. Virol. **20:**281–297. http://dx.doi.org/10.1002/rmv.654.
12. **Scott CC, Gruenberg J.** 2011. Ion flux and the function of endosomes and lysosomes. pH is just the start: the flux of ions across endosomal membranes influences endosome function not only through regulation of the luminal pH. Bioessays **33:**103–110. http://dx.doi.org/10.1002/bies.201000108.
13. **Heikkilä O, Susi P, Tevaluoto T, Härmä H, Marjomäki V, Hyypiä T, Kiljunen S.** 2010. Internalization of coxsackievirus A9 is mediated by β2-microglobulin, dynamin, and Arf6 but not by caveolin-1 or clathrin. J. Virol. **84:**3666–3681. http://dx.doi.org/10.1128/JVI.01340-09.
14. **Shakeel S, Seitsonen JJ, Kajander T, Laurinmäki P, Hyypiä T, Susi P, Butcher SJ.** 2013. Structural and functional analysis of coxsackievirus A9 integrin αvβ6 binding and uncoating. J. Virol. **87:**3943–3951. http://dx.doi.org/10.1128/JVI.02989-12.
15. **Karjalainen M, Rintanen N, Lehkonen M, Kallio K, Mäki A, Hellström K, Siljamäki V, Upla P, Marjomäki V.** 2011. Echovirus 1 infection depends on biogenesis of novel multivesicular bodies. Cell. Microbiol. **13:**1975–1995. http://dx.doi.org/10.1111/j.1462-5822.2011.01685.x.
16. **Rintanen N, Karjalainen M, Alanko J, Paavolainen L, Mäki A, Nissinen L, Lehkonen M, Kallio K, Cheng RH, Upla P, Ivaska J, Marjomäki V.** 2012. Calpains promote α2β1 integrin turnover in nonrecycling integrin pathway. Mol. Biol. Cell **23:**448–463. http://dx.doi.org/10.1091/mbc.E11-06-0548.
17. **Hanson PI, Cashikar A.** 2012. Multivesicular body morphogenesis. Annu. Rev. Cell Dev. Biol. **28:**337–362. http://dx.doi.org/10.1146/annurev-cellbio-092910-154152.
18. **Matsuo H, Chevallier J, Mayran N, Le Blanc I, Ferguson C, Faure J, Blanc NS, Matile S, Dubochet J, Sadoul R, Parton RG, Vilbois F, Gruenberg J.** 2004. Role of LBPA and Alix in multivesicular liposome formation and endosome organization. Science **303:**531–534. http://dx.doi.org/10.1126/science.1092425.
19. **Hendry E, Hatanaka H, Fry E, Smyth M, Tate J, Stanway G, Santti J, Maaronen M, Hyypiä T, Stuart D.** 1999. The crystal structure of coxsackievirus A9: new insights into the uncoating mechanisms of enteroviruses. Structure. **7:**1527–1538.
20. **Abraham G, Colonno RJ.** 1984. Many rhinovirus serotypes share the same cellular receptor. J. Virol. **51:**340–345.
21. **Pulli T, Roivainen M, Hovi T, Hyypiä T.** 1998. Induction of neutralizing antibodies by synthetic peptides representing the C terminus of coxsackievirus A9 capsid protein VP1. J. Gen. Virol. **79:**2249–2253.
22. **Buttinelli G, Donati V, Ruggeri FM, Joki-Korpela P, Hyypiä T, Fiore L.** 2003. Antigenic sites of coxsackie A9 virus inducing neutralizing monoclonal antibodies protective in mice. Virology **312:**74–83. http://dx.doi.org/10.1016/S0042-6822(03)00182-X.
23. **Upla P, Marjomäki V, Nissinen L, Nylund C, Waris M, Hyypiä T, Heino J.** 2008. Calpain 1 and 2 are required for RNA replication of echovirus 1. J. Virol. **82:**1581–1590. http://dx.doi.org/10.1128/JVI.01375-07.
24. **Upla P, Marjomäki V, Kankaanpää P, Ivaska J, Hyypiä T, Van Der Goot FG, Heino J.** 2004. Clustering induces a lateral redistribution of alpha 2 beta 1 integrin from membrane rafts to caveolae and subsequent protein kinase C-dependent internalization. Mol. Biol. Cell **15:**625–636. http://dx.doi.org/10.1091/mbc.E03-08-0588.
25. **Slot JW, Geuze HJ.** 2007. Cryosectioning and immunolabeling. Nat. Protoc. **2:**2480–2491. http://dx.doi.org/10.1038/nprot.2007.365.
26. **Kankaanpää P, Paavolainen L, Tiitta S, Karjalainen M, Päivärinne J, Nieminen J, Marjomäki V, Heino J, White DJ.** 2012. BioImageXD: an open, general-purpose and high-throughput image-processing platform. Nat. Methods **9:**683–689. http://dx.doi.org/10.1038/nmeth.2047.
27. **Costes SV, Daelemans D, Cho EH, Dobbin Z, Pavlakis G, Lockett S.** 2004. Automatic and quantitative measurement of protein-protein colocalization in live cells. Biophys. J. **86:**3993–4003. http://dx.doi.org/10.1529/biophysj.103.038422.
28. **Brandenburg B, Lee LY, Lakadamyali M, Rust MJ, Zhuang X, Hogle JM.** 2007. Imaging poliovirus entry in live cells. PLoS Biol. **5**(7)**:**e183. http://dx.doi.org/10.1371/journal.pbio.0050183.
29. **Karjalainen M, Kakkonen E, Upla P, Paloranta H, Kankaanpää P, Liberali P, Renkema GH, Hyypiä T, Heino J, Marjomäki V.** 2008. A Raft-derived, Pak1-regulated entry participates in α2β1 integrin-dependent sorting to caveosomes. Mol. Biol. Cell **19:**2857–2869. http://dx.doi.org/10.1091/mbc.E07-10-1094.
30. **Gruenberg J, Griffiths G, Howell KE.** 1989. Characterization of the early endosome and putative endocytic carrier vesicles in vivo and with an assay of vesicle fusion in vitro. J. Cell Biol. **108:**1301–1316.
31. **Gruenberg J, Stenmark H.** 2004. The biogenesis of multivesicular endosomes. Nat. Rev. Mol. Cell Biol. **5:**317–323. http://dx.doi.org/10.1038/nrm1360.
32. **Hirsch JG, Fedorko ME, Cohn ZA.** 1968. Vesicle fusion and formation at the surface of pinocytic vacuoles in macrophages. J. Cell Biol. **38:**629–632.
33. **Raiborg C, Malerod L, Pedersen NM, Stenmark H.** 2008. Differential functions of Hrs and ESCRT proteins in endocytic membrane trafficking. Exp. Cell Res. **314:**801–813. http://dx.doi.org/10.1016/j.yexcr.2007.10.014.
34. **Urbe S, Sachse M, Row PE, Preisinger C, Barr FA, Strous G, Klumperman J, Clague MJ.** 2003. The UIM domain of Hrs couples receptor sorting to vesicle formation. J. Cell Sci. **116:**4169–4179. http://dx.doi.org/10.1242/jcs.00723.
35. **Katzmann DJ, Odorizzi G, Emr SD.** 2002. Receptor downregulation and multivesicular-body sorting. Nat. Rev. Mol. Cell Biol. **3:**893–905. http://dx.doi.org/10.1038/nrm973.
36. **Futai M, Oka T, Sun-Wada G, Moriyama Y, Kanazawa H, Wada Y.** 2000. Luminal acidification of diverse organelles by v-ATPase in animal cells. J. Exp. Biol. **203:**107–116.
37. **Clague MJ, Urbe S, Aniento F, Gruenberg J.** 1994. Vacuolar ATPase activity is required for endosomal carrier vesicle formation. J. Biol. Chem. **269:**21–24.
38. **van Deurs B, Holm PK, Kayser L, Sandvig K.** 1995. Delivery to lysosomes in the human carcinoma cell line HEp-2 involves an actin filament-facilitated fusion between mature endosomes and preexisting lysosomes. Eur. J. Cell Biol. **66:**309–323.
39. **Bayer N, Schober D, Prchla E, Murphy RF, Blaas D, Fuchs R.** 1998. Effect of bafilomycin A1 and nocodazole on endocytic transport in HeLa cells: implications for viral uncoating and infection. J. Virol. **72:**9645–9655.
40. **Siljamäki E, Rintanen N, Kirsi M, Upla P, Wang W, Karjalainen M, Ikonen E, Marjomäki V.** 2013. Cholesterol dependence of collagen and echovirus 1 trafficking along the novel α2β1 integrin internalization pathway. PLoS One **8**(2)**:** e55465. http://dx.doi.org/10.1371/journal.pone.0055465.
41. **Pietiäinen V, Marjomäki V, Upla P, Pelkmans L, Helenius A, Hyypiä T.** 2004. Echovirus 1 endocytosis into caveosomes requires lipid rafts, dynamin II, and signaling events. Mol. Biol. Cell **15:**4911–4925. http://dx.doi.org/10.1091/mbc.E04-01-0070.
42. **Coyne CB, Kim KS, Bergelson JM.** 2007. Poliovirus entry into human brain microvascular cells requires receptor-induced activation of SHP-2. EMBO J. **26:**4016–4028. http://dx.doi.org/10.1038/sj.emboj.7601831.
43. **Gazina EV, Harrison DN, Jefferies M, Tan H, Williams D, Anderson DA, Petrou S.** 2005. Ion transport blockers inhibit human rhinovirus 2 release. Antiviral Res. **67:**98–106. http://dx.doi.org/10.1016/j.antiviral.2005.05.003.
44. **Harrison DN, Gazina EV, Purcell DF, Anderson DA, Petrou S.** 2008. Amiloride derivatives inhibit coxsackievirus B3 RNA replication. J. Virol. **82:**1465–1473. http://dx.doi.org/10.1128/JVI.01374-07.
45. **Koivusalo M, Welch C, Hayashi H, Scott CC, Kim M, Alexander T, Touret N, Hahn KM, Grinstein S.** 2010. Amiloride inhibits macropinocytosis by lowering submembranous pH and preventing Rac1 and Cdc42 signaling. J. Cell Biol. **188:**547–563. http://dx.doi.org/10.1083/jcb.200908086.
46. **Liberali P, Kakkonen E, Turacchio G, Valente C, Spaar A, Perinetti G, Bockmann RA, Corda D, Colanzi A, Marjomäki V, Luini A.** 2008. The closure of Pak1-dependent macropinosomes requires the phosphorylation of CtBP1/BARS. EMBO J. **27:**970–981. http://dx.doi.org/10.1038/emboj.2008.59.
47. **Bosco EE, Mulloy JC, Zheng Y.** 2009. Rac1 GTPase: a "Rac" of all trades. Cell. Mol. Life Sci. **66:**370–374. http://dx.doi.org/10.1007/s00018-008-8552-x.
48. **Morel E, Parton RG, Gruenberg J.** 2009. Annexin A2-dependent polymerization of actin mediates endosome biogenesis. Dev. Cell **16:**445–457. http://dx.doi.org/10.1016/j.devcel.2009.01.007.
49. **Doedens J, Maynell LA, Klymkowsky MW, Kirkegaard K.** 1994. Secretory pathway function, but not cytoskeletal integrity, is required in poliovirus infection. Arch. Virol. Suppl. **9:**159–172.
50. **Gromeier M, Wetz K.** 1990. Kinetics of poliovirus uncoating in HeLa cells in a nonacidic environment. J. Virol. **64:**3590–3597.
51. **Perez L, Carrasco L.** 1993. Entry of poliovirus into cells does not require a low-pH step. J. Virol. **67:**4543–4548.
52. **Patel KP, Coyne CB, Bergelson JM.** 2009. Dynamin- and lipid raft-dependent entry of decay-accelerating factor (DAF)-binding and non-DAF-binding coxsackieviruses into nonpolarized cells. J. Virol. **83:**11064–11077. http://dx.doi.org/10.1128/JVI.01016-09.

III

ECHOVIRUS 1 INTERNALIZATION NEGATIVELY REGULATES EGFR DOWNREGULATION

by

Moona Huttunen, Paula Turkki, Anita Mäki, Paavolainen Lassi, Pekka Ruusuvuori & Varpu Marjomäki

Manuscript